The Higgs Boson in Less Constrained Supersymmetric Models

by
Helge Pettersen

Master's Thesis in Theoretical Particle Physics

Department of Physics and Technology
University of Bergen
Norway

June 2012

Acknowledgements

I would like to thank my supervisor, Professor Per Osland, for being an excellent guide in the creation of this thesis. Thank you for teaching me particle physics, and for being able to give great advice whenever I needed it.

I wouldn't have been able to do any of this without all the help I've received from the wonderful people at IFT. Dr. Nils-Erik Bomark is able to answer every question imaginable and Dr. Thomas Burgess could debug an ant colony.

Thanks for all the enlightening and engaging conversations during and in between the numerous coffee breaks. Anders Haarr and Ørjan Dale. Steffen Mæland and Knut Morå. Jan Lindroos and Justas Zalieckas. Without your friendship and help this wouldn't have been possible!

For all their love, support and proofreading, I would like to thank my family and friends. And of course, to Jorid, who shows me the beauty in the smallest of things.

Helge Pettersen
June 1, 2012

Contents

List of Figures

List of Tables

Chapter 1

Introduction

1.1 History and introduction

When J. J. Thompson discovered the electron at the end of the 19th century, he started a revolution in physics. During the following decades, quantum mechanics and the theory of relativity were developed, collectively called "modern physics".

Before this discovery, Newtonian physics had described the world adequately. The atom was, eponymously, the smallest known structure and thus the heart of all matter. The unification of the electric and magnetic forces by James Clerk Maxwell in 1865 was followed by new insights into the nature of light, and in 1887 Heinrich Hertz discovered the photoelectric effect: Where high-intensity light is directed towards a material, which then emits electrons. However, none of these breakthroughs were inconceivable in the Newtonian paradigm.

So when the first hint of a novel substructure – that of the electron, with its quantized charge – appeared in 1897, a paradigm shift was needed. In 1905 Albert Einstein added to the enigma by explaining the photoelectric effect with the quantized photon. During the next ten years (in which time his predictions about the photoelectric effect were proved to be true), he developed his theories: Special and general relativity. Together, these theories unified space, time and gravity. Today his work stands unaltered at one side of this two-faced modern revolution.

At the other side, the European effort of constructing a quantum theory gained momentum. Around 1911 Niels Bohr and Ernest Rutherford came up with new models of the atom. Rutherford hypothesized a heavy nucleus surrounded by an electron cloud. Bohr later added "sudden" or "quantum" leaps of the electron, which would then emit or absorb photons. With this theory, it was possible to describe the by then well-known spectrum of hydrogen.

Add a few years, and a more complete picture emerged. In 1925 Erwin Schrödinger had

formulated the quantum analogue of Newton's laws. Still in use today, it can in principle describe every (non-relativistic) quantum phenomenon. An extension to account for the special relativity of Einstein was quickly developed by Paul Dirac. Every new equation predicted new and unknown phenomena, and they were often discovered shortly after. The abstract "spin" of the electron, as an example, could be read off directly from the Dirac equation. It should be noted that a consistent extension of the Schrödinger Equation for general relativity (or gravity) has not been found yet.

Enter the age of the atom smashers. At the end of the 1920s, only three elementary particles were needed to describe the world: The electron, the proton, and the neutron (to account for large atomic masses). During the next decades, a plethora of new particles emerged. Some of these were suggested by theorists, like the neutrino of Enrico Fermi. However, the vast number of new detector signatures were surprises, in forms of mesons and baryons. The different pions, omegas, xis, rhos and lambdas were all just manifestations of different quark configurations, although the physicists had no way of guessing at this novel substructure yet.

This chaotic situation was resolved by the quark model in 1964, which could account for the SU(3) symmetries observed between the new states. At this point, theoretical progress had come a long way. Gauge theories like Quantum Electrodynamics (a quantum version of Maxwell's electrodynamics) and the electroweak theory had been formulated, and the existence of a "Higgs" boson had been proposed to solve the problem of electroweak symmetry breaking. Together with the full description of the strong interactions through Quantum Chromodynamics in 1974, the *Standard Model* took its current form.

1.2 The Standard Model

The Standard Model (SM) as a theory describes elementary particles, together with how they interact. From this, it is possible to reconstruct the classical laws of physics. In later chapters we will give the SM a more thorough treatment, but for now it is convenient to outline its phenomenology.

There are many ways to describe the particles. A usual way to do this is to use their spin. The spin-$\frac{1}{2}$ particles, or *fermions*, are divided into *quarks* and *leptons*. Both of these can be characterized by their *family*, or *generation*, where the heavier particles belong to a higher generation: 3 in total. There are two leptons and two quarks for each generation, and each can be further separated by the *weak isospin*: Isospin "up" (or $+\frac{1}{2}$) are the up-type quarks u, c, t and the nearly massless neutrinos ν_e, ν_μ, ν_τ. Isospin "down" (or $-\frac{1}{2}$) are the down-type quarks d, s, b and charged leptons e, μ, τ. Each of the quarks comes in sets of three, labeled arbitrarily with the *color* charge.

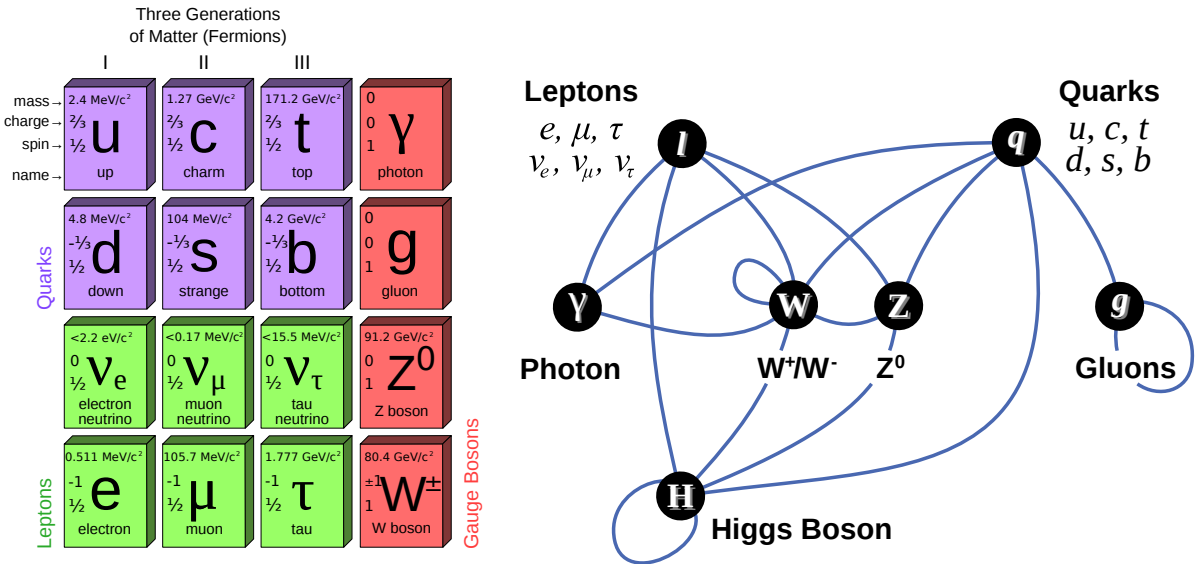

Figure 1.1: **Left***: The particles of the SM, including some of their properties. From Wikipedia* [1]*, where the numbers are checked against the Review of Particle Physics by the Particle Data Group (PDG)* [2]*.* **Right***: The interactions between the SM particles, where the lines signify possible interactions. From Wikipedia* [3]*.*

The integer spin particles are called *bosons*. There are four spin-1 bosons, which are also the force carriers. They are: The massless photon, which propagates the electric force, the massive gauge bosons $W^{\pm}$ and Z^0 for the weak force, and for the strong force, the massless gluon which only interacts in the quark sector. The gluon carries one color and one anti-color, and comes in eight different configurations.

In addition, there is the spin 0 scalar particle called the Higgs boson. Still hypothetical, the finalization of this thesis may well coincide with its official discovery at the Large Hadron Collider at CERN. All these particles, as well as how they interact, are listed in Fig. 1.1.

1.3 Motivation

Since 1974, there has been little theoretical progress. Put another way, many extensions of the Standard Model have been proposed, but in lieu of striking experimental anomalies the SM still stands firmly.

With the discovery of the Higgs boson, the last parameter of the SM is fixed. Precision measurements may then tell us whether we have found "our" Higgs boson, or if we have found one from another theory. Many theories predict a Higgs boson with slightly different

properties than the familiar Standard Model Higgs boson. A theory based on *supersymmetry* is one such possibility.

In this thesis, we will assume that the emerging results from the LHC are real, so that we have indeed found a Higgs boson. We will use the preliminary measurements of its mass and cross section to see how this can be accommodated in a supersymmetric theory. We will also use a less constrained supersymmetric theory than many analyses often do, and it will be interesting to see how such a theory fares against Nature: After every physical constraint has been imposed, is there still any possibility for models based on supersymmetry?

We will begin by reconstructing the Standard Model in Chapter 2. After explaining how and why we need the different components of the SM, we move on to Chapter 3 where we extend the discussion to properties of the SM Higgs boson. In Chapter 4 we explain why and where the SM is inadequate, and propose some of its extensions. Focus will be placed on supersymmetry and the Minimal Supersymmetric Standard Model (MSSM). In Chapter 5 we repeat the exercise of describing the properties of the Higgs boson, but this time in the MSSM sector. Here we use its SM counterpart as a benchmark. In Chapter 6 we look at how to practically study properties of the MSSM Higgs bosons through scans of the parameter space. We will also look at which constraints we need to impose to have a physical (and undetected) theory. At the end, we will put it all together in Chapter 7, where we compare the Standard Model and the MSSM, and enter the preliminary results from the LHC and other collaborations. A conclusion follows in Chapter 8.

Chapter 2

The Standard Model of particle physics

We begin this thesis by outlining the Standard Model. In Section 2.1, the different kinematical equations by Schrödinger, Dirac and Klein-Gordon will be shown. In the following sections, the different gauge groups and symmetries are added: First U(1) QED and SU(2) Yang-Mills, then their combination SU(2) $\times$ U(1). We explain the Higgs mechanism in Section 2.6, and use it to find the Weinberg-Salam broken SU(2) $\times$ U(1) model. After discussing SU(3) QCD in Section 2.9, we look at some of the tools and concepts we will need later: Feynman diagrams in Section 2.10 and higher-order loop diagrams in Section 2.11.

2.1 The Dirac and Klein-Gordon equations

The foundations upon which the Standard Model are built are special relativity and quantum mechanics. Classically, the Hamiltonian for a free particle can be written as

$$H = \frac{\mathbf{p}^2}{2m}. \tag{2.1}$$

The quantization of this Hamiltonian can be done by taking both energy (H) and momentum ($\mathbf{p}$) as operators. With natural units ($\hbar = c = 1$), this transcription is

$$H \to i\frac{\partial}{\partial t}, \qquad \mathbf{p} \to -i\nabla. \tag{2.2}$$

Combining Eqs. (2.1) and (2.2), we find the Schrödinger Equation for a free particle,

$$i\frac{\partial}{\partial t}\psi(\mathbf{x}, t) = \frac{-\nabla^2}{2m}\psi(\mathbf{x}, t). \tag{2.3}$$

It was formulated in the 1920s by Erwin Schrödinger [4, 5]. It is non-relativistic and follows all the requirements for a quantum theory: About how the state function ψ should behave, how only eigenstates are observed and about probability distributions. For the latter, the probability of a particle being in the box $\mathrm{d}^3\mathbf{x}$ around $\mathbf{x}$ at time t_0 is $\mathrm{d}^3\mathbf{x}|\psi(\mathbf{x}, t_0)|^2$.

A relativistic extension of Eq. (2.3) is needed for us to have a Lorentz covariant framework on which to build the Standard Model. This can be done by rewriting the Hamiltonian to its relativistic version. Still using natural units, the relativistic energy is

$$H = \sqrt{\mathbf{p}^2 + m^2}. \tag{2.4}$$

We square it, and get $H^2 = \mathbf{p}^2 + m^2$. Now, the possibility of a *negative* energy state is introduced, given by $H = -\sqrt{\mathbf{p}^2 + m^2}$. By inserting the squared relation into the Schrödinger Equation (2.3), we find the Klein-Gordon second order equation

$$\frac{\partial^2}{\partial t^2}\phi(x) - \nabla^2\phi(x) + m^2\phi(x) = 0, \tag{2.5}$$

which describes a scalar wavefunction $\phi(x) \equiv \phi(x_\mu) \equiv \phi(\mathbf{x}, t)$ for a spin 1 particle.

Since the Klein-Gordon equation is second order in both time and space derivatives, some problems arise. It is impossible to have a physical interpretation of the negative energy and to keep the probability density positive at the same time, see Chapter 2 of Bjorken and Drell [5]. This problem is solved through a linearization of Eq. (2.5), and we will see that the interpretation of such negative-energy solutions is the *anti*-particles, like the positron for the regular electron.

We want to have a linear version of the Klein-Gordon equation, so we take the square root of Eq. (2.5) and introduce the gamma matrices γ^μ, where $\mu = 0, 1, 2, 3$. When two identical indices arise, they are summed over: $\gamma^\mu\partial_\mu = \gamma^0\partial_0 - \boldsymbol{\gamma}\cdot\nabla$. From P. A. M. Dirac's groundbreaking 1928 paper [6], we have

$$i\gamma^\mu\frac{\partial}{\partial x^\mu}\psi(x) - m\psi(x) = 0. \tag{2.6}$$

This is the Dirac equation, which describes a spin $\frac{1}{2}$ particle with the wavefunction $\psi(x)$. $\psi(x)$ is called a spinor due to its mathematical construct: It needs to be rotated 720° to regain itself (instead of the regular 360°, which would flip its sign). This is to incorporate the spin $\frac{1}{2}$ structure. γ^μ are four matrices that follow the relation

$$\{\gamma^\mu, \gamma^\nu\} \equiv \gamma^\mu\gamma^\nu + \gamma^\nu\gamma^\mu = 2g^{\mu\nu}, \tag{2.7}$$

where $g^{\mu\nu}$ is the Minkowski metric with signature ($+$ $-$ $-$ $-$).

2.1.1 Lorentz covariance of the Dirac equation

If the Dirac equation (2.6) is Lorentz covariant, it should be the same for observer $\mathcal{O}'$ with wavefunction $\psi'(x')$ as for observer $\mathcal{O}$ with $\psi(x)$. Defining

$$(x^\nu)' = \frac{\partial x'^\nu}{\partial x^\mu} x^\mu = a^\nu{}_\mu x^\mu = ax, \qquad \psi'(x') = \psi'(ax) = S(a)\psi(x), \tag{2.8}$$

we start with left-multiplying Eq. (2.6) with $S(a)$ and insert $S^{-1}(a)S(a) = 1$:

$$\left(iS(a)\gamma^\mu S^{-1}(a) S(a) \frac{\partial}{\partial x^\mu} - mS(a) \right) \psi(x) = 0 \tag{2.9}$$

$$\left(iS(a)\gamma^\mu S^{-1}(a) \frac{\partial}{\partial x^\mu} - m \right) S(a)\psi(x) = 0. \tag{2.10}$$

With

$$\frac{\partial}{\partial x^\mu} = \frac{\partial x'^\nu}{\partial x^\mu} \frac{\partial}{\partial x'^\nu} = a^\nu{}_\mu \frac{\partial}{\partial x'^\nu}, \tag{2.11}$$

we can write Eq. (2.10) as

$$\left(iS(a)\gamma^\mu S^{-1}(a) a^\nu{}_\mu \frac{\partial}{\partial x'^\nu} - m \right) \psi'(x') = 0. \tag{2.12}$$

The Lorentz covariance of Eq. (2.6) is then secured if we require the following identity to hold:

$$a^\nu{}_\mu \gamma^\mu = S^{-1}(a)\gamma^\nu S(a). \tag{2.13}$$

With this, Eq. (2.12) can written as a primed version of the Dirac equation (2.6),

$$\left(i\gamma^\nu \frac{\partial}{\partial x'^\nu} - m \right) \psi'(x') = 0. \tag{2.14}$$

The transformations can be more explicitly defined as

$$\begin{aligned} a^\nu{}_\mu &= g^\nu{}_\mu + \Delta\omega^\nu{}_\mu \\ S &= 1 - \frac{i}{4}\sigma_{\mu\nu}\Delta\omega^{\mu\nu}, \end{aligned} \tag{2.15}$$

with $\Delta\omega$ as the "angle of rotation" (a 4×4 matrix), and with $\sigma_{\mu\nu}$ related to the Pauli matrices

$$\sigma_{\mu\nu} = \frac{i}{2}[\gamma_\mu, \gamma_\nu]. \tag{2.16}$$

2.2 U(1) QED

Quantum Electrodynamics (QED) was the first and is the simplest gauge theory. It couples the massless spin 1 electromagnetic field A_μ with the spin $\frac{1}{2}$ fermion field ψ. The field ψ has mass m and charge eQ. The QED Lagrangian is

$$\mathcal{L} = -\frac{1}{4}F_{\mu\nu}F^{\mu\nu} + \bar{\psi}(x)\left[i\gamma^\mu D_\mu - m\right]\psi(x), \tag{2.17}$$

where $F_{\mu\nu}$ is the electromagnetic field tensor:

$$F_{\mu\nu} = \partial_\nu A_\mu - \partial_\mu A_\nu, \tag{2.18}$$

and D_μ is the covariant derivative which couples A_μ and $\psi(x)$:

$$D_\mu = \partial_\mu + ieQA_\mu. \tag{2.19}$$

The fields A_μ and ψ can be expanded as

$$\begin{aligned}
A_\mu(x) = A_\mu^+(x) + A_\mu^-(x) &= \sum_{r,\mathbf{k}} \frac{1}{\sqrt{2V\omega_\mathbf{k}}}\varepsilon_{r\mu}(\mathbf{k})\left[a_r(\mathbf{k})\ \mathrm{e}^{-ik\cdot x} + a_r^\dagger(\mathbf{k})\ \mathrm{e}^{ik\cdot x}\right], \\
\psi(x) = \psi^+(x) + \psi^-(x) &= \sum_{r,\mathbf{p}} \sqrt{\frac{m}{VE_\mathbf{p}}}\left[c_r(\mathbf{p})u_r(\mathbf{p})\ \mathrm{e}^{-ip\cdot x} + d_r^\dagger(x)v_r(\mathbf{p})\ \mathrm{e}^{ip\cdot x}\right], \\
\bar{\psi}(x) = \bar{\psi}^+(x) + \bar{\psi}^-(x) &= \sum_{r,\mathbf{p}} \sqrt{\frac{m}{VE_\mathbf{p}}}\left[d_r(\mathbf{p})\bar{v}_r(\mathbf{p})\ \mathrm{e}^{-ip\cdot x} + c_r^\dagger(\mathbf{p})\bar{u}_r(\mathbf{p})\ \mathrm{e}^{ip\cdot x}\right],
\end{aligned} \tag{2.20}$$

where V is the quantization volume (taken to be large but finite) and $\varepsilon_{r\mu}$ is the photon polarization. a_r, c_r and d_r are the annihilation operators for the different fields, while $a_r^\dagger, c_r^\dagger$ and $d_r^\dagger$ are the creation operators. u_r (v_r) are the spinors that arise as positive (negative) energy solutions to the Dirac equation. The sums are over spin (r) and quantized momentum: $\mathbf{p}$ for fermions, $\mathbf{k}$ for bosons.

These fields are also solutions to the Dirac and Klein-Gordon equations, but it should be noted that they are *not* wavefunctions like the $\psi(x)$ and $\phi(x)$ of Section 2.1. For example, the wavefunction $\psi(x)$ could be compared to the Fourier transformed spinors $\sum_\mathbf{p} u_r(\mathbf{p})\ \mathrm{e}^{-ip\cdot x}$ of the field $\psi(x)$. A squared wavefunction yields the probability distribution, while observables for fields are less trivial to find.

2.3 The symmetries of QED

2.3.1 Noether's theorem

Noether's theorem, originally formulated by Emily Noether in 1918 [7], states that when $\mathcal{L}$ is invariant under global transformations[†], we get a conserved quantity. If we adopt the notation $\phi(x) = \psi(x)$ and $\phi^\dagger(x) = \bar{\psi}(x)\gamma^0$, we can write any transformation as

$$\phi_r(x) \to \phi_r'(x) = \phi_r(x) + \delta\phi_r(x). \tag{2.21}$$

The index r points to the different independent fields, and is summed over. In QED, $\phi_r = \psi, \psi^\dagger$. Demanding the invariance of $\mathcal{L} = \mathcal{L}(\phi_r(x), \partial_\mu\phi_r(x))$, we can set $\delta\mathcal{L} = 0$:

$$\delta\mathcal{L} = \frac{\partial\mathcal{L}}{\partial\phi_r(x)}\delta\phi_r(x) + \frac{\partial\mathcal{L}}{\partial(\partial_\mu\phi_r(x))}\partial_\mu\delta\phi_r(x) = 0. \tag{2.22}$$

We look for a constant f^μ, such that $\partial_\mu f^\mu = 0$. With the Euler-Lagrange equation

$$\frac{\partial\mathcal{L}}{\partial\phi_r(x)} - \partial_\alpha\left(\frac{\partial\mathcal{L}}{\partial(\partial_\alpha\phi_r(x))}\right) = 0, \tag{2.23}$$

Eq. (2.22) becomes

$$\begin{aligned}
\delta\mathcal{L} &= \partial_\mu\left(\frac{\partial\mathcal{L}}{\partial(\partial_\mu\phi_r(x))}\right)\delta\phi_r(x) + \frac{\partial\mathcal{L}}{\partial(\partial_\mu\phi_r(x))}\partial_\mu\delta\phi_r(x) \\
&= \partial_\mu\left(\frac{\partial\mathcal{L}}{\partial(\partial_\mu\phi_r(x))}\delta\phi_r(x)\right) \\
&\equiv \partial_\mu f^\mu \\
&= 0.
\end{aligned} \tag{2.24}$$

The last line follows from the requirement $\delta\mathcal{L} = 0$. To find the conserved quantity, F^0, we integrate the zeroth component of f^μ over the volume:

$$F^0 = \int \mathrm{d}^3\mathbf{x}\; f^0 = \int \mathrm{d}^3\mathbf{x}\; \frac{\partial\mathcal{L}}{\partial(\partial_0\phi_r(x))}\delta\phi_r(x). \tag{2.25}$$

In the case of the global phase transformations

$$\begin{aligned}
\phi_r(x) &\to \phi_r'(x) = e^{i\varepsilon}\phi_r(x) \simeq (1 + i\varepsilon)\phi_r(x) \\
\phi_r^\dagger(x) &\to \phi_r^{\dagger\prime}(x) = e^{-i\varepsilon}\phi_r^\dagger(x) \simeq (1 - i\varepsilon)\phi_r^\dagger(x),
\end{aligned} \tag{2.26}$$

[†]A global transformation is the same everywhere, like $\mathrm{e}^{i\delta}$, while a local one will depend on x, like $\mathrm{e}^{i\alpha(x)}$.

we set $\delta\phi_r(x) = i\varepsilon\phi_r(x)$ and $\delta\phi_r^\dagger(x) = -i\varepsilon\phi_r^\dagger(x)$. In QED, we find f^μ by inspecting $\mathcal{L}$ from Eq. (2.17):

$$\begin{aligned} f^\mu &= \frac{\partial\mathcal{L}}{\partial(\partial_\mu\psi(x))}\delta\psi(x) + \frac{\partial\mathcal{L}}{\partial(\partial_\mu\psi^\dagger(x))}\delta\psi^\dagger(x) \\ &= \left(i\psi^\dagger(x)\gamma^0\gamma^\mu\right) i\varepsilon\psi(x) \\ &= -\varepsilon\psi^\dagger(x)\gamma^0\gamma^\mu\psi(x). \end{aligned} \tag{2.27}$$

Note that $\mathcal{L}$ does not contain any term $\partial_\mu\psi^\dagger(x)$. Since we now have $\partial_\mu f^\mu = 0$, we can also set $(-eQ/\varepsilon)\partial_\mu f^\mu = 0$. We find the conserved quantity with Eq. (2.25):

$$Q = F^0 = eQ\int \mathrm{d}^3\mathbf{x}\ \psi^\dagger(x)\gamma^0\gamma^0\psi(x) = eQ\int \mathrm{d}^3\mathbf{x}\ \psi^\dagger(x)\psi(x). \tag{2.28}$$

From Eq. (2.7), $\gamma^0\gamma^0 = g^{00} = 1$. It is possible to show that Eq. (2.28) can be written as

$$Q = -e\sum_{r,\mathbf{p}}\left[c_r^\dagger(\mathbf{p})c_r(\mathbf{p}) - d_r^\dagger(\mathbf{p})d_r(\mathbf{p})\right] \equiv -e\sum_{r,\mathbf{p}}\left[N_r(\mathbf{p}) - \bar{N}_r(\mathbf{p})\right], \tag{2.29}$$

where N_r ($\bar{N}_r$) is the number of electrons (positrons) with momentum $\mathbf{p}$ and spin r.

Similarly, one can use the invariance of $\mathcal{L}$ through translations and rotations to find the conservation of, respectively, momentum and angular momentum. This arises as a property of the spinor solutions of the Dirac (for fermions) and Klein-Gordon equation (for bosons), and will thus hold for every gauge theory which is based upon them. The field $\psi(x)$ is covariant (see Section 2.1.1), so we can write

$$\bar{\psi}'(x')\psi'(x') = (\bar{\psi}(x)S^{-1}(a))(S(a)\psi(x)) = \bar{\psi}(x)\psi(x). \tag{2.30}$$

$S(a)$ is unitary, and we can use $S^{-1}(a)S(a) = 1$. Since the Lagrangian of Eq. (2.17) only contains bilinear spinor terms $\propto \bar{\psi}(x)\psi(x)$, it is invariant under Lorentz transformations.

2.3.2 Gauge invariance

The gauge invariance of QED is the invariance of $\mathcal{L}$ under the local phase transformations

$$\begin{aligned} \psi(x) &\to \psi'(x) = \psi(x)\ \mathrm{e}^{-ieQ\alpha(x)} \\ \bar{\psi}(x) &\to \bar{\psi}'(x) = \bar{\psi}(x)\ \mathrm{e}^{ieQ\alpha(x)} \\ A_\mu(x) &\to A'_\mu(x) = A_\mu(x) + \partial_\mu\alpha(x), \end{aligned} \tag{2.31}$$

where $\alpha(x)$ is an arbitrary function. Inserting Eq. (2.31) into the QED Lagrangian, Eq. (2.17), we find

$$\begin{aligned} \bar{\psi}'\left(i\gamma^\mu D'_\mu - m\right)\psi' &= \bar{\psi}\ \mathrm{e}^{ieQ\alpha(x)}\left(i\gamma^\mu\left[\partial_\mu + ieQA'_\mu\right] - m\right)\ \mathrm{e}^{-ieQ\alpha(x)}\psi \\ &= \bar{\psi}\left(i\gamma^\mu\ \mathrm{e}^{ieQ\alpha(x)}\left[\partial_\mu + ieQA_\mu + ieQ\left(\partial_\mu\alpha(x)\right)\right]\ \mathrm{e}^{-ieQ\alpha(x)} - m\right)\psi \end{aligned} \tag{2.32}$$

We use

$$\partial_\mu \, \mathrm{e}^{-ieQ\alpha(x)} = \, \mathrm{e}^{-ieQ\alpha(x)} \left(\partial_\mu - ieQ \left(\partial_\mu \alpha(x)\right)\right), \tag{2.33}$$

inserting it into Eq. (2.32) (the rest of the factors will be unaffected by the transformation):

$$\begin{aligned} \bar{\psi}' \left(i\gamma^\mu D'_\mu - m\right) \psi' &= \bar{\psi} \left(i\gamma^\mu \left[\partial_\mu - ieQ \left(\partial_\mu \alpha(x)\right) + ieQA_\mu + ieQ \left(\partial_\mu \alpha(x)\right)\right] - m\right) \psi \\ &= \bar{\psi} \left(i\gamma^\mu \left[\partial_\mu + ieQA_\mu\right] - m\right) \psi \\ &= \bar{\psi} \left(i\gamma^\mu D_\mu - m\right) \psi. \end{aligned} \tag{2.34}$$

For the field tensor $F_{\mu\nu}$,

$$\begin{aligned} F'_{\mu\nu} &= \partial_\nu A'_\mu - \partial_\mu A'_\nu \\ &= \partial_\nu A_\mu + \partial_\nu(\partial_\mu \alpha(x)) - \partial_\mu A_\nu - \partial_\mu(\partial_\nu \alpha(x)) \\ &= F_{\mu\nu} + \partial_\mu(\partial_\nu \alpha(x)) - \partial_\mu(\partial_\nu \alpha(x)) \\ &= F_{\mu\nu}. \end{aligned} \tag{2.35}$$

Thus $\mathcal{L}$ is invariant under the transformations of Eqs. (2.31). Gauge transformations are local phase transformations which generate the interactions between the gauge and fermion fields. Without the term $ieQA_\mu$ in the covariant derivative D_μ, $\mathcal{L}$ would not be invariant under such transformations.

2.4 SU(2) Yang-Mills theory

The step from QED to weak theory is an important one. We introduce a new triplet $\mathbf{W}_\mu$, with generators $\mathbf{T}$ which correspond to the Pauli matrices. They do not commute, creating a non-Abelian theory with many interesting properties. Following V. Barger and R. Philips in their Collider Physics [8], we find

$$\mathcal{L} = \bar{\psi}(x) \left[i\gamma^\mu D_\mu - m\right] \psi(x) - \frac{1}{4} \mathbf{W}_{\mu\nu} \cdot \mathbf{W}^{\mu\nu}. \tag{2.36}$$

In QED, the field tensor $F_{\mu\nu}$ is linear in the fields A_μ. In non-Abelian theories like SU(2), an additional bilinear term is needed, where the two fields $\mathbf{W}_\mu$ and $\mathbf{W}_\nu$ are multiplied according to the properties of the theory. Here,

$$\mathbf{W}_{\mu\nu} = \partial_\nu \mathbf{W}_\mu - \partial_\mu \mathbf{W}_\mu - g\mathbf{W}_\mu \times \mathbf{W}_\nu. \tag{2.37}$$

The interactions between the fields are described by

$$D_\mu = \partial_\mu + ig\mathbf{W}_\mu \cdot \mathbf{T}. \tag{2.38}$$

Since the theory is non-Abelian, the generators $\mathbf{T}$ follow certain commutation rules. For SU(2) Yang-Mills theory, this is

$$[T_i, T_j] = i\epsilon_{ijk}T_k. \tag{2.39}$$

The generators are traceless, and satisfy the identity $\mathrm{Tr}(T_iT_j) = \frac{1}{2}\delta_{ij}$. The *structure constant* ϵ_{ijk} is the Levi-Civita symbol. Using this, one may rewrite the field tensor as

$$W_{i\mu\nu} = \partial_\nu W_{i\mu} - \partial_\mu W_{i\nu} - g\epsilon_{ijk}W_{j\mu}W_{k\nu}. \tag{2.40}$$

The Yang-Mills theory is invariant under the SU(2) transformations

$$\begin{aligned} \psi(x) &\to \psi'(x) = \ \mathrm{e}^{-ig\boldsymbol{\alpha}(x)\cdot\mathbf{T}}\psi(x) \\ \bar{\psi}(x) &\to \bar{\psi}'(x) = \bar{\psi}(x)\ \mathrm{e}^{ig\boldsymbol{\alpha}(x)\cdot\mathbf{T}} \\ \mathbf{W}_\mu(x) &\to \mathbf{W}'_\mu(x) = \mathbf{W}_\mu + \partial_\mu\boldsymbol{\alpha}(x) + g\boldsymbol{\alpha}(x)\times\mathbf{W}_\mu(x). \end{aligned} \tag{2.41}$$

In order for the theory to be gauge invariant, gauge boson mass terms like $M^2\mathbf{W}^\mu\cdot\mathbf{W}_\mu$ are excluded. In other terms, this is a theory for the interactions between three massless gauge bosons and the fermion field. In order for it to be a physical theory for the SU(2)-interactions, it needs to describe the three massive vector bosons $W^\pm$ and Z^0, interacting only with left-handed fermion fields.

2.5 Unbroken SU(2) × U(1) theory

The unification of QED and Yang-Mills into the electroweak theory is the construction of a gauge theory which describes interactions between fermions, photons and the three massive gauge bosons. The theory should be gauge invariant under both SU(2) and U(1) transformations. Introducing the field B_μ (as a mix between Z^0 and A_μ, as we will see in Eq. (2.49)), we define the Lagrangian:

$$\mathcal{L} = \bar{\psi}(x)\left[i\gamma^\mu D_\mu\right]\psi(x) - \frac{1}{4}\mathbf{W}_{\mu\nu}\cdot\mathbf{W}^{\mu\nu} - \frac{1}{4}B_{\mu\nu}B^{\mu\nu}. \tag{2.42}$$

The $\mathrm{U}(1)_Y$ field B_μ is defined as an Abelian field:

$$B_{\mu\nu} = \partial_\nu B_\mu - \partial_\mu B_\nu. \tag{2.43}$$

We need to redefine $\psi(x)$, since $\mathrm{SU}(2)_\mathrm{L}$ interactions only affect left-handed fermion fields

$$\psi_\mathrm{L}(x) = \frac{1}{2}(1+\gamma_5)\psi(x), \qquad \psi_\mathrm{R}(x) = \frac{1}{2}(1-\gamma_5)\psi(x). \tag{2.44}$$

	$\mathbf{T}$	T_3	$\frac{1}{2}Y$	Q
$\nu_{e\mathrm{L}}$	1/2	1/2	-1/2	0
e_{L}	1/2	-1/2	-1/2	-1
u_{L}	1/2	1/2	1/6	2/3
d_{L}	1/2	-1/2	1/6	-1/3
e_{R}	0	0	-1	-1
u_{R}	0	0	2/3	2/3
d_{R}	0	0	-1/3	-1/3

Table 2.1: The quantum numbers isospin, hypercharge and charge for the different fields.

With this definition, a mass term $m\bar{\psi}\psi$ would be split into terms like $m\bar{\psi}_{\mathrm{R}}\psi_{\mathrm{L}}$, which violates the gauge invariance. Therefore, fermions are considered massless until further notice. The covariant derivative must reflect this "heliciticism". A way of describing that is

$$D_\mu = \partial_\mu + ig\mathbf{W}_\mu \cdot \mathbf{T} + ig'\frac{1}{2}YB_\mu, \tag{2.45}$$

using different $\mathrm{SU}(2)_{\mathrm{L}}$ quantum numbers for ψ_{R} and ψ_{L}. The Gell-Mann-Nishijima formula,

$$Q = T_3 + \frac{1}{2}Y, \tag{2.46}$$

specifies the relationship between the third component of the weak isospin T_3, the hypercharge Y and the electric charge Q. The different quantum numbers for the fields $\nu_{e\mathrm{L}}, e_{\mathrm{L}}, u_{\mathrm{L}}, d_{\mathrm{L}}$ and $e_{\mathrm{R}}, u_{\mathrm{R}}, d_{\mathrm{R}}$ are listed in Table 2.1, and their transformations under $\mathrm{SU}(2)_{\mathrm{L}}$ and $\mathrm{U}(1)_Y$ in Table 2.2. In order to unify this theory with the electromagnetic theory, we first define the

$\mathrm{SU}(2)_{\mathrm{L}}$			$\mathrm{U}(1)_Y$		
$\psi_{\mathrm{L}}(x)$	$\rightarrow$	$[1 - ig\mathbf{T}\cdot\boldsymbol{\alpha}(x)]\psi_{\mathrm{L}}(x)$	$\psi_{\mathrm{L}}(x)$	$\rightarrow$	$[1 - ig'\frac{1}{2}Y\beta(x)]\psi_{\mathrm{L}}(x)$
$\psi_{\mathrm{R}}(x)$	$\rightarrow$	$\psi_{\mathrm{R}}(x)$	$\psi_{\mathrm{R}}(x)$	$\rightarrow$	$[1 - ig'\frac{1}{2}Y\beta(x)]\psi_{\mathrm{R}}(x)$
$\mathbf{W}_\mu$	$\rightarrow$	$\mathbf{W}_\mu + \partial\boldsymbol{\alpha}(x) + g\boldsymbol{\alpha}(x)\times\mathbf{W}_\mu$	$\mathbf{W}_\mu$	$\rightarrow$	$\mathbf{W}_\mu$
B_μ	$\rightarrow$	B_μ	B_μ	$\rightarrow$	$B_\mu + \partial_\mu\beta(x)$

Table 2.2: SU(2)$_L$ and U(1)$_Y$ gauge transformations.

generators as raising and lowering operators. We do the same for the field $\mathbf{W}_\mu$,

$$\begin{aligned} T^\pm &= \frac{1}{\sqrt{2}}(T_1 \pm iT_2), \\ W_\mu^\pm &= \frac{1}{\sqrt{2}}(W_{1\mu} \mp iW_{2\mu}). \end{aligned} \tag{2.47}$$

Their dot product becomes

$$\mathbf{W}_\mu \cdot \mathbf{T} = W_\mu^+ T^+ + W_\mu^- T^- + W_{3\mu} T_3, \tag{2.48}$$

and we have separated $\mathbf{W}_\mu$ into two of its (still massless) physical fields plus $W_{3\mu}$. With help from the Gell-Mann-Nishijima formula, Eq. (2.46), the electromagnetic term $ieQA_\mu$ must be contained in the neutral term of D_μ, i.e. $i(gW_{3\mu}T_3 + g'\frac{1}{2}YB_\mu)$. This is done by rotating a vector with $W_{3\mu}$ and B_μ by an angle θ_W, defining two new fields A_μ and Z_μ:

$$\begin{pmatrix} W_{3\mu} \\ B_\mu \end{pmatrix} = \begin{pmatrix} \cos\theta_W & \sin\theta_W \\ -\sin\theta_W & \cos\theta_W \end{pmatrix} \begin{pmatrix} Z_\mu \\ A_\mu \end{pmatrix}. \tag{2.49}$$

With these physical fields and some redefinitions in the couplings, we can write down the Lagrangian, Eq. (2.42), in terms of the currents:

$$\begin{aligned} -\mathcal{L} = e\mathcal{J}^\mu_{e.m.} A_\mu + \frac{g}{\sqrt{2}} \left(\mathcal{J}_{\mathrm{L}}^{+\mu} W_\mu^+ + \mathcal{J}_{\mathrm{L}}^{-\mu} W_\mu^- \right) \\ + g_Z \mathcal{J}^\mu_{\mathrm{Z}} Z_\mu + \frac{1}{4} \mathbf{W}_{\mu\nu} \cdot \mathbf{W}^{\mu\nu} + \frac{1}{4} B_{\mu\nu} B^{\mu\nu}, \end{aligned} \tag{2.50}$$

where

$$\begin{aligned} \mathcal{J}_{\mathrm{L}}^{\pm\mu} &= \sqrt{2}\bar{\psi}(x)\gamma^\mu T_{\mathrm{L}}^\pm \psi(x), \\ \mathcal{J}_Z^\mu &= \bar{\psi}(x)\gamma^\mu \left[T_3 - Q\sin^2\theta_W \right] \psi(x), \\ \mathcal{J}^\mu_{e.m.} &= \bar{\psi}(x)\gamma^\mu Q \psi(x), \end{aligned} \tag{2.51}$$

and

$$g_Z = \frac{e}{\sin\theta_W \cos\theta_W}, \qquad g = \frac{e}{\sin\theta_W}. \tag{2.52}$$

And in accordance with Table 2.1, $\mathbf{T}_{\mathrm{L}} = \frac{1}{2}\boldsymbol{\tau}$ on ψ_{L}, while $\mathbf{T}_{\mathrm{L}} = \mathbf{0}$ on ψ_{R}.

2.6 The Higgs mechanism

Any term like $M^2 A_\mu A^\mu$ in a gauge theory violates the gauge invariance. Since the physical gauge bosons $W^\pm$ and Z^0 are not massless, a method for implementing mass terms must be found. The Higgs mechanism (see the Gunion *et al.* Higgs Hunter's Guide [9] for a good introduction) starts with an invariant Lagrangian and massless gauge bosons, and through transformations on $\mathcal{L}$ we get massive gauge bosons, breaking the gauge symmetry. Such a theory for the Abelian case would be

$$\mathcal{L} = (D_\mu\phi)^*(D^\mu\phi) - \mu^2\phi^*\phi - \lambda(\phi^*\phi)^2 - \frac{1}{4}F_{\mu\nu}F^{\mu\nu}, \tag{2.53}$$

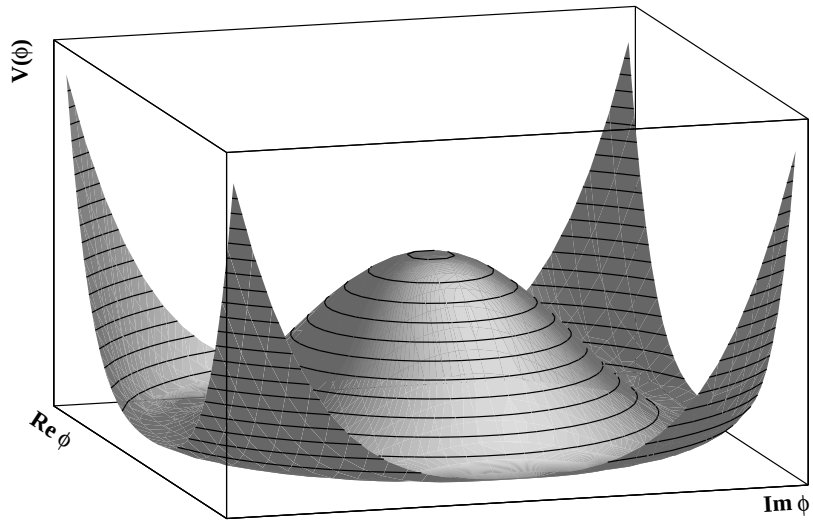

Figure 2.1: The Higgs potential $V(\phi)$. At the minimum of $V(\phi)$, we have a non-zero minimal value of ϕ.

where ϕ is the field for a complex scalar boson. $F_{\mu\nu} = \partial_\nu A_\mu - \partial_\mu A_\nu$ for a massless gauge boson A_μ, and we require

$$D_\mu = \partial_\mu + igA_\mu, \tag{2.54}$$

if $\mathcal{L}$ is to be invariant under the transformations

$$\begin{aligned} \phi \to \phi' = \ & \mathrm{e}^{ig\chi(x)}\phi, \\ A_\mu \to A'_\mu = A_\mu & - \partial_\mu \chi(x). \end{aligned} \tag{2.55}$$

The potential

$$V(\phi) = \mu^2 \phi^* \phi + \lambda(\phi^* \phi)^2 \tag{2.56}$$

is shown in Fig. 2.1, for a set of values $\mu^2 < 0$ and $\lambda > 0$. Solving $V'(\phi) = 0$, we find the minimum value at $\phi = \sqrt{-\mu^2/2\lambda} \equiv v/\sqrt{2}$. We expand $\phi(x)$ near this point, and use a U(1) gauge transformation to remove the complex phase. We arrive at the *unitary gauge*, where ϕ is split into a real field $h(x)$ plus a constant term v to describe the *vacuum expectation value*,

$$\phi(x) = [v + h(x)]/\sqrt{2}, \tag{2.57}$$

Writing Eq. (2.53) in terms of the unitary gauge:

$$\begin{aligned} \mathcal{L}' = \frac{1}{2}[(\partial_\mu - igA_\mu)(v + h)(\partial^\mu + igA^\mu)(v + h)] \\ + \frac{1}{2}\mu^2(v + h)^2 - \frac{1}{4}\lambda(v + h)^4 - \frac{1}{4}F_{\mu\nu}F^{\mu\nu}, \end{aligned} \tag{2.58}$$

we find the terms

$$\mathcal{L} \supseteq \frac{g^2 v^2}{2} A_\mu A^\mu - \mu^2 h^2. \tag{2.59}$$

They are the mass terms for A_μ and h, respectively. The act of choosing a direction with the gauge transformation of Eq. (2.57) will ruin the gauge invariance of $\mathcal{L}$. This is caused by the non-zero minimum value of the field $\phi(x)$.

The complex scalar $\phi(x)$ has two degrees of freedom (DoF), while the real $h(x)$ has only one. The last DoF is transferred to the gauge boson, where it will become the longitudinal polarization – the mass. This act of transferring the DoF to give mass to the gauge bosons is called the *Higgs mechanism*, named after P. Higgs [10]. Other people also contributed when this mechanism was developed in the early sixties, like Englert and Brout in [11], and Guralnik, Hagen and Kibble in [12].

The parameter v can be found from the mass of the gauge bosons, and is given by the Particle Data Group (PDG) in their *Review of Particle Physics* [2] as

$$v \simeq 246 \text{ GeV}. \tag{2.60}$$

Furthermore, μ (or λ) is a free parameter, and cannot be decided *a priori*. Thus the mass of the Higgs boson is completely free, with very few theoretical bounds. Gunion *et al.* [9] discuss mass ranges from 1 MeV to about 1 TeV, while new experimental results hint at $m_h \sim 125$ GeV [13, 14]. In the next session, we will discuss the Higgs boson in the context of SU(2) × U(1) – the points we've mentioned apply there as well, if we set $m_H = \sqrt{-2\mu^2}$.

2.7 The Weinberg-Salam broken SU(2) × U(1) model

The generalization of the Higgs mechanism from U(1) to SU(2)×U(1) is trivial, and can be found in a number of texts – the method from Barger and Philips [8] is used here. Instead of a complex scalar ϕ, we use an isodoublet of two complex scalars

$$\Phi = \begin{pmatrix} \phi^+ \\ \phi^0 \end{pmatrix} = \begin{pmatrix} \eta_1 + i\eta_2 \\ \eta_3 + i\eta_4 \end{pmatrix}, \tag{2.61}$$

with the quantum numbers as listed in Table 2.3. The Lagrangian is

$$\mathcal{L}_\Phi = |D_\mu \Phi|^2 - V\left(|\Phi|^2\right) = |D_\mu \Phi|^2 - \mu^2 |\Phi|^2 - \lambda |\Phi|^4, \tag{2.62}$$

and the neutral part of Φ, i.e. ϕ^0, can be expanded from its minimal value $|\Phi|^2 = -\mu^2/2\lambda$. An SU(2) gauge transformation with $\boldsymbol{\alpha}(x) = \boldsymbol{\xi}(x)/2v$ will then transfer the 3 DoF from $\boldsymbol{\xi}$ to

	$\mathbf{T}$	T_3	$\frac{1}{2}Y$	Q
ϕ^+	1/2	1/2	1/2	1
ϕ^0	1/2	-1/2	1/2	0

Table 2.3: The quantum numbers for Φ.

the three gauge fields W_μ^+, W_μ^- and Z_μ^0, giving them mass:

$$\Phi(x) = \exp\left(\frac{i\boldsymbol{\xi}(x)\cdot\boldsymbol{\tau}}{2v}\right)\begin{pmatrix}0\\(v+H(x))/\sqrt{2}\end{pmatrix} \xrightarrow{\text{SU(2)}} \frac{1}{\sqrt{2}}\begin{pmatrix}0\\v+H(x)\end{pmatrix} \tag{2.63}$$

Inserting this into the Lagrangian, with D_μ defined in terms of the physical fields,

$$D_\mu = \partial_\mu + ieQA_\mu + ig(T^+W_\mu^+ + T^-W_\mu^-) + ig_Z\left(T_3 - Q\sin^2\theta_W\right)Z_\mu, \tag{2.64}$$

yields the same result as we found in the U(1) case: Mass terms for the gauge bosons and interaction terms between the Higgs boson and the different particles. That is,

$$\begin{aligned}\mathcal{L}'_\Phi = \frac{1}{2}(\partial_\mu H)^2 + \frac{1}{4}g^2W_\mu^+W^{-\mu}(v+H)^2 \\ + \frac{1}{8}g_Z^2Z_\mu Z^\mu(v+H)^2 - \mu^2\left[\frac{1}{2}(v+H)^2\right]^2 - \lambda\left[\frac{1}{2}(v+H)^2\right]^4\end{aligned} \tag{2.65}$$

With $M_W = \frac{1}{2}gv$ and $M_Z = M_W/\cos\theta_W$, we find the mass terms

$$\mathcal{L}'_\Phi \supseteq M_W^2W_\mu^+W^{-\mu} + \frac{1}{2}M_Z^2Z_\mu Z^\mu. \tag{2.66}$$

We also find the terms (from the kinetic and potential part)

$$\mathcal{L}'_\Phi \supseteq \frac{1}{2}(\partial_\mu H)^2 - \frac{1}{2}m_H^2H^2 + \frac{1}{4}\mu^2v^2\left[-1 + \frac{4H^3}{v^3} + \frac{H^4}{v^4}\right]. \tag{2.67}$$

Here are the cubic and quartic self interactions of H, together with a mass term $\frac{1}{2}m_H^2H^2$, where

$$m_H = \sqrt{-2\mu^2}. \tag{2.68}$$

The interactions of H are given by Eq. (2.65):

$$\mathcal{L}'_\Phi \supseteq \left(\frac{1}{4}g^2W_\mu^+W^{-\mu} + \frac{1}{8}g_Z^2Z_\mu Z^\mu\right)\left(H^2 + 2vH\right). \tag{2.69}$$

Note that no electromagnetic interactions are involved. This is due to H having $Q = 0$.

2.8 Yukawa interactions

In the last section, the mechanism for generating the masses of the gauge bosons was discussed. They arise by adding a field to the Lagrangian, resulting in mass terms for the $W^{\pm}$ and Z^0. In addition we get a new particle, the Higgs boson.

However, fermion masses were not introduced. This can be done in a seemingly *ad hoc* way, by adding a gauge invariant term which generates interactions between the Higgs fields and fermions under spontaneous symmetry breaking. With an electron isodoublet

$$\ell_{\mathrm{L}} = \begin{pmatrix} \nu_e \\ e \end{pmatrix}_{\mathrm{L}}, \tag{2.70}$$

we can write

$$\mathcal{L} = -G_e \left[\bar{e}_{\mathrm{R}} \left(\Phi^{\dagger} \ell_{\mathrm{L}} \right) + \left(\bar{\ell}_{\mathrm{L}} \Phi \right) e_{\mathrm{R}} \right]. \tag{2.71}$$

The coupling G_e is arbitrary, but inspection of the resulting terms shows that it needs to be proportional to the electron mass: $G_e = \sqrt{2} m_e / v$. In the unitary gauge, Eq. (2.71) becomes

$$\mathcal{L} = -m_e \bar{e} e - \frac{m_e}{v} H \bar{e} e, \tag{2.72}$$

with an electron mass term and an interaction term between H and the electron. For the other lepton generations,

$$\mathcal{L} = -m_e \bar{e} e - m_\mu \bar{\mu} \mu - m_\tau \bar{\tau} \tau - v \left(m_e H \bar{e} e + m_\mu H \bar{\mu} \mu + m_\tau H \bar{\tau} \tau \right). \tag{2.73}$$

Quark masses are generated in the same way, but since their weak and mass eigenstates are not the same, many new couplings and mass matrices are introduced.

2.9 SU(3) QCD

Quantum Chromodynamics (QCD) can be generalized from the Weinberg-Salam theory, but contains many novel features. It describes the interactions between the color-charged quarks and new massless gauge bosons: The gluons. In the sixties, H. Greenberg [15] showed that in order for the Pauli exclusion principle to allow certain quarks to exist, a new 3-fold charge was needed. Later, the experimentalists found that hadron creation processes needed an additional factor 3 to match the data, see Section 10.9 of Henley and García [16]. This charge was dubbed *color*. Quarks can be defined as a color vector

$$\psi = \begin{pmatrix} \psi_{\mathrm{red}} \\ \psi_{\mathrm{green}} \\ \psi_{\mathrm{blue}} \end{pmatrix} = \begin{pmatrix} \psi_r \\ \psi_g \\ \psi_b \end{pmatrix}. \tag{2.74}$$

A word of caution: The mapping of the SU(3) charges to the color spectrum is just a convenient definition. A color neutral (*white*) state is created by combining color + anticolor, or three different colors or anticolors.

The gauge theory to describe the interactions between quarks and gluons is the non-Abelian SU(3) theory. The Lagrangian has the usual form, but with $\psi(x)$ as color triplets:

$$\mathcal{L} = \sum_{\text{flav.}} \bar{\psi}_{\text{flav.}}(x) \left[i\gamma^\mu D_\mu - m_{\text{flav.}} \right] \psi_{\text{flav.}}(x) - \frac{1}{4} \sum_{a=1}^{8} F^a_{\mu\nu}(x) F^{a\mu\nu}(x). \tag{2.75}$$

The first sum is over the 6 different quark flavors defined in the introduction: Up, down, charm, strange, top and bottom. The second sum, over a, is connected to the eight generators T^a. They are analogous to the three generators $\mathbf{T}$ in the SU(2) theory.

The generators T^a and the corresponding structure constants f^{abc} depend on the representation of the theory, but can easily be defined. The covariant derivative is

$$D_\mu = \partial_\mu + i g_s \sum_{a=1}^{8} T^a A^a_\mu(x), \tag{2.76}$$

where A^a_μ is the massless gluon field and g_s the SU(3) coupling constant. The field tensor $F^a_{\mu\nu}$ follows from Eq. (2.40)

$$F^a_{\mu\nu} = \partial_\nu A^a_\mu - \partial_\mu A^a_\nu + g_s f^{abc} A^b_\mu A^c_\nu. \tag{2.77}$$

The SU(3) transformations under which the Lagrangian is invariant are

$$\begin{aligned} \psi(x) &\to \psi'(x) = \ \mathrm{e}^{i g_s T_a \omega_a(x)} \psi(x) \\ \bar{\psi}(x) &\to \bar{\psi}'(x) = \bar{\psi}(x)\ \mathrm{e}^{-i g_s T_a \omega_a(x)} \\ A^\mu_a(x) &\to A'^\mu_a(x) = A^\mu_a(x) - \partial^\mu \omega_a(x) - g_s f_{abc}\ \omega_b(x) A^\mu_c(x), \end{aligned} \tag{2.78}$$

where $\omega_a(x)$ is an arbitrary function.

The eight generators correspond to eight different gluons, or gluons with eight different color charge configurations. Since they themselves are charged, they have the ability to exchange colors. This is a feature absent in the photons of U(1), and gives rise to self interactions between the gluons. The different gluons will be linear superpositions of the color-anticolor states $r\bar{g}$, $b\bar{r}$, $b\bar{b}$ etc. An r quark, sending out a $g\bar{r}$ gluon, will itself become a g quark (converting another quark from g to r). In this way, colors are conserved. As for the electromagnetic quantum numbers, for the gluon we have $Q_g = 0$. For up-type quarks, $Q_u = 2/3$, and for down-type quarks $Q_d = -1/3$.

The massless photon has an infinite range, while the massive gauge bosons are limited by their mass to about 10^{-18} m. Yet the massless gluons have a very limited range due to

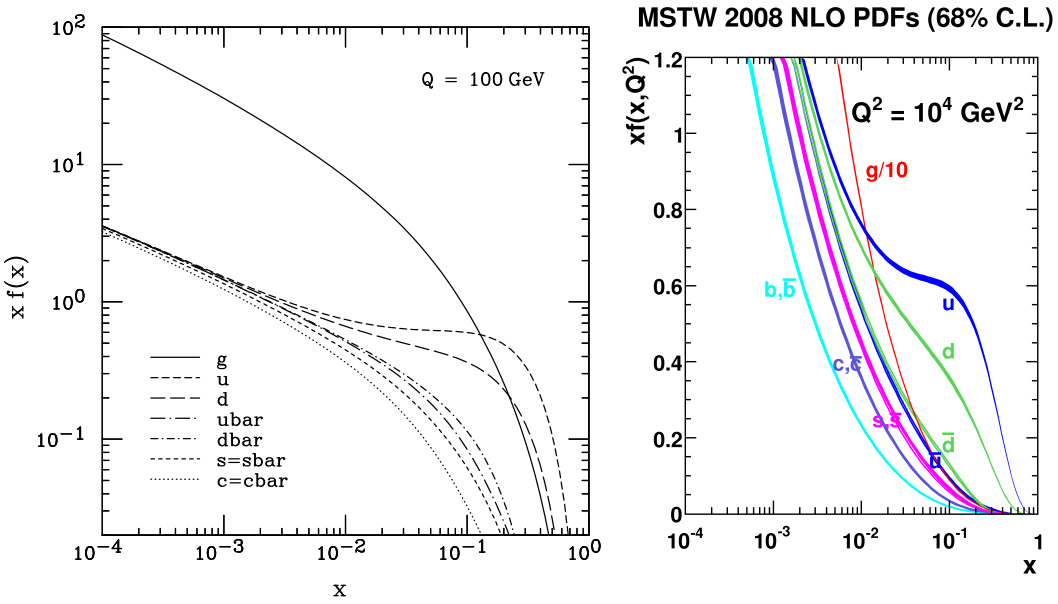

Figure 2.2: Different parton density functions, taken at $Q^2 = (100\text{ GeV})^2$. **Left***:* CTEQ6 [19], **Right***:* MSTW2008 [20].

color confinement (See K. G. Wilson [17]): No free colors can be observed, and only trios of rgb or $\bar{r}\bar{g}\bar{b}$ (baryons, like the proton and neutron) and pairs of $r\bar{r}, g\bar{g}$ or $b\bar{b}$ (mesons, like the pion and kaon) can be found as free states[†]. As two quarks separate, the separation energy of the gluon field will be converted into a quark-antiquark pair from the vacuum, creating a color-neutral meson. With high enough energy this process will be repeated, and a high energy $q\bar{q}$ pair from a collision will be seen as two *jets* of hadrons.

Since the gluons are massless, we do not need to introduce a Higgs triplet to create their mass terms. We do, however, need to add the Yukawa interactions for the quarks, as was done for the leptons in Section 2.8.

The Standard Model of particle physics will then be given by the product $\mathrm{SU(3)_C} \times \mathrm{SU(2)_L} \times \mathrm{U(1)_Y}$, which is separately gauge invariant under all three gauge transformations.

2.9.1 Parton Density Functions

In the time scales of collisions, protons can be treated in the *impulse approximation* where they consist of free quarks and gluons, historically called *partons*. This history can be found in Section 6.9 of Henley and García [16]. The different partons will each carry a certain fraction x of the momentum,

$$x = \frac{\text{parton momentum}}{\text{proton momentum}}. \tag{2.79}$$

This x is sometimes referred to as the Bjorken x scaling variable, from J. D. Bjorken [21]. The parton q will have the probability distribution $q(x, Q^2)$, and $q_i(x, Q^2)\,\mathrm{d}x$ is the probability of finding q_i within the interval $\mathrm{d}x$ at x, at momentum transfer Q^2. The inclusive cross section for a process must be multiplied with its luminosity. For the $gg \to H$ process, this is

$$\frac{\mathrm{d}\mathcal{L}^{gg}}{\mathrm{d}x} = \int_\tau^1 \frac{\mathrm{d}x}{x} g(x, Q^2) g(\tau/x, Q^2). \tag{2.80}$$

Here, $g(x, Q^2)$ is the gluon parton density function (PDF), and τ is the Higgs mass squared normalized to the CoM energy: $\tau = m_H^2/s$. These PDFs will depend on the momentum transfer Q and the parton flavor or type. Today, many different PDFs exist for different applications. CTEQ6 [19] and MSTW2008 [20] are two for general usage. Examples of these at $Q^2 = (100\ \text{GeV})^2$ are reproduced in Fig. 2.2. The MSTW2008 NLO PDF is used for calculating the Higgs production cross section in Section 3.6.1.

2.10 Feynman diagrams

There are a number of ways of displaying and computing processes from the different Lagrangians given in the above sections. One way is looking at the transition probability between two states, as a perturbation in orders of the interaction Hamiltonian. This method was streamlined by R. Feynman, with the development of Feynman diagrams and their corresponding rules. Fig. 2.3 displays such a diagram. It is read against the arrows, and every time a particle is created, emitted or propagated from one place to another, a factor is picked up. The factor of every such action is specified by the Feynman rules, and in this example shown in the figure. In this diagram, the *amplitude* $\mathcal{M}$ becomes

$$\mathcal{M} = \bar{v}_r(\mathbf{p}_2)(-ie\gamma^\alpha)u_r(\mathbf{p}_1)\frac{-ig_{\alpha\beta}}{k^2 + i\varepsilon}\bar{u}_r(\mathbf{p}_1')(-ie\gamma^\beta)v_r(\mathbf{p}_2'). \tag{2.81}$$

[†]Other exotic combinations are theorized, like glueballs (color neutral bound states of gluons) and tetraquarks (combinations $qq\bar{q}\bar{q}$). These are not yet found experimentally, as summarized by E. Klempt and A. Zaitsev [18].

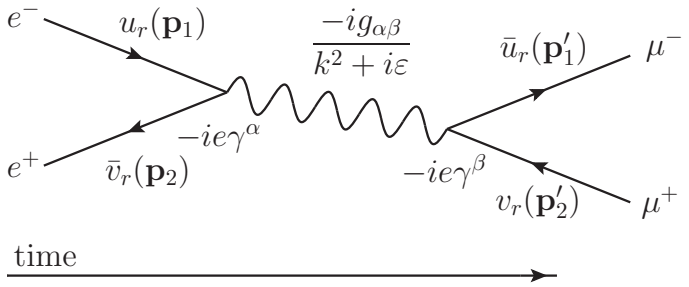

Figure 2.3: Example of a Feynman diagram: The annihilation process $e^+e^- \to \mu^+\mu^-$.

The squared amplitude $|\mathcal{M}|^2$ is then multiplied with different factors: The phase space, field normalizations and the particle fluxes. The conservation of four-momentum is also demanded at every vertex. For collision processes we arrive at:

$$\mathrm{d}\sigma = (2\pi)^4\delta^{(4)}\left(\sum_f p'_f - \sum_i p_i\right)\frac{1}{4E_1E_2v_{rel.}}\prod_l(2m_l)\prod\frac{\mathrm{d}^3\mathbf{p}'_f}{(2\pi)^3 2E'_f}|\mathcal{M}|^2, \tag{2.82}$$

where the index l is for the external leptons, $v_{rel.}$ is the relative velocity between the colliding particles and p'_f (p_i) is the final (initial) four-momentum. We can simplify: The differential cross section in the Centre of Mass (CoM) frame, for a collision between two particles p_1 and p_2, is

$$\left(\frac{\mathrm{d}\sigma}{\mathrm{d}\Omega'_1}\right) = \frac{1}{64\pi^2(E_1+E_2)^2}\frac{|\mathbf{p}'_1|}{|\mathbf{p}_1|}\left(\prod_l 2m_l\right)|\mathcal{M}|^2. \tag{2.83}$$

In order to obtain the end result, we combine Eqs. (2.81) and (2.83), use different identities for the combination of spinors and take a sum over the spins r. This should be true for every theory, however the procedure and complexity may vary. Rules like the ones specified in Fig. 2.3 can be derived from the Lagrangian of a theory. Vertex factors will correspond to the couplings between the different fields and propagators to the vacuum expectation values of time ordered combinations of two field operators.

To finalize the example of Eqs. (2.81) and (2.83), after a somewhat lengthy calculation and some approximations, the differential cross section of the process $e^+e^- \to \mu^+\mu^-$ becomes

$$\left(\frac{\mathrm{d}\sigma}{\mathrm{d}\Omega'_1}\right) = \frac{\alpha^2}{16E^2}\left(1+\cos^2\theta\right). \tag{2.84}$$

Fig. 2.4 shows one experimental measurement of this process by B. Adeva [22]. The theoretical value is calculated at loop level (see Section 2.11). This forward-backward asymmetry is induced by the exchange of a Z^0 boson, and cannot be calculated from QED alone.

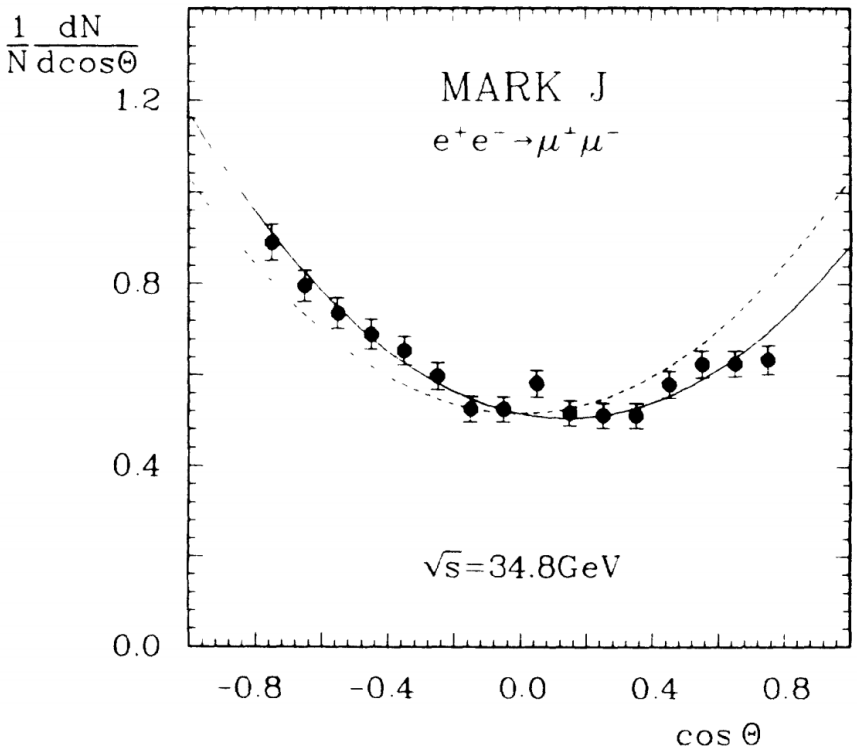

Figure 2.4: Measurement of the differential cross section of the process $e^+e^- \to \mu^+\mu^-$. The full line is the theoretical value. The dashed line, while not important to this discussion, is a fit to a polynomial in $\cos^n\theta$. *From* [22].

Often, there is more than one diagram with the same initial and final state. This may happen in calculations where a higher order of perturbation theory is used, or where different channels contribute. An example of the latter is $e^+e^- \to e^+e^-$, which may happen both as an annihilation and a scattering process. These diagrams must be summed over in order to find the amplitude:

$$\mathcal{M} = \sum_i \mathcal{M}_i. \tag{2.85}$$

2.11 Loop diagrams and renormalizability

The principle of uncertainty, discovered by W. Heisenberg [23] in 1927, defines the relationship

$$\Delta E \Delta t \geq h. \tag{2.86}$$

This means that, during the short interval Δt, ΔE may be "borrowed" from the vacuum without violating any physical laws.

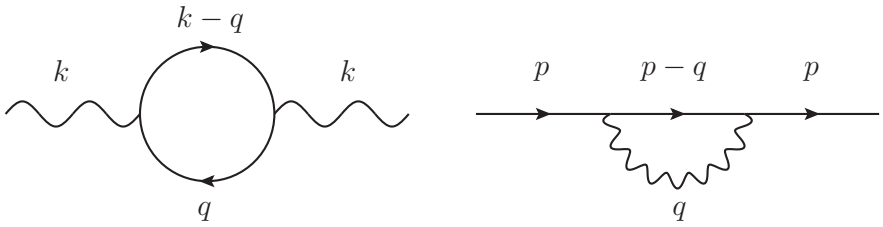

Figure 2.5: Loop processes. **Left:** *A propagating photon,* **Right***: A propagating electron.*

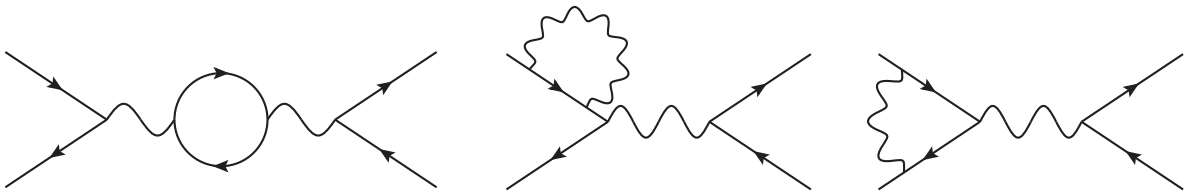

Figure 2.6: Some of the loops in the process $e^+e^- \to \mu^+\mu^-$.

Physically, particles can use this energy to emit and absorb new *virtual* particles, which appear as internal lines in Feynman diagrams. Such particles can never be observed, however their effects can be large. A propagating photon can undergo the process $\gamma \to e^{*+}e^{*-} \to \gamma$, while an electron $e^- \to \gamma^* e^- \to e^-$. The star signifies virtuality. This process creates a *loop* in the propagator, see Chapter 9 of F. Mandl and G. Shaw [24]. Fig. 2.5 shows this process for an electron and a photon.

These effects will take place everywhere, creating a number of new amplitudes to be calculated. For the $e^+e^- \to \mu^+\mu^-$ annihilation discussed earlier, additional diagrams are created: See Fig. 2.6 for a few examples of these. Since these diagrams have more vertices than the lowest order *tree* level diagrams, they arise as higher-order corrections. This is usually done in terms of the coupling constant, in QED this is e. The internal energy-momentum of a loop (q in Fig. 2.5) is not fixed by conservation at the vertices, and must be integrated over. This is sometimes a convergent integral, and in those cases we get a finite correction to a physical variable. The loop integrals are on the form

$$\int^{\Lambda} \mathrm{d}^4k \; f(k, \text{external momenta}), \tag{2.87}$$

where k is the internal momentum and the *cut-off* scale Λ is the maximum momentum transfer to where the theory is supposed to be valid. When the amplitudes diverge, we get infinite corrections.

In QED, loops of the lowest order diverge, which cause the mass and charge of the electron

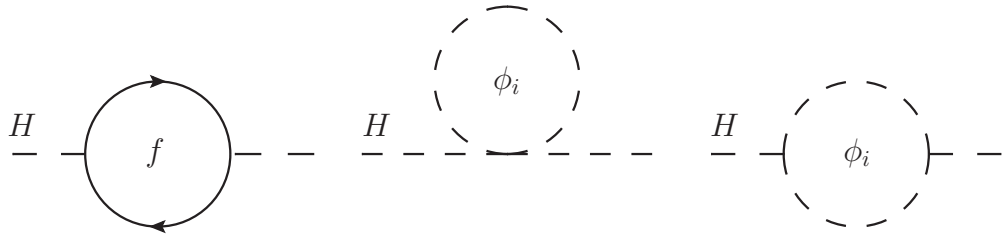

Figure 2.7: One-loop self energy graphs for the Higgs boson. **Left***: Fermion (top) contribution.* **Center and right***: Scalar Higgs contributions.*

to be infinite. Considerations show that e.g. the electron mass will diverge logarithmically as $\delta m \sim \alpha m \ln \Lambda$. At Planck scales $\Lambda \sim m_P$, this is only a correction $\delta m \sim m$, as showed in Chapter 1 of I. Aitchison [25]. However, we want the theory to be convergent even at the scale $\Lambda \to \infty$. The procedure is to redefine the mass and charge as *bare* properties m_0, e_0; which cannot be measured, and physical observables m, e. The relationship between these will depend on Λ, like for the mass

$$m = m_0 + \delta m. \tag{2.88}$$

The bare variables e_0 and m_0 are then divergent, while the physical ones stay finite. Although the bare variables go into the Lagrangian, every observable is expressed using the physical ones, so the theory itself is finite. Every observable can therefore be calculated to a given order. This is a *renormalizable* theory: The physical parameters remain finite even when the cut-off is removed.

A non-renormalizable theory will still be well-defined with a finite Λ, but the physical predictions diverge in the limit $\Lambda \to \infty$. One interpretation is that the cut-off parameter Λ is *not* infinite, but rather should be placed at the threshold where the theory is no longer valid. This often hints at an underlying theory to be found.

The Higgs mechanism is renormalizable. However, the self-energy of the Standard Model (SM) Higgs boson is quadratically divergent. This can be explained by the absence of a symmetry protecting the Higgs mass from large radiative corrections. The fermions have the *chiral symmetry*, the breaking of which only generates logarithmic corrections. In the same way, the photons are protected from mass terms by the local gauge symmetry.

Without such a symmetry, the Higgs mass gets corrections from the fermionic loops shown in Fig. 2.7. In I. Aitchison [25] these are written as

$$\lambda \int^{\Lambda} \mathrm{d}^4 k \, \frac{1}{k^2 - m_H^2}. \tag{2.89}$$

The divergence can be guessed at: By power counting, we have k^4 in the numerator and k^2 in the denominator. Thus a Λ^2, or quadratic, divergence should be the result. Careful analysis shows that the fermionic contribution for N_f fermions is just that, see A. Djouadi [26]. The correction is

$$\Delta m_H^2 = N_f \frac{2m_f^2}{8v^2\pi^2}\left[-\Lambda^2 + 6m_f^2 \ln\frac{\Lambda}{m_f} - 2m_f^2\right] + \mathcal{O}(1/\Lambda^2). \tag{2.90}$$

The leading order of Eq. (2.90) is $\sim \Lambda^2$.

In QED, we defined physical and bare parameters. Now, we do the same and define a parameter $\mu_{\text{phys.}}$,

$$\mu_{\text{phys.}}^2 = \mu^2 - \lambda\Lambda^2. \tag{2.91}$$

Remember that all the different masses m_i in the SM depend on μ somehow. In the Yukawa interactions of Section 2.8, we have $m_i \propto \mu$, and for the gauge bosons we have e.g. $M_W = g\mu/\sqrt{\lambda}$.

The theory is valid up to the momentum transfer scale Λ^2. From the definition

$$4\mu^2 = v^2\lambda, \tag{2.92}$$

and using I. Aitchison [25], we find that $\mu_{\text{phys.}} \simeq \sqrt{\lambda}123$ GeV. Since we generally want to be able to treat the Higgs couplings pertubatively[†], λ should be below unity. From these constraints,

$$\mu_{\text{phys.}} \sim 100 \text{ GeV}, \tag{2.93}$$

and to be able to obtain this value we need

$$\mu \sim \Lambda. \tag{2.94}$$

A natural choice for Λ is the Planck scale, $m_P \sim 10^{19}$ GeV. In that case, μ must be chosen with a precision of $10^2 : 10^{19}$. This is called the *fine tuning problem*, one of the problems a theory *Beyond the Standard Model* must endeavour to solve.

[†]This is not a physical constraint, but rather based on the wishful idea that nature is simple.

Chapter 3

The Standard Model Higgs Boson

A general treatment of the Higgs boson of the Standard Model was given in Section 2.6. In this part, we focus on the different decay modes of H. Recently, hints of a 125 GeV Higgs boson were given by the CMS [13] and ATLAS [14] collaborations at the LHC. One of the most sensitive channels in the detection of a Higgs boson in this mass range is the diphoton channel, where the Higgs decays via a triangle diagram into two photons. Since this is a process only happening at loop level, it is very sensitive to new physics. An unknown charged particle in the triangle could distort the decay width away from its SM value. In the following sections, tools for calculating the width and branching ratio of this decay channel are presented, as well as for the other interesting channels. Another phenomenologically important channel is the $H \to W^+W^-$.

The outline of this chapter is the following: In the two first sections, we find the decay width, including corrections, to the process $H \to \gamma\gamma$. We will also see in Section 3.3 how new physics can affect this process. Then, in Section 3.5 we find the widths of the other possible decay processes of H, and in the last section we look at some of the production mechanisms for the Higgs boson.

First, a definition. H is the standard model Higgs, while h will signify an unspecified charge-parity-even (CP-even) Higgs boson in the minimal supersymmetric extension of the SM (MSSM): h^0 or H^0.

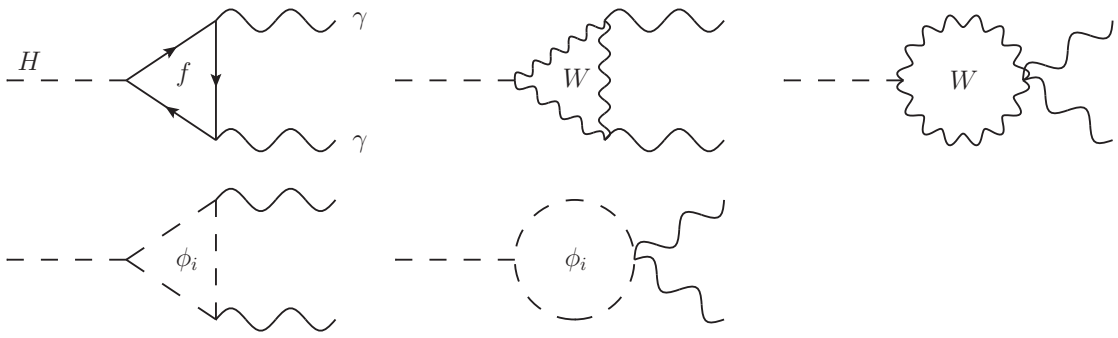

Figure 3.1: The different tree-level triangle diagrams for the process $H \to \gamma\gamma$. They can be characterized as spin 1/2 (f), spin 1 (W) and spin 0 (ϕ_i).

3.1 The width of $H \to \gamma\gamma$

The width is calculated using triangle loops, as shown in Fig. 3.1. From J. Gunion *et al.* [9], we have

$$\Gamma(H \to \gamma\gamma) = \frac{\alpha^2 G_F m_H^3}{128\sqrt{2}\pi^3} \left| \sum_i N_{ci} e_i^2 F_i \right|^2 , \tag{3.1}$$

where i is the spin of the different loop particles ($i = 1/2, 1, 0$), and e_i the electric charge. N_{ci} is the color charge multiplicity, 1 for leptons and 3 for quarks. Furthermore,

$$\begin{aligned} F_1 &= 2 + 3\tau + 3\tau(2-\tau)f(\tau) \\ F_{1/2} &= -2\tau[1 + (1-\tau)f(\tau)] \\ F_0 &= \tau[1 - \tau f(\tau)], \end{aligned} \tag{3.2}$$

where τ is defined as

$$\tau = 4m_i^2/m_h^2, \tag{3.3}$$

and the function $f(\tau)$ is

$$f(\tau) = \begin{cases} \left[\sin^{-1}\left(\sqrt{1/\tau}\right)\right]^2 & \text{if } m_i \geq 0.5\ m_H \\ -\frac{1}{4}\left[\ln\left(\frac{1+\sqrt{1-\tau}}{1-\sqrt{1-\tau}}\right) - i\pi\right]^2 & \text{if } m_i < 0.5\ m_H. \end{cases} \tag{3.4}$$

To get a precise value, we need to include all the possible particles that can participate in these loops, shown in Fig. 3.1.

3.2 Corrections to $\Gamma(H \to \gamma\gamma)$

The tree level width of the diphoton decay is given by Eq. (3.1). Different kinds of higher-order correction can be included: Electroweak radiative corrections on G_F and higher order loop will be used here. Also, running quark masses in the modified minimal subtraction-scheme ($\overline{\text{MS}}$) are used on the heavy quarks, introduced by G. t'Hooft [27] and S. Weinberg [28] in 1973. Each of these will be discussed in the following section.

3.2.1 Electroweak corrections

The electroweak corrections can be controlled through a single variable: Δr. It is the sum of many different loop corrections, e.g. on the gauge boson propagators. Following B. Kniehl [29], we alter the value of Fermi's constant

$$G_F = \frac{\sqrt{2}g^2}{8M_W^2} = 1.16637 \cdot 10^{-5}\ \text{GeV}^{-2} \to \frac{\sqrt{2}g^2}{8M_W^2}\frac{1}{1-\Delta r}. \tag{3.5}$$

The value of Δr is given by the PDG [2], and is

$$\Delta r = 0.0362. \tag{3.6}$$

Then, we find the corrected value

$$G_F = 1.21018 \cdot 10^{-5}\ \text{GeV}^{-2}. \tag{3.7}$$

This correction will propagate to all the other electroweak constants, like $\alpha_{e.m.}, \sin^2\theta_W$ and M_W, M_Z. Therefore, we will keep them at their "standard" value of $\alpha_{e.m.} = 1/137.036$, $\sin^2\theta_W = 0.2310$, $m_W = 80.399$ GeV and $m_Z = 91.1876$ GeV, which are all given in the PDG [2].

3.2.2 Running of quark masses

From [9] we have the relation between the pole (m_q) and $\overline{\text{MS}}$ ($\overline{m}_q$) masses:

$$m_{LL}(m_H) = m_q \left[\frac{\ln\left(m_H^2/\Lambda_{\text{QCD}}^2\right)}{\ln\left(m_q^2/\Lambda_{\text{QCD}}^2\right)}\right]^{\gamma_0/2\beta_0} \tag{3.8}$$

$$\overline{m}_q = m_{LL}(m_H)\left[1 + \alpha_s(m_H)\left(\frac{\gamma_0\beta_1}{2\beta_0^2}\ln\ln\left(m_H^2/\Lambda_{\text{QCD}}^2\right) + \frac{\gamma_0\beta_1 - \gamma_1\beta_0}{2\beta_0^2}\right)\right], \tag{3.9}$$

where the scale μ in $m_{LL}(\mu)$ is chosen to be the Higgs mass, $\mu = m_H$[†]. The parameters are given by $\gamma_0 = -8$, $\gamma_1 = -(404/3) + (40/9)N_f$, $\beta_0 = 11 - (2/3)N_f$ and $\beta_1 = 102 - (38/3)N_f$. N_f is the number of active flavours (5 with the Higgs mass $m_b < m_H < m_t$). $\alpha_s(\mu)$ is the value of the strong coupling constant at the scale μ, given by

$$\alpha_s(\mu) = \frac{1}{\beta_0 \ln\left(\mu^2/\Lambda^2_{\rm QCD}\right)}. \tag{3.10}$$

The renormalized mass $\overline{m}_q$ is now used in the function $f(\tau)$ of Eq. (3.4), instead of the pole mass m_q. This is done every time we encounter m_q.

3.2.3 Two-loop contributions to $\Gamma(H \to \gamma\gamma)$

Two-loop corrections to the diphoton decay are mainly given by t quark loops and other QCD loops, see G. Degrassi and F. Maltoni [31]. In the high t quark mass limit, the electroweak two-loop correction is given by a term $\mathcal{F}_t^{2l}$ which goes into the sum in Eq. (3.1):

$$\mathcal{F}_t^{2l} = -\frac{\alpha}{4\pi \sin^2(\theta_W)} N_c Q_t^2 \frac{m_t^2}{m_W^2} \left(\frac{367}{96} + \frac{11}{16} h_{4w} + \frac{19}{56} h_{4w}^2 + \frac{29}{140} h_{4w}^3 + \mathcal{O}\left(h_{4w}^4\right) \right), \tag{3.11}$$

where $N_c = 3$ is the color factor, $Q_t = 2/3$ and $h_{4w} = m_H^2/4m_W^2$. The term for the two-loop QCD corrections is

$$\mathcal{F}_{\rm QCD}^{2l} = \frac{\alpha_s}{\pi} \frac{4Q_t^2 N_c}{3} \left(1 - \frac{122}{135} h_{4t} - \frac{8864}{14175} h_{4t}^2 - \frac{209186}{496125} h_{4t}^3 + \mathcal{O}\left(h_{4t}^4\right) \right), \tag{3.12}$$

Here, $h_{4t} = m_H^2/4m_t^2$.

Note that these two corrections will almost cancel for $m_H \in [100, 150]$ GeV, and exactly at $m_H \simeq 130$ GeV: See Fig. 6 in [31] for this.

3.3 The effects of new physics

A plot of the different contributions to the $\gamma\gamma$ decay rate is given in Fig. 3.2. Since the gauge bosons give the largest (and positive) contribution to the amplitude, we can add new heavy quarks, which give a negative contribution: This will create a destructive interference in the amplitude. Since the width is proportional to the amplitude squared, the width is reduced. This effect is shown in Fig. 3.2.

[†]Note that some set $\mu = \frac{1}{2}m_H$, but this choice is somewhat arbitrary. Section 2.3 of S. Dittmaier [30] argues that $\mu < m_H$ leads to more consistent calculations of the Higgs production cross section.

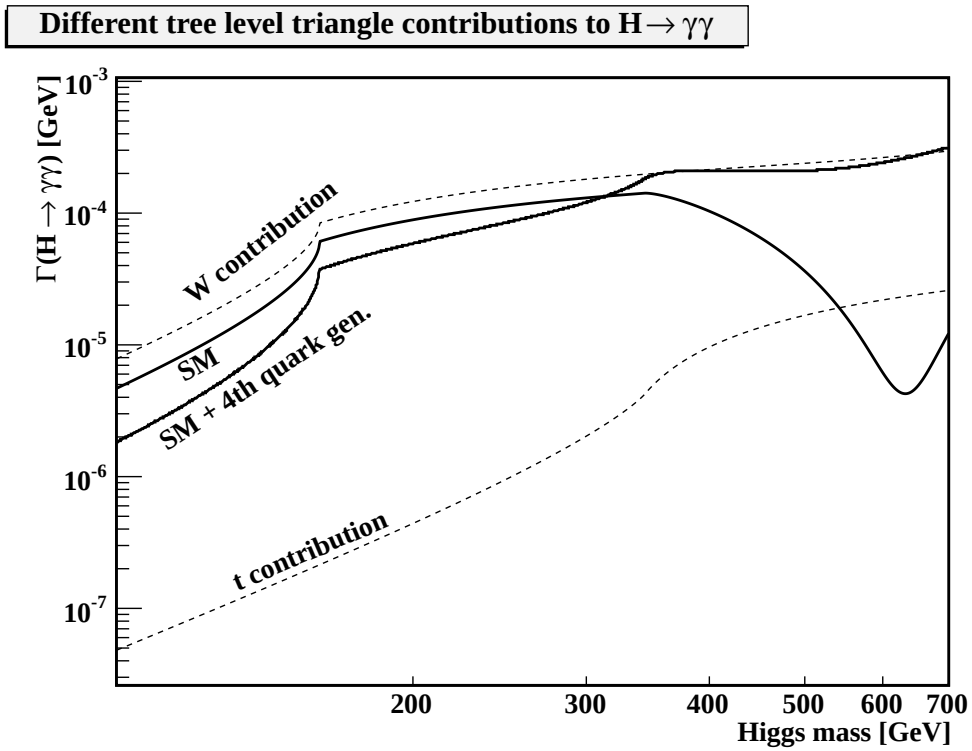

Figure 3.2: The width of $H \to \gamma\gamma$, given different triangle contributions. The W and t triangle will interfere, putting the sum ("SM") below the W contribution. The top quark contribution is negative, and a 4th quark generation will further decrease the sum.

In general, following the discussion from J. Gunion *et al.* [9], the limits of Eq. (3.2) when $m_{\text{triangle}}/m_H \to \infty$ are

$$F_0 \to -\frac{1}{3}, \qquad F_{1/2} \to -\frac{4}{3}, \qquad F_1 \to 7. \tag{3.13}$$

Adding new heavy particles of spin 1 will increase the width, while new spin 1/2 or 0 particles will decrease it. Thus a 4th quark generation would create *constructive* interference. However, such effects in this toy model are isolated. For the interesting variables (like the branching ratios and cross sections), adding new particles will affect existing channels or create new ones, and the end result is not as easily discerned. One of these effects is that when the total decay width is increased, existing particles get a smaller share of the width – and their BRs are decreased.

In supersymmetric theories, the extra participating particles will be the sfermions $\tilde{f}_{\text{L}}, \tilde{f}_{\text{R}}$ and charginos $\tilde{\chi}_i^{\pm}$.

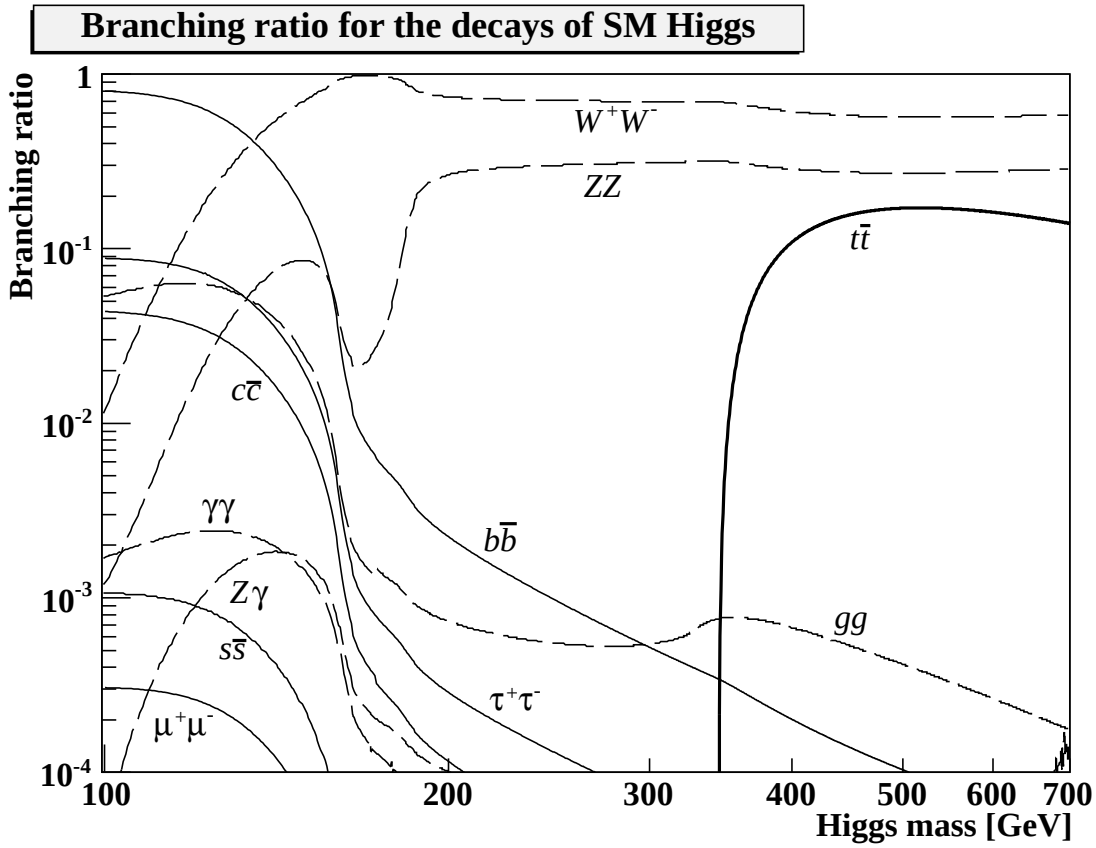

Figure 3.3: Branching ratios for the main decays of the SM Higgs boson, computed with the formulae in sections 3.2.3 and 3.5.

3.4 Branching Ratios

The branching ratio (BR) is defined as the ratio between the width of a channel and the sum of all the channels:

$$\mathrm{BR}(H \to \gamma\gamma) \equiv \frac{\Gamma(H \to \gamma\gamma)}{\Gamma_{H,\mathrm{tot}}} \tag{3.14}$$

We then need to know the widths of all the channels. From [9, 29, 32] we get the widths (including loop corrections) for the decay processes: $H \to f\bar{f}$, $H \to VV$ (including contributions from virtual vectors V^*V and V^*V^* at the mass regime $m_H < 2m_V$), $H \to Z\gamma$ and $H \to gg$.

To get the branching ratios, each channel is normalized to the sum of all the channels. The result is shown in Fig. 3.3. At low m_H (around 120 GeV), the contributions from W^*W and $b\bar{b}$ are the most substantial ones.

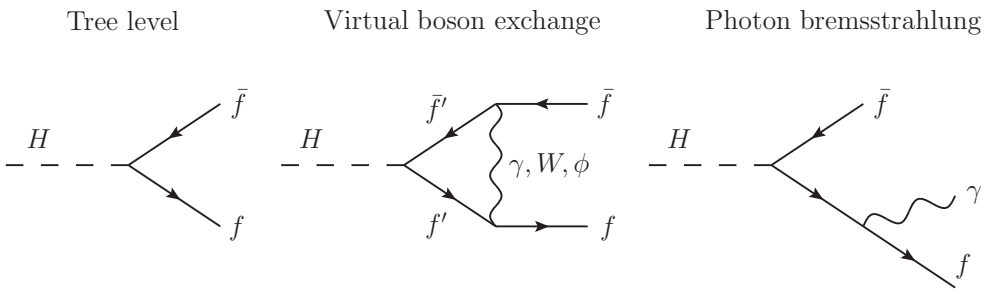

Figure 3.4: Some of the one-loop corrections to $H \to f\bar{f}$.

3.5 The width of other channels

As mentioned above, knowledge about the various decay channels is required to find the normalized width, or branching ratio. Below, each channel will be discussed briefly. When applicable, contributions from loop corrections and other effects are included. They are outlined in B. Kniehl [33].

3.5.1 $H \to l^+l^-$

The lepton channel is extracted from the fermion width in J. Gunion *et al.* [9]. It is given by

$$\Gamma_0(H \to l^+l^-) = \frac{G_F m_l^2 m_H}{4\pi\sqrt{2}} \left(1 - 4\frac{m_l^2}{m_H^2}\right)^{3/2} \tag{3.15}$$

Some examples of one-loop electroweak corrections to the more general $H \to f\bar{f}$ are shown in Fig. 3.4. They are given by B. Kniehl [29]:

$$\Gamma(H \to l^+l^-) = \Gamma_0(H \to l^+l^-)\left[1 + (\alpha/\pi)Q_f^2\Delta_{\text{em}}\right](1 + \Delta_{\text{weak}}), \tag{3.16}$$

where Q_f is the electric charge, and

$$\Delta_{\text{em}} = -\frac{3}{2}\ln\frac{m_H^2}{m_f^2} + \frac{9}{4} \tag{3.17}$$

$$\begin{aligned}\Delta_{\text{weak}} = \frac{G_F}{8\pi^2\sqrt{2}}\Bigg\{&C_f m_t^2 + M_W^2\left(\frac{3}{\sin^2(\theta_W)}\ln\cos^2(\theta_W) - 5\right)\\ &+M_Z^2\left[\frac{1}{2} - 3\left(1 - 4\sin^2(\theta_W)\right)|Q_f|^2\right]\Bigg\}\end{aligned} \tag{3.18}$$

With one-loop corrections, $C_f = 7$. Two-loop corrections can be included through this constant, which yields

$$C_f = 7 - 2\left(\frac{\pi}{3} + \frac{3}{\pi}\right)\alpha_s. \tag{3.19}$$

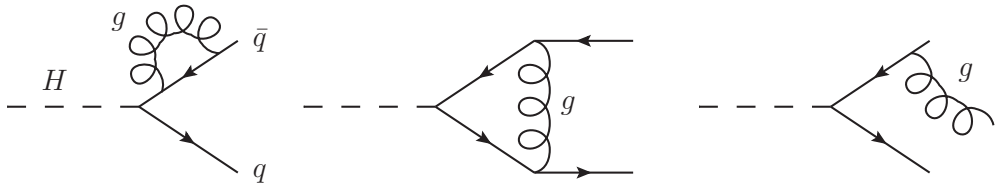

Figure 3.5: Some of the one-loop QCD-corrections to $H \to q\bar{q}$.

3.5.2 $H \to q\bar{q}$

Apart from a color factor of 3, the quark channel is the same as Eq. (3.15) at tree level. Including corrections, the electroweak ones mentioned above are the same. We need to include QCD effects, as shown in Fig. 3.5. Up to $\mathcal{O}(\alpha_s^2)$, we have from B. Kniehl [29]

$$\begin{aligned}\Gamma(H \to q\bar{q}) = \frac{3G_F m_H \overline{m}_q^2}{4\pi\sqrt{2}} \Bigg\{ &\left(1 - 4\frac{\overline{m}_q^2}{m_H^2}\right)^{3/2} + C_F \frac{\alpha_s}{\pi}\left(\frac{17}{4} - 30\frac{\overline{m}_q^2}{m_H^2}\right) \\ &+ \left(\frac{\alpha_s}{\pi}\right)^2 \Bigg[K_1 + K_2 \frac{\overline{m}_q^2}{m_H^2} + 12 \sum_{i=u,d,s,b} \frac{\overline{m}_q^2}{m_H^2} \\ &+ \frac{1}{3}\left(\frac{1}{3}\ln^2\frac{m_H^2}{\overline{m}_q^2} - 2\ln\frac{m_H^2}{\overline{m}_t^2} + 8 - 2\zeta(2)\right)\Bigg]\Bigg\}\end{aligned} \tag{3.20}$$

We have used $K_1 = 35.93996 - 1.3586N_f$, $K_2 = -129.72924 + 6.00093N_f$, where N_f is the number of active quark flavours at $\mu = m_H$. $\zeta(2) = \pi^2/6$ is the Riemann Zeta function, and $C_F = (N_c^2 - 1)/2N_c = 4/3$ where $N_c = 3$ is the number of colors.

The electroweak corrections Eqs. (3.17) and (3.18) apply here as well, with Eq. (3.16). The C_f of Eq. (3.19) is valid for the u, d, s, c quarks, but for the b quark another definition must be used:

$$C_b = 1 - 2\left(\frac{\pi}{3} + \frac{2}{\pi}\right)\alpha_s. \tag{3.21}$$

3.5.3 $H \to VV$

The decays into the massive vector bosons are split into three parts, depending on the Higgs mass. Each of them is shown in Fig. 3.6. First, for $m_H > 2m_V$, the on-shell decays are given for $H \to WW, ZZ$ in J. Fleischer and F. Jegerlehner [34]:

$$\Gamma_0(H \to VV) = \frac{\sigma_V G_F m_H^3}{16\pi\sqrt{2}}\sqrt{1 - x_V}\left(1 - x_V + \frac{3}{4}x_V^2\right), \tag{3.22}$$

for $V = W, Z$. We define $\sigma_W = 2, \sigma_Z = 1$ and $x_V = 4m_V^2/m_H^2$. For better precision, complicated loop functions can be used, as done by B. Kniehl [35,36]. They include evaluation of the

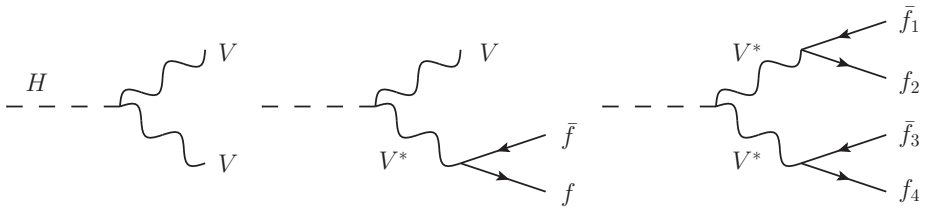

Figure 3.6: Two-, three- and four-body decays of H into the massive vector bosons V.

three-point scalar functions and different regularization schemes. We use an approximation from J. Gunion *et al.* [9],

$$\Gamma = \Gamma_0 \left[1 + \frac{G_F m_H^2}{\sqrt{2}\pi^2} \left(\frac{19}{16} - \frac{3\sqrt{3}\pi}{8} + \frac{5\pi^2}{48} \right) \right]. \tag{3.23}$$

For a lighter Higgs, decays into V^*V (one virtual, one real vector boson) are considered. These are valid for $m_V < m_H < 2m_V$,

$$\begin{aligned} \Gamma(H \to W^*W) &= \frac{3G_F^2 m_W^4 m_H}{16\pi^3} F(m_W/m_H) \\ \Gamma(H \to Z^*Z) &= \frac{G_F^2 m_W^4 m_H}{64\pi^3} \frac{7 - \frac{40}{3}\sin^2\theta_W + \frac{160}{9}\sin^4\theta_W}{\cos^4\theta_W} F(m_Z/m_H), \end{aligned} \tag{3.24}$$

where $F(x)$ is a phase space integral for the different possible decays of V^*. From W-Y Keung and W. Marciano [37],

$$F(x) = \int_{2x}^{1+x^2} \frac{\mathrm{d}y\sqrt{y^2-4x^2}}{(1-y)^2}(y^2 - 12x^2y + 8x^2 + 12x^4) \tag{3.25}$$

$$\begin{aligned} &= -|1-x^2| \left(\frac{47}{2}x^2 - \frac{13}{2} + \frac{1}{x^2} \right) + 3(1 - 6x^2 + 4x^4)|\ln x| \\ &\quad + \frac{3(1-8x^2+20x^4)}{\sqrt{4x^2-1}} \cos^{-1}\left(\frac{3x^2-1}{2x^3} \right). \end{aligned} \tag{3.26}$$

When $x \to 1/2$ (or when $m_H \to 2m_V$), a correction for the gauge boson Breit-Wigner width must be included. In this case,

$$F(x) = \int_{2x}^{1+x^2} \frac{\mathrm{d}y\sqrt{y^2-4x^2}}{(1-y)^2 + x^2\Gamma_V^2/m_H^2}(y^2 - 12x^2y + 8x^2 + 12x^4), \tag{3.27}$$

where Γ_V is the width of the V boson. This integral is harder to solve analytically, so it is evaluated numerically using the `SciPy.quad` package for Python [38]. For convenience, the widths Γ_V are given in the PDG [2]:

$$\Gamma_W = 2.085 \text{ GeV}, \qquad \Gamma_Z = 2.4952 \text{ GeV}. \tag{3.28}$$

Lastly, the most general and computational demanding method is to consider two off-shell vectors, i.e. $H \to V^*V^*$. This is done with a double integration, evaluated with `SciPy.dblquad` [39]. From A. Djouadi [40],

$$\Gamma(H \to V^*V^*) = \frac{1}{\pi^2}\int_0^{m_H^2} \frac{\mathrm{d}q_1^2 m_V \Gamma_V}{(q_1^2 - m_V^2)^2 + m_V^2\Gamma_V^2} \int_0^{(m_H - q_1)^2} \frac{\mathrm{d}q_2^2 m_V \Gamma_V}{(q_2^2 - m_V^2)^2 + m_V^2\Gamma_V^2} \Gamma_0, \tag{3.29}$$

where

$$\Gamma_0 = \frac{G_F m_H^3}{16\sqrt{2}\pi}\sigma_V \sqrt{\lambda(q_1^2, q_2^2; m_H^2)} \left[\lambda(q_1^2, q_2^2; m_H^2) + \frac{12 q_1^2 q_2^2}{m_H^4}\right]. \tag{3.30}$$

The function λ is given by

$$\lambda(x, y; z) = (1 - x/z - y/z)^2 - 4xy/z^2. \tag{3.31}$$

This expression is general and includes the lower-order expressions, so it should be used *instead* of Eqs. (3.23) + (3.24). It is only a minor correction, although it reaches the percent level at around 100 (110) GeV for W (Z) decays.

3.5.4 $H \to Z\gamma$

Decays of H into a Z and γ are given by triangle diagrams in J. Gunion *et al.* [9]. This becomes important when we add new particles into the theory. The diagrams are similar to the ones for $\gamma\gamma$, but here the W boson plays a even bigger role. According to A. Djouadi [40], this is true for masses up to $m_H \sim 400$ GeV. The decay width is

$$\Gamma(H \to Z\gamma) = \frac{G_F \alpha^2 m_H^3}{16\sqrt{2}\pi^3} \left|A_F + A_W\right|^2 \left(1 - \frac{m_Z^2}{m_H^2}\right)^3, \tag{3.32}$$

where the functions for fermion and W triangles (A_F and A_W, respectively) are given by

$$A_F = \sum_f N_{cf} \frac{-2e_f(T_{3f} - 2e_f \sin^2\theta_W)}{\sin\theta_W \cos\theta_W} \left[I_1(\tau_f, \lambda_f) - I_2(\tau_f, \lambda_f)\right] \tag{3.33}$$

$$\begin{aligned} A_W = -\cot\theta_W \Bigg\{ & 4(3 - \tan^2\theta_W) I_2(\tau_W, \lambda_W) \\ & + \left[\left(1 + \frac{2}{\tau_W}\right)\tan^2\theta_W - \left(5 + \frac{2}{\tau_W}\right)\right] I_1(\tau_W, \lambda_W) \Bigg\}. \end{aligned} \tag{3.34}$$

Here, e_f is the charge of f given in units of e and T_{3f} is the 3rd component of the weak isospin. N_{cf} is the color multiplicity of a fermion f. τ and λ are defined by

$$\tau_f = \frac{4m_f^2}{m_H^2}, \quad \lambda_f = \frac{4m_f^2}{m_Z^2}, \quad \tau_W = \frac{4m_W^2}{m_H^2}, \quad \lambda_W = \frac{4m_W^2}{m_Z^2}. \tag{3.35}$$

The integrals I_i are given by

$$I_1(a,b) = \frac{ab}{2(a-b)} + \frac{a^2b^2}{2(a-b)^2}[f(a) - f(b)] + \frac{a^2b}{(a-b)^2}[g(a) - g(b)], \tag{3.36}$$

$$I_2(a,b) = -\frac{ab}{2(a-b)}[f(a) - f(b)]. \tag{3.37}$$

$f(\tau)$ is defined in Eq. (3.4), while

$$g(\tau) = \begin{cases} \sqrt{\tau - 1}\sin^{-1}(1/\sqrt{\tau}), & \text{if } \tau \geq 1 \\ \frac{1}{2}\sqrt{1-\tau}\left[\ln\left(\frac{1+\sqrt{1-\tau}}{1-\sqrt{1-\tau}}\right) - i\pi\right], & \text{if } \tau < 1. \end{cases} \tag{3.38}$$

A minor QCD correction from M. Spira *et al.* [41] can be applied to the top quark amplitude A_F:

$$A_F \to A_F\left[1 + D(\tau_f)\frac{\alpha_s}{\pi}\right], \tag{3.39}$$

where $D(\tau_f) \simeq -0.6$ for $m_H \sim 125$ GeV. The total correction is at the percent level.

3.5.5 $H \to gg$

A treatment of the $H \to gg$ channel is given by J. Gunion *et al.* [9], and corrections are defined by M. Steinhauser [32], albeit with a low Higgs mass approximation. It is an important channel, as it is through gluon fusion that most of the Higgs production happens at the LHC, and $\sigma(gg \to H) \propto \Gamma(H \to gg)$. At one loop, the decay width is

$$\Gamma_0(H \to gg) = \frac{\alpha_s^2 G_F m_H^3}{16\pi^3\sqrt{2}}\left|\sum_i \tau_i[1 + (1-\tau_i)f(\tau_i)]\right|^2, \tag{3.40}$$

where the sum is over the different quarks that contribute. τ_i and $f(\tau_i)$ are defined in Eqs. (3.3) and (3.4). QCD corrections are important for this channel, with some diagrams shown in Fig. 3.7 (again, see A. Djouadi [40]). M. Steinhauser gave a parametrization up to $\mathcal{O}(\alpha_s^3 G_F m_t^2)$ in [32]:

$$\begin{aligned}\Gamma(H \to gg) = \Gamma_0\Bigg[1 + x_t + \frac{\alpha_s(m_H)}{\pi}\left[17.917 + x_t\left(33.004 + 2\ln\frac{m_H^2}{\overline{m}_t^2}\right)\right] \\ + \left(\frac{\alpha_s(m_H)}{\pi}\right)^2\left[156.808 + 5.708\ln\frac{m_H^2}{\overline{m}_t^2}\right]\Bigg],\end{aligned} \tag{3.41}$$

with the electroweak corrections parametrized as

$$x_t = \frac{G_F\overline{m}_t^2}{8\pi^2\sqrt{2}}. \tag{3.42}$$

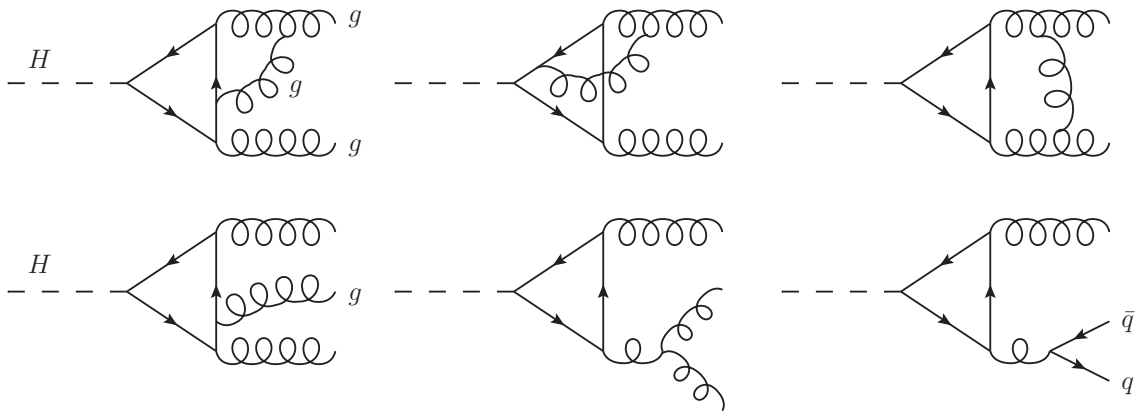

Figure 3.7: Corrections to $\Gamma(H \to gg)$. **Above***: Virtual corrections not present in* $H \to \gamma\gamma$. **Below***: Real corrections, with additional final particles.*

3.6 Production of *H*

Up until this point, we have been looking at widths and branching ratios for the Higgs boson. In order to get a complete picture of the probability of seeing a specific decay, it is important to know the probability of *creating* a Higgs. This depends on the type of collider, as well as its energy. As commented in Section 3.5.5, gluon fusion is the single most important channel in hadron colliders like the LHC. In addition, the other production channels are vector boson fusion (VBF), Higgs-strahlung and $Q\bar{Q}$ associated production, see A. Djouadi [42]. Fig. 3.8 shows the diagrams for these channels.

Although less interesting at the present time, at e^+e^- colliders the prominent production channels are from Higgs-strahlung $e^+e^- \to \nu\bar{\nu} + H$ (see R. Barger and V. Philips [8]), via W^+W^- fusion, as well as $e^+e^- \to Z^* \to Z + H$. The latter is treated in J. Gunion *et al.* [9]. Future e^+e^- colliders like the International Linear Collider (ILC) will use these production channels to make precision measurements of the Higgs, as T. Nelson [43] proposes.

3.6.1 $gg \to H$

Production of the Higgs through gluon fusion is analogous to the decay channel $H \to \gamma\gamma$, and differ at two points: The phase space is different, and in order to get physical answers, the *parton density functions* (PDFs) of Section 2.9.1 must be considered. Following A. Djouadi [40], the lowest-order inclusive cross section is

$$\sigma_0(pp \to H + X) = \frac{G_F \alpha_s^2 \tau}{288\sqrt{2}\pi} \left| \sum_Q A_Q(\tau_Q) \right|^2 \int_\tau^1 \frac{\mathrm{d}x}{x} g(x, Q^2) g(\tau/x, Q^2). \tag{3.43}$$

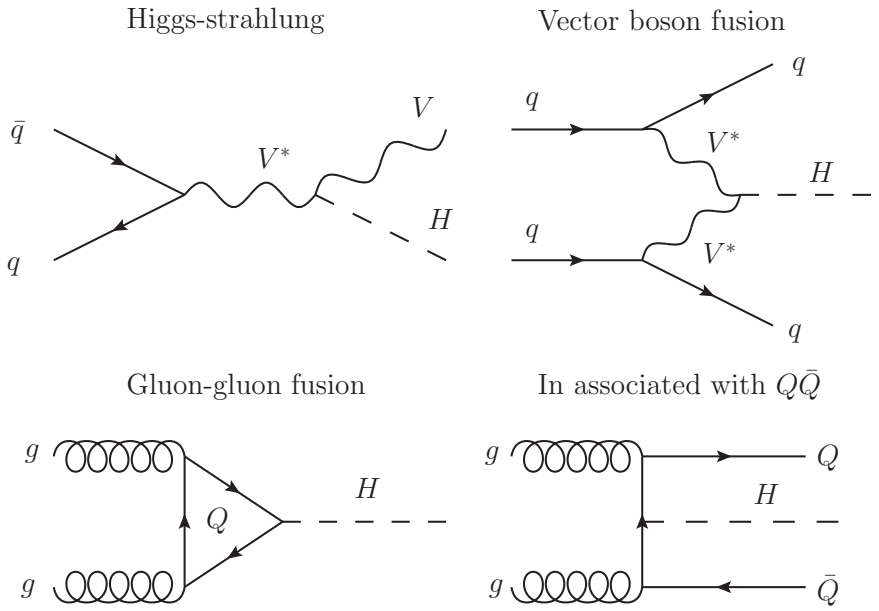

Figure 3.8: Feynman diagrams for the leading production mechanisms for the SM Higgs boson.

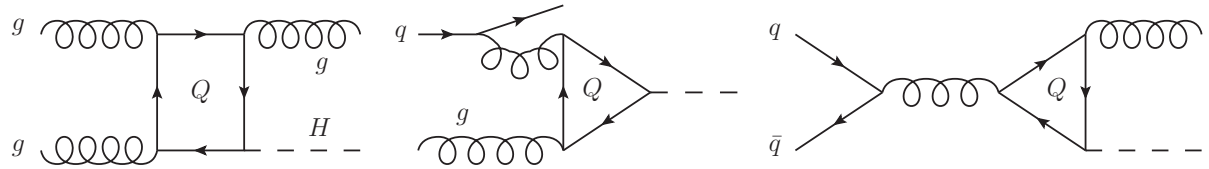

Figure 3.9: Some of the real QCD corrections to $gg \to H$.

The variables τ and τ_Q refer to the quark and Higgs masses: If s is the CoM energy squared,

$$\tau_Q = \frac{4\overline{m}_Q^2}{m_H^2}, \qquad \tau = \frac{m_H^2}{s}. \tag{3.44}$$

Without the integral over the PDF, the resulting cross section would be between two individual gluons, $\sigma(gg \to H)$. Integrating over the gluon parton density in the colliding protons, we find the gluon *contribution* to the cross section $\sigma(pp \to H)$, where other final states may or may not be produced.

Higher order QCD corrections described by A. Djouadi [44] will increase the lowest-order cross section σ_0 by about 50%. They consist of self energy corrections, extra gluon final states and initial-state rescattering of the gluons. This is done by adding terms for the different contributions. From Chapter 2.1 of the `HIGLU` manual [45],

$$\sigma(pp \to H + X) = \sigma_0 + \Delta\sigma_{\text{virt.}} + \Delta\sigma_{gg} + \Delta\sigma_{gq} + \Delta\sigma_{q\bar{q}}, \tag{3.45}$$

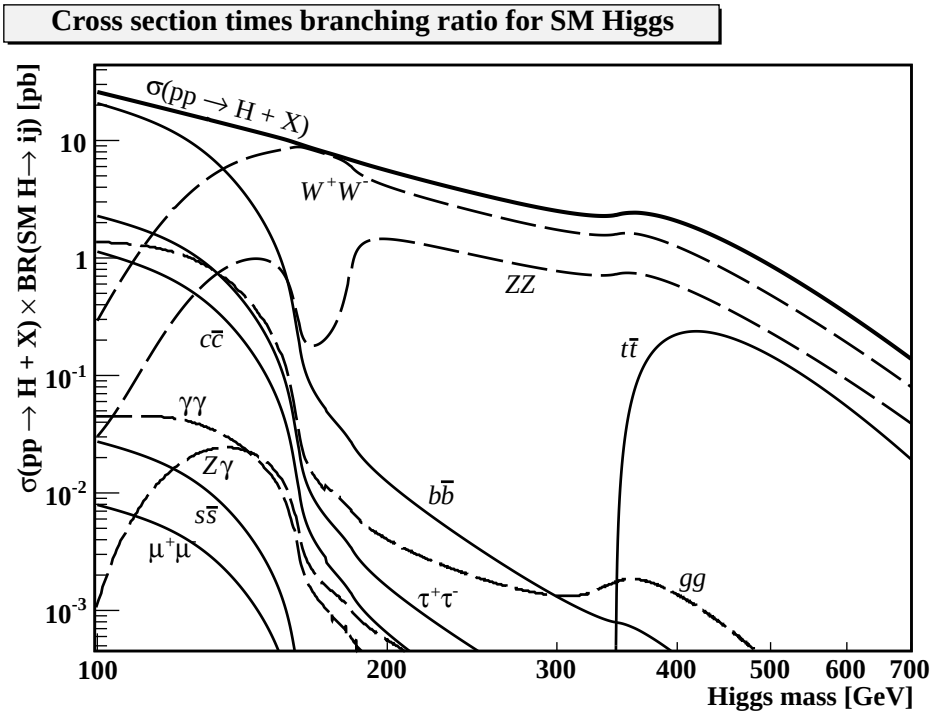

Figure 3.10: Branching ratios times the cross section for the main decays of the SM Higgs boson. The CoM energy is for the 2011 LHC run, $\sqrt{s} = 7$ TeV.

where $\Delta\sigma_{\text{virt.}}$ is the infrared virtual two-loop corrections, and $\Delta\sigma_{ij}$ $(i, j = g, q, \bar{q})$ are the real one-loop corrections for the subprocesses shown in Fig. 3.9:

$$gg \to Hg, \qquad gq \to Hq, \qquad q\bar{q} \to Hg. \tag{3.46}$$

Due to the complicated nature of the parton density functions in Eq. (3.43), the program `HIGLU` [45] is used for calculation of the complete gluon fusion process. See Section 6.3.3 for more information on this program.

Choosing a CoM energy $\sqrt{s}$, the cross section will fall with increasing m_H. After calculation of the different cross sections with `HIGLU`, these can be used to redraw Fig. 3.3, with

$$\sigma(pp \to H + X) \times \text{BR}(H \to ij) \tag{3.47}$$

instead of just the branching fractions. See Fig. 3.10 for this. The full cross section is also included in the figure, corresponding to the sum $\sum_{ij} \text{BR}(H \to ij) = 1$.

There are a few sources of error in calculating this uncertainty, mainly from the PDFs. S. Dittmaier *et al.* estimate an error of $\mathcal{O}(10\%)$ from the MSTW2008NLO PDF in Section 2.3 of [30].

Chapter 4

Beyond the Standard Model

The Standard Model (SM) has been remarkably successful in precisely explaining the rich phenomenology of nature. See the PDG [2] in its entirety for such examples. There are, however, both observations not explained by the standard model, and theoretical arguments for wanting to go beyond it.

In this chapter, we will explain why we want to go further than the SM. In Sections 4.1 and 4.2 we will list the experimental and theoretical problems with the SM. Then we will use the rest of the chapter to discuss the different models beyond the standard model: The Two-Higgs-Doublet Model and different versions of supersymmetric theories.

4.1 Experimental issues with the Standard Model

4.1.1 Gravity

While the general relativity (GR) of Einstein [46] and the SM are equally successful, they cannot be explained within the same framework. See B. Bertotti *et al.* [47] for precision tests of the GR. Phenomena like black holes are in the domains of both quantum theory and GR. Put more precisely: A black hole is a classic (GR) concept, but some of its properties need quantum theory to be explained. Hawking radiation, described by G. t'Hooft in [48] is one such example. The merging of these two is an ongoing task, with almost a century of history. These attempts are usually made in the context of merging all the elementary forces, creating a *Theory of Everything* (ToE). Some examples of ToEs will come later in this chapter.

4.1.2 Dark Matter

To quote S. Maurer from a 2001 SLAC article [49],

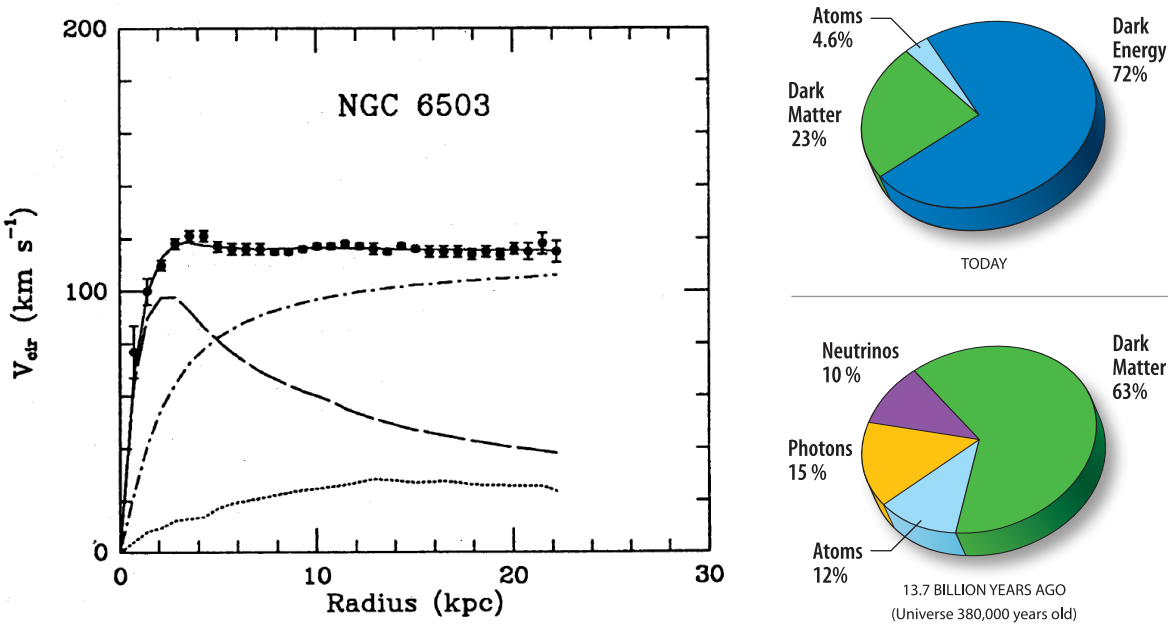

Figure 4.1: **Left***: Rotation curves for the galaxy* NGC 6503*, from K. G. Begeman* et al. [53]*. The dashed curve is for the visible component, while the dash-dotted curve is for a dark matter "halo" component.* **Right***: The contents of the universe, from the* WMAP *project* [54]*.*

> When researchers talk about neutron stars, dark matter, and gravitational lenses, they all start the same way: "Zwicky noticed this problem in the 1930s. Back then, nobody listened..."

In 1933, F. Zwicky used the *Virial theorem* [50, 51] on the Coma cluster to show that the galaxies rotated faster than the visible mass could account for. Such a rotational curve is shown in Fig. 4.1. J. Oort had by then already proved [52] that there is a discrepancy between stellar motions in the local galactic neighbourhood, compared to the visible mass. This unseen mass was dubbed *dark matter* (DM).

Today, there is an abundance of different observations that point towards the existence of DM. More specifically in the form of a new kind of particle, not interacting electromagnetically: A Weakly Interacting Massive Particle (WIMP). In addition to the rotational evidence listed above, *gravitational lensing* in levels exceeding the visible mass of galaxies have been observed, see R. Massey *et al.* [55].

There are many experiments looking for direct and indirect scattering effects from such a WIMP, like the XENON [56] and IceCube [57] collaborations where they search for direct recoil effects of a WIMP. The Fermi Large Angle Telescope (Fermi-LAT) [58] and Cherenkov telescopes like HESS [59] are searching for indirect photon energy signatures from relic WIMP

annihilations. So far, they have been inconclusive [60–62], but set limits on cross sections.

In the SM, there is no candidate for a WIMP. Neutrinos are too light, since the abundance needs to be *cold*, or non-relativistic, to keep its structure (see standard texts, like [63]). From theories *Beyond the Standard Model* (BSM), we have potential candidates. From supergravity, the spin 3/2 *gravitino* [64]. As a solution to the strong CP problem, the Peccei-Quinn theory theorizes a scalar particle, the *axion* [65]. From supersymmetric theories, the fermionic *neutralino* $\tilde{\chi}_1^0$.

The current Standard Model of cosmology is the ΛCDM (Λ Cold Dark Matter), where Λ signifies the *dark energy*. An estimate of the fraction of baryonic matter, DM and Λ is found from the Wilkinson Microwave Anisotropy Probe (WMAP) in Fig. 4.1. It is usually parametrized as the normalized density $\Omega = \rho/\rho_c$, where the critical density for a *flat* universe is $\rho_c \simeq 11h^2$ keV/cm^3. The dimensionless Hubble parameter h is defined later in Eq. (4.4).

Roughly speaking, $\Omega = 1$ would allow the universe to keep its expansion rate at a constant value, while a value $\Omega > 1$ or $\Omega_\Lambda < 0$ would cause the universe to re-collapse. Here we have defined Ω_Λ as the dark energy component of the normalized density. A value $\Omega < 1$ would slow down the expansion rate (see T. Padmanabhan [66]). We can define the components of Ω as

$$\Omega \simeq \Omega_{\text{baryonic}} + \Omega_{\text{DM}} + \Omega_\Lambda, \tag{4.1}$$

where each component has the value (from the WMAP project [54])

$$\Omega_{\text{DM}} = 0.23 \pm 0.04, \qquad \Omega_\Lambda = 0.73 \pm 0.04, \qquad \Omega_{\text{baryonic}} = 0.044 \pm 0.004. \tag{4.2}$$

Including a small fraction for relativistic particles, the numbers add up to

$$\Omega = 1.02 \pm 0.02. \tag{4.3}$$

The WMAP project [54] has measured the curvature of the universe to be flat, which is consistent with $\Omega = 1$. This is done by constructing a triangle between galaxies, and checking if the angles add up to 180°.

In this thesis, we assume the DM to consist of neutralinos. More specifically, the lightest neutralino $\tilde{\chi}_1^0$, which is also the LSP. Its different properties will be calculated to match (or at least not be larger than) the current limits set by telescope and scattering experiments [58–62, 67].

It is convenient to introduce the dimensionless Hubble parameter h, which is defined as

$$H_0 = \frac{\text{proper distance to galaxy}}{\text{“velocity” of galaxy}} = h \times 100 \ \frac{\text{km}}{\text{sec Mps}}. \tag{4.4}$$

Measurements of the Hubble parameter H_0 give h. The “velocity” is the derivative of the proper distance with respect to the cosmological time coordinate. This equation is referred to

as Hubble's law, but was originally derived in a 1927 article by the priest and astronomer G. Lemaître [68].

The parameter h is often used together with other quantities: From the WMAP 7 year Cosmological parameter survey [69], the dark matter *relic* density (after thermal equilibrium was reached) is given as

$$\Omega_{\mathrm{DM}}h^2 = 0.1123 \pm 0.0035. \tag{4.5}$$

This number will later be compared to a calculated DM relic density in our scans. More information about these constraints in Section 6.5.

4.1.3 Dark Energy

Although a similarity of name with dark matter, *dark energy* is a far more enigmatic subject. Historically, Einstein's cosmological constant appears in his modified field equation as Λ [46],

$$R_{\mu\nu} - \frac{1}{2}Rg_{\mu\nu} + g_{\mu\nu}\Lambda = \frac{8\pi G}{c^4}T_{\mu\nu}. \tag{4.6}$$

By putting $\Lambda = 0$, Eq. (4.6) is reduced to the original field equation of general relativity. He later rejected the idea of a cosmological constant.

Combining the WMAP data (requiring $\Omega = 1$) and the fact that the baryonic and dark matter only add up to a non-relativistic component of about $\Omega_{\mathrm{NR}} = 0.3$, see P. Peebles and B. Ratra [70], discarding the cosmological constant was (in hindsight) a bad idea.

Yielding the 2011 Nobel Prize in physics, the measurement of Ω_Λ and its identification with an accelerating expansion of the universe was done in the 1990s by Perlmutter *et al.* [71]. These measurements were done by studying high red-shift type Ia supernovae.

We see that around 70% of the universe needs to consist of a novel kind of energy. It was dubbed dark energy, and is supposed to have a large negative pressure. It is this property that makes the expansion accelerate. In contrast to DM, which stack up about galaxies and galaxy clusters, dark energy is uniform through the whole universe, and has a far lower density: See P. Peebles and B. Ratra [70].

4.1.4 Matter-antimatter asymmetry

Shortly after the Big Bang, different annihilation and creation processes were in equilibrium. According to the SM, matter and antimatter should have been produced in almost equal amounts.

Experiments looking for primordial antimatter, summarized by P. Ahlen [72] have not revealed any. This is a discrepancy, as the universe has a huge imbalance of ordinary matter.

The only known source of CP violation in the SM is through the weak interactions. However, it can only account for a very small fraction of the observed asymmetry.

4.1.5 Neutrino masses

Neutrino masses are not incorporated in the SM today. Mixing and oscillation in the neutrino sector has shown that such terms are necessary, but their nature is still unclear: Whether they are Dirac or Majorana particles, their masses and how they mix. A good review of this can be found in the PDG [2].

4.2 Theoretical issues with the Standard Model

4.2.1 Fine-tuning, or the Hierarchy problem

The Higgs boson gets very large corrections from virtual top quarks. The corrections can be canceled by fine-tuning some of the SM-parameters with a precision of 10^{-17}, but this is not an elegant or natural solution. See Section 2.11 for more details. The *Hierarchy problem* is analogous, and refers to the *orders* of magnitude between the lightest (ν) and heaviest (t) observed particles.

4.2.2 Number of parameters

The standard model contains 19 parameters[†] which must be input to match experimental data. Even though many BSM theories add to this number, ultimately we want to find why the parameters of the SM (or a theory beyond) are what they are. String theory tries to explain every phenomenon with *one* parameter – the tension of its eponymous strings. A review of string theory can be found in K. Dienes [73].

4.2.3 Unification of forces

More than once in history have different forces been found to have a shared parent force, often at higher energies. The electromagnetic force of J. Maxwell combined the electric and magnetic forces [74], while the electroweak interactions of A. Salam, S. Glashow and S. Weinberg combined electromagnetism and the weak force [75].

[†]They are: 9 fermion masses, 3 CKM angles, 1 CKM CP-violating phase, 3 gauge couplings, 1 QCD vacuum angle and the 2 Higgs parameters for its quadratic coupling and self-coupling strength. The neutrino mass sector is not included here.

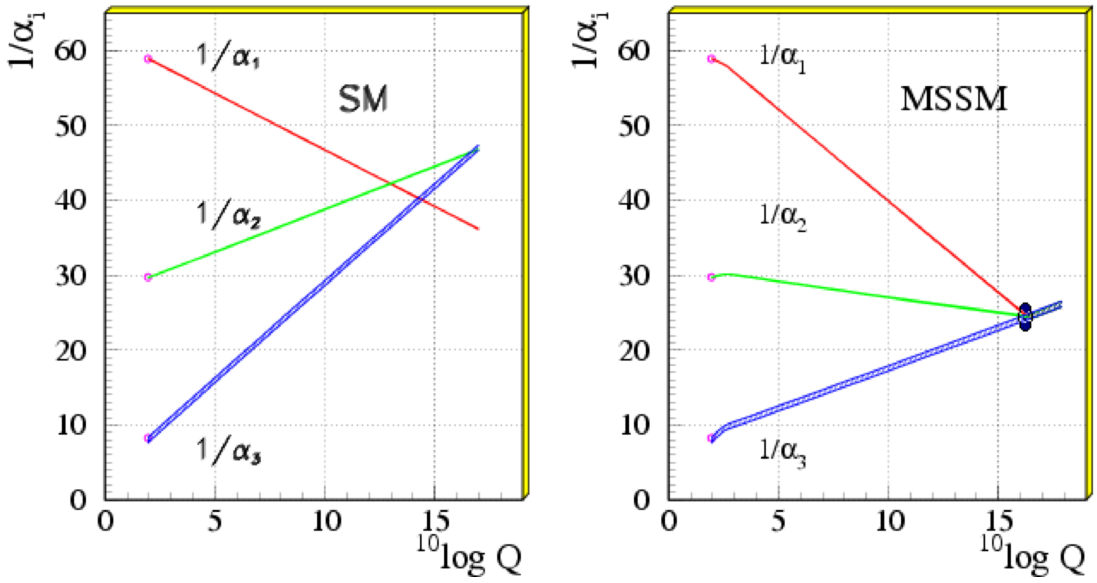

Figure 4.2: Gauge coupling unification using LEP data from the PDG [2]. **Left***: Non-supersymmetric GUTs,* **Right***: Supersymmetric GUTs.*

A *Grand Unification Theory* (GUT) tries to unify all the forces (*sans* gravity). Running of the different coupling constants shows that this is almost possible in the SM at high energies, where the three coupling constants (strong, weak and electromagnetic) just fail to meet at $\Lambda_{\text{GUT}} \sim 10^{16}$ GeV.

One of the most well-known examples of a GUT is the SU(5) extension of the Standard Model. It was shown in 1974 by H. Georgi and S. Glashow [76] that it is possible to unify quarks and leptons by introducing a SU(5) gauge group, which is broken down into SU(3) $\times$ SU(2) $\times$ U(1) below the GUT scale. With this unification, the proton gets a finite lifetime. Since such a decay has not been observed, we can either keep fiddling with the theory to increase the proton lifetime, or abandon it. The gauge symmetry SO(10) has also been proposed.

Supersymmetric theories can provide heavy particles which modify the running of the couplings, so that they meet at Λ_{GUT}, see Fig. 4.2. These kinds of theories will be treated in the next chapter.

A *Theory of Everything* is a unification of the forces *including* gravity, described in the *Nature* article by J. Ellis [77]. The idea of unifying gravity and electromagnetism came shortly after Einstein discovered general relativity. T. Kaluza and O. Klein [78, 79] found that if a fourth (rolled-up) spatial dimension was entered into Einstein's theory, equations similar to Maxwell's equations appeared. Einstein devoted most of his life to develop this

idea, but without success – the fourth dimension could not be dynamical, as the electron charge depended on its size. Without a dynamical metric, GR would not work.

There are also other ways to include gravity. String theory tries to construct a new theory bottom-up at Planck energies, and is therefore experimentally tricky to probe. Loop Quantum Gravity, reviewed by A. Ashtekar [80], is a fusion of general relativity and quantum theory. Since there is a strong duality between the dynamics and the metric in GR, both of these are quantized: The dynamical equations are quantized on a quantum Riemannian geometry.

In the next section, a selection of the proposed BSM models will be presented, with focus on the phenomenology of the Higgs boson.

4.3 The Two-Higgs-Doublet Model

The minimal extension to the SM for the mechanism of electroweak symmetry breaking is described in Section 2.6, and consists of *one* new scalar Φ. More complex varieties can be constructed, however there are two major restrictions on how this can be done – see J. Gunion *et al.* [9].

First, the parameter $\rho = m_W^2/(m_Z^2 \cos^2\theta_W)$ should be very close to 1. It is given by the sum over Higgs multiplets with weak isospins T_i, hypercharges Y_i and vevs v_i:

$$\rho = \frac{\sum_i \left[T_i(T_i+1) - Y_i^2\right] v_i^2}{\sum_i 2Y_i^2 v_i^2} \simeq 1. \tag{4.7}$$

The choice $T = 1/2$ and $Y = \pm 1$ is one possible solution to Eq. (4.7).

The second requirement comes from the experimental non-observation of flavor-changing neutral currents (FCNCs). These are automatically absent at tree-level in models with one doublet, because the Higgs-fermion couplings are always diagonalized. With more than one doublet, a theorem from Glashow and Weinberg [81] states that if all fermions of a given charge couple to only *one* doublet, FCNCs at tree level are absent.

The Two-Higgs-Doublet Model (2HDM), described in V. Barger and R. Philips [8], is created with both requirements in mind. The extension is needed for supersymmetric models, but can also be used as a minimal extension to the SM Higgs. Two SU(2) Higgs doublets are introduced,

$$\Phi_1 = \begin{pmatrix} \phi_1^0 \\ -\phi_1^- \end{pmatrix}, \qquad \Phi_2 = \begin{pmatrix} \phi_2^+ \\ \phi_2^0 \end{pmatrix}, \tag{4.8}$$

with hypercharge $Y = 1$.

To cope with the FCNCs, different versions of the 2HDM exist. In type I models, all the fermions couple to Φ_2. In type II models, up-type quarks couple to Φ_2, while down-type

	VV	$u\bar{u}$	$d\bar{d}$
H^0	$\cos(\beta-\alpha)$	$\dfrac{\sin\alpha}{\sin\beta}$	$\dfrac{\cos\alpha}{\cos\beta}$
h^0	$\sin(\beta-\alpha)$	$\dfrac{\cos\alpha}{\sin\beta}$	$\dfrac{-\sin\alpha}{\cos\beta}$

Table 4.1: Couplings between h^0, H^0 and VV, $u\bar{u}$ and $d\bar{d}$ for the type II 2HDM, normalized to the SM Higgs coupling. The $d\bar{d}$ coupling also apply for the charged leptons.

quarks and leptons couple to Φ_1. While these are the most important, there exist other possibilities: In type III models, FCNCs are allowed at tree level. *Lepton-specific* models couple the quarks to Φ_2 as with type I, but couple the leptons to Φ_1. *Flipped models* mimic type II models, but here leptons couple to Φ_2. Of these, type II models are the most widely studied, and is also responsible for the Higgs sector in the Minimal Supersymmetric Model of Section 4.5. See Chapter 2 of G. Branco *et al.* [82] for a information about the different coupling schemes of the 2HDMs.

In contrast to the SM, in the 2HDM we have eight degrees of freedom (DoF), and two *vacuum expectation values* (vevs) v_1 and v_2. The relation between G_F and the vevs is

$$\sqrt{v_1^2+v_2^2} = v = \frac{2^{-1/4}}{\sqrt{G_F}}. \tag{4.9}$$

Two new parameters are introduced, in addition to the coefficients of the potential. They are

$$\tan\beta = v_2/v_1, \tag{4.10}$$

and a mixing angle α between the ϕ_i^0 and the physical neutral CP-even Higgs bosons. This is a result of the 2HDM being a CP-invariant theory: α and β decouple the complex states into the real CP-even states h^0, H^0 and the imaginary CP-odd state A^0.

The DoF needed to give the gauge bosons mass are the same as with the SM, so we are left with *five* physical states in the unitary gauge: Two CP-even neutral particles h^0 and H^0 (where by definition $m_{H^0} > m_{h^0}$), one C-odd pseudoscalar A^0 and two charged states $H^\pm$. These states are given by

$$\begin{aligned}
\begin{pmatrix} H^0 \\ h^0 \end{pmatrix} &= \sqrt{2}\begin{pmatrix} \cos\alpha & \sin\alpha \\ -\sin\alpha & \cos\alpha \end{pmatrix}\begin{pmatrix} \mathrm{Re}\ \phi_1^0 - v_1 \\ \mathrm{Re}\ \phi_2^0 - v_2 \end{pmatrix}, \\
A^0 &= \sqrt{2}\left(-\mathrm{Im}\ \phi_1^0 \sin\beta + \mathrm{Im}\ \phi_2^0 \cos\beta\right), \\
H^\pm &= -\phi_0^\pm \sin\beta + \phi_2^\pm \cos\beta.
\end{aligned} \tag{4.11}$$

Couplings between these 2HDM Higgs bosons, fermions and gauge bosons are modified by trigonometric factors of α, β. These are given in Table 4.1 for the type II model. The

phenomenology of 2HDM will be explored further in the context of *supersymmetry*, which is the theme of the next sections.

4.4 Supersymmetry

In Section 2.11, the divergence of the mass corrections to the Higgs boson was discussed. The *lack of a symmetry* to protect the Higgs was proposed as the source of this divergence. This problem was also briefly referred to as the Hierarchy problem in Section 4.2.1.

Extending to that discussion, a symmetry connecting scalar and fermionic particles would provide such a protection. From Fig. 2.7 and A. Djouadi [26], we can add scalar partners S to Eq. (2.90), in addition to the fermions already contributing. The trilinear and quadrilinear couplings of S to the Higgs boson are $v\lambda_S$ and λ_S. From Chapter 1 of A. Djouadi [26], the contribution from N_S scalar partners is

$$\Delta m_H^2 = \frac{\lambda_S N_S}{16\pi^2}\left[-\Lambda^2 + 2m_S^2 \ln\left(\frac{\Lambda}{m_S}\right)\right] - \frac{\lambda_S^2 N_S}{16\pi^2} v^2 \left[-1 + 2\ln\left(\frac{\Lambda}{m_S}\right)\right] + \mathcal{O}\left(\frac{1}{\Lambda^2}\right). \quad (4.12)$$

If such a symmetry exists in a way that $\lambda_f^2 = 2m_f^2/v^2 = -\lambda_S$ and $N_S = 2N_f$, then a combination of Eqs. (2.90) and (4.12) becomes

$$\Delta m_H^2 = \lambda m_f^2 N_f 4\pi^2 v^2 \left[(m_f^2 - m_S^2)\ln\left(\frac{\Lambda}{m_S}\right) + 3m_f^2 \ln\left(\frac{m_S}{m_f}\right)\right] + \mathcal{O}\left(\frac{1}{\Lambda^2}\right). \quad (4.13)$$

If the symmetry between f and S is exact, $m_S = m_f$ and then $\Delta m_H^2 = \mathcal{O}(\Lambda^{-2})$. Other particles will also contribute to the mass correction. The process can be repeated (and the new quadratic corrections canceled) by introducing fermionic partners to $W^{\pm}$, Z^0, and to the Higgs bosons.

The symmetry cannot be exact, since we have not observed partner scalars at any of the fermion masses. Luckily, the quadratic divergences are still canceled, but a logarithmic one remains. To keep the Higgs mass at $\mathcal{O}(100\text{ GeV})$ and avoid more fine-tuning, the partners should not be heavier than the TeV scale.

Supersymmetry (SUSY) is such a symmetry, relating particles with integer and half-integer spin. The SUSY generators $\mathcal{Q}$ transform back and forth between fermions and bosons:

$$\mathcal{Q}|\text{fermion}\rangle = |\text{boson}\rangle, \qquad \mathcal{Q}|\text{boson}\rangle = |\text{fermion}\rangle. \quad (4.14)$$

When the symmetry is exact, the only difference between a normal state and a transformed *superpartner* state is their spin. In this case, supersymmetry is fully specified, with no new parameters (other than the form of the Higgs potential W).

Superfield	$SU(3)_C$	$SU(2)_L$	$U(1)_Y$	Particle content
$\hat{G}_a$	8	1	0	$G_a^\mu,\ \tilde{G}_a$
$\hat{W}_a$	1	3	0	$W_a^\mu,\ \tilde{W}_a$
$\hat{B}$	1	1	0	$B^\mu,\ \tilde{B}$

Table 4.2: The MSSM superpartners of the gauge boson and their quantum numbers.

We will not go into details on the algebra behind supersymmetry here. Roughly speaking, the operator $\mathcal{Q}$ correspond to the square root of the energy-momentum operator P_μ. Formally, from Eq. (4.48) in [25] we have the anticommutation relation

$$\left\{\mathcal{Q}_a, \mathcal{Q}_b^\dagger\right\} = (\sigma^\mu)_{ab} P_\mu. \tag{4.15}$$

Particles are combined with their superpartners into *superfields*, denoted with a hat. They can consist of a complex scalar field S with two degrees of freedom, plus a Weyl fermionic field with two components ζ. The Weyl fields correspond to the u_r and v_r spinors of the standard fermionic field $\psi(x)$ of Eq. (2.20), see P. Labelle [83]. There are other possible superfield constructions, however this is the one used in the minimal supersymmetric extension of the SM, which is the theme of the next section.

4.5 Minimal Supersymmetric Standard Model

Supersymmetry as a usable theory is incomplete. As two examples, it does not specify any particle content, nor which gauge symmetries to use. Its main idea is to provide an algebra behind this new symmetry we need to protect the Higgs.

The Minimal Supersymmetric Standard Model (MSSM) is the minimal realization of SUSY. It follows four basic assumptions [26]:

1. **Minimal gauge group**: The SM gauge symmetry $SU(3)_C \times SU(2)_L \times U(1)_Y$ is reproduced in MSSM. This requires the spin-$\frac{1}{2}$ superpartners of the gauge bosons, the *gauginos*, to mimic the SM: The bino $\tilde{B}$ for the B^μ, the three winos $\tilde{W}_{1-3}$ for $\mathbf{W}^\mu$ and the eight gluinos $\tilde{G}_{1-8}$ for $\mathbf{G}^\mu$. Their quantum numbers are listed in Table 4.2.

2. **Minimal particle content**: Three scalar *sfermion* generations are introduced. Chiral superfields contain the spin-$\frac{1}{2}$ SM particles, together with their spin-0 partners: $\hat{Q}, \hat{U}_R, \hat{D}_R, \hat{L}, \hat{E}_R$. In order to break the electroweak symmetry, the Higgs sector from the 2HDM is adopted (see Section 4.3). The two chiral superfields $\hat{H}_1$ and $\hat{H}_2$ contain both the two Higgs doublets and their Higgsino partners. Their quantum numbers are listed in

Superfield	$SU(3)_C$	$SU(2)_L$	$U(1)_Y$	Particle content
$\hat{Q}$	3	2	$\frac{1}{3}$	$(u_L, d_L), (\tilde{u}_L, \tilde{d}_L)$
$\hat{U}^c$	$\bar{3}$	1	$-\frac{4}{3}$	$\bar{u}_R, \tilde{u}_R^*$
$\hat{D}^c$	$\bar{3}$	1	$\frac{2}{3}$	$\bar{d}_R, \tilde{d}_R^*$
$\hat{L}$	1	2	-1	$(\nu_L, e_L), (\tilde{\nu}_L, \tilde{e}_L)$
$\hat{E}^c$	1	1	2	$\bar{e}_R, \tilde{e}_R^*$
$\hat{H}_1$	1	2	-1	$H_1, \tilde{H}_1$
$\hat{H}_2$	1	2	1	$H_2, \tilde{H}_2$

Table 4.3: The MSSM superpartners of the fermions and their quantum numbers.

Table 4.3. The Higgsinos mix with the winos and the bino, with the resulting particles as the two charginos $\tilde{\chi}^{\pm}_{1,2}$ and the four neutralinos $\tilde{\chi}^0_{1,2,3,4}$.

3. **Minimal Yukawa interactions and R-parity conservation**: R-parity requires that the lepton and baryon numbers (L and B) are conserved. This parity is defined by

$$R_p = (-1)^{2s+3B+L}, \tag{4.16}$$

where s is the spin. Now, $R_p = 1$ for ordinary particles, and $R_p = -1$ for superpartners. When R_p is conserved, supersymmetric particles can only be produced in pairs, and the lightest SUSY particle (LSP) is stable. The minimal Yukawa superpotential is given by

$$W = \sum_{i,j=\text{gen.}} \left(-Y^u_{ij} \hat{u}_{Ri} \hat{H}_2 \cdot \hat{Q}_j + Y^d_{ij} \hat{d}_{Ri} \hat{H}_1 \cdot \hat{Q}_j + Y^\ell_{ij} \hat{\ell}_{Ri} \hat{H}_1 \cdot \hat{L}_j \right) + \mu \hat{H}_1 \cdot \hat{H}_2. \tag{4.17}$$

$Y^{u,d,l}_{ij}$ are the Yukawa couplings, and $H \cdot Q \equiv \epsilon_{ab} H^a Q^b$, for ϵ_{ab} as the antisymmetric tensor. Note how only $\hat{H}_2$ couples to up-type quarks, and $\hat{H}_1$ to down-type (including leptons). This is due to the Glashow-Weinberg theorem mentioned earlier.

4. **Minimal set of soft SUSY-breaking terms**: The property *soft* refers to a breaking of SUSY, while preventing the reappearance of quadratic divergences. These terms are the masses and the different Higgs couplings, which are added to the Lagrangian. For convenience, they are listed below:

   (a) Mass terms for the gauginos:

$$-\mathcal{L}_{\text{gaugino}} = \frac{1}{2} \left[M_1 \tilde{B}\tilde{B} + M_2 \sum_{a=1}^{3} \tilde{W}^a \tilde{W}_b + M_3 \sum_{a=1}^{8} \tilde{G}^a \tilde{G}_a + \text{h.c.} \right] \tag{4.18}$$

(b) Mass terms for the sfermions:

$$-\mathcal{L}_{\text{sfermions}} = \sum_{i=\text{gen.}} \left(m^2_{\tilde{Q}_i} \tilde{Q}^\dagger_i \tilde{Q}_i + m^2_{\tilde{L}_i} \tilde{L}^\dagger_i \tilde{L}_i + m^2_{\tilde{u}_i} |\tilde{u}_{\text{R}i}|^2 + m^2_{\tilde{d}_i} |\tilde{d}_{\text{R}i}|^2 + m^2_{\tilde{\ell}_i} |\tilde{\ell}_{\text{R}i}|^2 \right) \quad (4.19)$$

(c) Mass and trilinear terms for the Higgs bosons:

$$-\mathcal{L}_{\text{Higgs}} = m^2_{H_2} H^\dagger_2 H_2 + m^2_{H_1} H^\dagger_1 H_1 + B\mu (H_2 \cdot H_1 + \text{h.c.}) \quad (4.20)$$

(d) Trilinear couplings between sfermions and the Higgs bosons:

$$-\mathcal{L}_{\text{tril.}} = \sum_{i,j=\text{gen.}} \left[A^u_{ij} Y^u_{ij} \tilde{u}^*_{\text{R}i} H_2 \cdot \tilde{Q}_j + A^d_{ij} Y^d_{ij} \tilde{d}^*_{\text{R}i} H_1 \cdot \tilde{Q}_j + A^\ell_{ij} Y^\ell_{ij} \tilde{\ell}^*_{\text{R}i} H_1 \cdot \tilde{L}_j + \text{h.c.} \right] \quad (4.21)$$

In all, we gain 110 parameters from the above considerations, which is the basis of this *unconstrained* MSSM. They are outlined in D. Sutter and S. Dimopoulos [84], and consist of 30 masses, 39 mixing angles and 41 phases.

4.6 Phenomenological MSSM

The unconstrained MSSM from the last section may lead to unphysical models, and contains many parameters. The *phenomenological MSSM* (pMSSM) model is a subset of the MSSM, with some additional constraints described in F. Gabbiani *et al.* [85]:

1. All the soft SUSY-breaking parameters are real, so no new sources of CP-violations. The CP-violations from the CKM matrix are kept.

2. The soft SUSY-breaking masses and trilinear couplings of the first and second generations are degenerate. This is to satisfy constraints from $K^0 - \bar{K}^0$-mixing.

3. The matrices for sfermion masses and trilinear couplings are diagonal. If not, inter-generational mixing would have allowed FCNCs at tree level.

Depending on the choice of the degenerate first two generations of trilinear couplings $A_{u,d,e}$, we are left with 19 ($A_{u,d,e} = A_{t,b,\tau}$ in C. Berger *et al.* [86]) or 22 parameters ($A_{u,d,e}$ and $A_{t,b,\tau}$ chosen separately in A. Djouadi [26]). This difference is not important, since the $A^{\text{gen.}}_i$ are multiplied with $m^{\text{gen.}}_i$, and $m^{1,2}_i < m^3_i$. There is also a choice on how to specify the Higgs masses: Either by the doublet masses $m^2_{H_1}$ and $m^2_{H_2}$, or by the pseudoscalar mass m^2_A and the Higgsino mass parameter μ.

These parameters are given in Table 4.4. It should be noted that even though the structure

$\tan\beta$	The ratio of the vevs of the 2HD field
m_A	The pseudoscalar Higgs mass
μ	The Higgsino mass parameter
M_1, M_2, M_3	The gaugino masses: $\tilde{B}$, $\tilde{W}_a$ and $\tilde{G}_a$
$m_{\tilde{q}}, m_{\tilde{u}_\mathrm{R}}, m_{\tilde{d}_\mathrm{R}}, m_{\tilde{\ell}}, m_{\tilde{e}_\mathrm{R}}$	The 1st/2nd gen. sfermion masses
(A_u, A_d, A_e)	(The 1st/2nd gen. trilinear couplings)
$m_{\tilde{Q}}, m_{\tilde{t}_\mathrm{R}}, m_{\tilde{b}_\mathrm{R}}, m_{\tilde{L}}, m_{\tilde{\tau}_\mathrm{R}}$	The 3rd gen. sfermion masses
A_t, A_b, A_τ	The 3rd gen. trilinear couplings

Table 4.4: The 19 (22) parameters of the pMSSM.

of the 2HDM is adopted by the MSSM, the choice of parameters are not the same. In the 2HDM, all the Higgs masses and the angles α, β can be input independently. In pMSSM, they are calculated from m_A, $\tan\beta$ and the Z^0 mass. The angle α is found by

$$\tan 2\alpha = \tan 2\beta \frac{M_A^2 + M_Z^2}{M_A^2 - M_Z^2}, \qquad -\frac{\pi}{2} \geq \alpha \geq 0. \tag{4.22}$$

We will focus on the CP-even particles h^0 and H^0. It may be worth mentioning that the mass of the SM Higgs is calculated by the quartic coupling λ, which is a free parameter. In the MSSM, this quartic coupling comes from the gauge coupling (through m_A, $\tan\beta$ and m_Z, as mentioned above), so the h^0 and H^0 masses are not free parameters! The masses and other properties of the MSSM Higgs bosons will be calculated in Chapter 5.

4.6.1 Mixing of the sfermions

In later chapters, the fermions are denoted as $\tilde{f}_{1,2}$. The index refers to the light and heavy mass eigenstates. In the sfermion sector, the chiral eigenstates are $\tilde{f}_\mathrm{R}$ and $\tilde{f}_\mathrm{L}$. These are mixed into the mass eigenstates $\tilde{f}_1$ and $\tilde{f}_2$, where by definition $m_{\tilde{f}_1} < m_{\tilde{f}_2}$. With

$$\begin{aligned} m_{\mathrm{LL}}^2 &= m_{\tilde{f}_\mathrm{L}}^2 + (T_3 - Q\sin^2\theta_W) m_Z^2 \cos 2\beta \\ m_{\mathrm{RR}}^2 &= m_{\tilde{f}_\mathrm{R}}^2 + Q\sin^2\theta_W m_Z^2 \cos 2\beta \\ X_f &= A_f - \mu(\tan\beta)^{-2T_3}, \end{aligned} \tag{4.23}$$

the mixing from the chiral into the mass eigenstates is (see [26]):

$$m_{\tilde{f}_{1,2}}^2 = m_f^2 + \frac{1}{2}\left[m_{\mathrm{LL}}^2 + m_{\mathrm{RR}}^2 \mp \sqrt{(m_{\mathrm{LL}}^2 - m_{\mathrm{RR}}^2)^2 + 4m_f^2 X_f^2}\right]. \tag{4.24}$$

Another way of looking at the mixing is as a rotation. In that case, the rotational angle between the chiral and mass eigenstates is

$$\theta_{\tilde{f}} = \frac{1}{2}\sin^{-1}\left[\frac{2m_f X_f}{m^2_{\tilde{f}_1} - m^2_{\tilde{f}_2}}\right] = \frac{1}{2}\cos^{-1}\left[\frac{m^2_{\mathrm{LL}} - m^2_{\mathrm{RR}}}{m^2_{\tilde{f}_1} - m^2_{\tilde{f}_2}}\right]. \tag{4.25}$$

This is most prominent in the $\tilde{t}$ (stop) sector. Large values of $X_t = A_t - \mu/\tan\beta$ give a large mass splitting between $\tilde{t}_1$ and $\tilde{t}_2$, and the lightest state may be comparable to the ordinary top mass. This is of interest, since it may increase the Higgs mass without too much *unnatural* strain on the parameter space, see Csaki *et al.* [87]. For the effect of a small $m_{\tilde{t}_1}$ on $\Gamma(h^0 \to \gamma\gamma)$, see Carmi *et al.* [88].

4.7 Constrained MSSM

While pMSSM is a constrained version of MSSM, it is possible to constrain the MSSM further. Such models are collectively called *constrained MSSMs* (cMSSMs). One of their main requirements is that of unification – that the couplings meet at M_{GUT}. This translates to fewer parameters which are input at the GUT scale: m_0, $m_{1/2}$, A_0, $\tan\beta$ and the sign of μ are the five parameters of *minimal supergravity* (mSUGRA) [89].

These models specify a *messenger*, which breaks the SUSY at a given scale. mSUGRA uses the gravitino for this, but there are also models which break the symmetry through loops (Anomaly Mediated Symmetry Breaking [90]), gauge interactions (Gauge Mediated Symmetry Breaking [91]) and gauginos [92].

With fewer parameters, it can be easier to probe the parameter space – and to exclude large parts of it using experimental data. We will briefly see this in Chapter 6, where a far smaller fraction of mSUGRA models pass our experimental constraints than with the pMSSM.

Chapter 5

The MSSM Higgs bosons

In this chapter, we will study the Higgs bosons of the MSSM. One of the differences with respect to the SM is that their masses are not free parameters. We will see how to calculate them in Section 5.1. We will then discuss how the different parameters affect this mass, before we continue to the decay widths and branching ratios in Section 5.3. After finding the production mechanisms in Section 5.4, we will round off with a quick discussion on loop-corrections to the parameters.

5.1 The masses of h^0 and H^0

In the MSSM, the tree-level masses of h^0 and H^0 are calculated as the eigenvalues from the mass matrix $\mathbf{V}$ with input parameters m_Z, the pseudoscalar Higgs mass m_{A^0}, and the ratio between the vacuum expectation values $\tan\beta$. From P. Labelle [83], the mass matrix is

$$\mathbf{V} = \begin{pmatrix} b\cot\beta + m_Z^2\sin^2\beta & -\frac{\sin 2\beta}{2}m_Z^2 - b \\ -\frac{\sin 2\beta}{2}m_Z^2 - b & b\tan\beta + m_Z^2\cos^2\beta \end{pmatrix}, \tag{5.1}$$

with $b = \frac{1}{2}m_{A^0}^2\sin 2\beta$. The eigenvalues of this matrix are the tree-level masses m_h^{tree}:

$$\left(m_{h^0}^{\text{tree}}\right)^2 = \frac{m_{A^0}^2 + m_Z^2}{2} - \frac{1}{2}\sqrt{(m_{A^0}^2 - m_Z^2)^2 - 4m_{A^0}^2 m_Z^2\cos^2 2\beta} \tag{5.2}$$

$$\left(m_{H^0}^{\text{tree}}\right)^2 = \frac{m_{A^0}^2 + m_Z^2}{2} + \frac{1}{2}\sqrt{(m_{A^0}^2 - m_Z^2)^2 - 4m_{A^0}^2 m_Z^2\cos^2 2\beta}. \tag{5.3}$$

In the $\beta \to 0$ and $m_{A^0} \to \infty$ limit, we get

$$m_{h^0}^{\text{tree}} \to m_Z, \qquad m_{H^0}^{\text{tree}} \to \infty. \tag{5.4}$$

This is called the *decoupling limit*, where h^0 acts as the SM Higgs. Then the gauge and Yukawa couplings will take their SM values. At tree level, $m_{h^0}^{\text{tree}}$ is bounded by $m_Z|\cos 2\beta|$. To match experimental data, we would like m_{h^0} to be higher.

To increase m_{h^0}, we introduce radiative corrections from B. Allanach [93], both to h^0 and to the particles participating in the loops. The dominating one-loop corrections increase the masses from $m_{h^0}^{\text{tree}}$ to m_{h^0}. Using $m_{h^0} = \sqrt{\left(m_{h^0}^{\text{tree}}\right)^2 + \epsilon}$, we find

$$\epsilon = \frac{3m_t^4}{2\pi^2 v^2}\left(\ln\frac{M_S^2}{m_t^2} + \frac{X_t^2}{2M_S^2} - \frac{X_t^4}{12M_S^4}\right) - \frac{3m_b^4}{2\pi^2 v^2}\frac{X_b^4}{12M_S^4}. \tag{5.5}$$

M_S is the common soft SUSY-breaking mass term for the third-generation squarks (often called the SUSY-scale), here defined by

$$M_S = \sqrt{m_{\tilde{t}_1} m_{\tilde{t}_2}}. \tag{5.6}$$

Some use another definition, that of the arithmetic average $M_S = \frac{1}{2}(m_{\tilde{t}_1} + m_{\tilde{t}_2})$. Notice the logarithmic dependence on M_S^2 – this is the remainder of the diverging Higgs mass we discussed in Section 4.4. X_t and X_b are the stop and sbottom mixing terms:

$$X_t = A_t - \mu\cot\beta, \qquad X_b = A_b - \mu\tan\beta. \tag{5.7}$$

These X_f are related to the stop and sbottom mixing angles $\theta_{\tilde{t},\tilde{b}}$, defined in Eq. (4.25).

Corrections up to two-loop order are needed for a satisfactory precision. In order to do this, the program `SuSpect` is used for the calculation of the pMSSM Higgs masses. The details on how this is done are located in Chapter 6.

Fig. 5.1 shows the result of a scan over the different pMSSM parameters, with the masses of h^0 and H^0 plotted. Section 6 describes how such scans are done. Note the peak around m_Z, due to this being the maximum tree-level value, and a broad peak around 120 GeV. No experimental constraints are imposed in this scan.

5.2 The effects of different parameters on the h^0 mass

In the preceding section, the h^0-mass was defined by parameters like $\tan\beta$, m_{A^0}, and the stop masses through radiative corrections.

The mass of h^0 has a nice dependence on the parameter X_t/M_S. See both Eq. (5.5) and Fig. 1 in A. Arbey [94]. Through the scans later described in Chapter 6, the figure is reproduced in Fig. 5.2. The lines at 125 ± 2 GeV are placed as reference to the possible h^0 candidate.

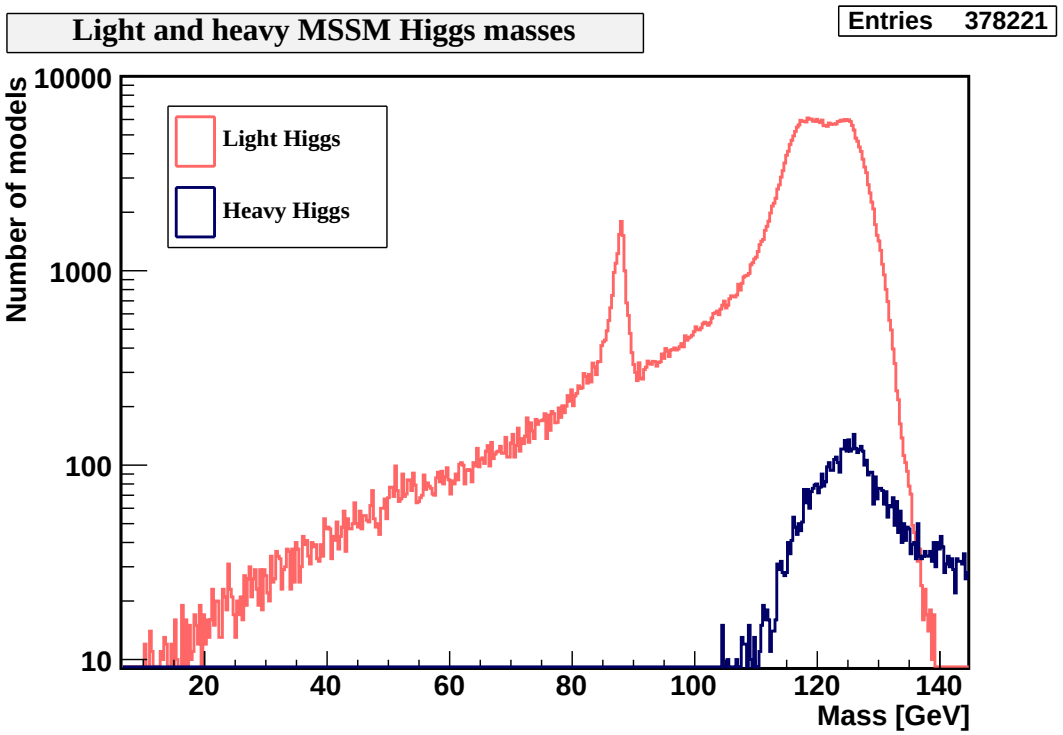

Figure 5.1: The masses of h^0 and H^0.

Another way of looking at this is by constraining the Higgs mass to 125 ± 2 GeV, and plotting X_t versus M_S. See Fig. 5.3. By doing this, it is easy to see how big the SUSY-scale needs to be to get a certain Higgs mass. One prominent feature is the disappearance of models with small stop mixing ($|X_t| \lesssim 2$ TeV). Two cuts are imposed: $\tan\beta < 60$ and $\tan\beta < 5$.

5.3 The width of the CP-even MSSM Higgs bosons

The MSSM Higgs bosons will have different couplings to the SM particles than the SM Higgs. The couplings will get additional factors, which are trigonometric functions of the angles α and β, adopting the 2HDM couplings. At tree-level, we retain a similarity of decay widths compared to the SM, up to these trigonometric factors. This does not include triangle diagrams however, where new mediating particles play a role, or decays with two final supersymmetric particles.

We can define R_i as the couplings between the light MSSM Higgs boson and i, normalized to the SM value. More explicitly,

$$R_W = \frac{g_W}{g_W^{\mathrm{SM}}}, \qquad R_Z = \frac{g_Z}{g_Z^{\mathrm{SM}}}, \qquad R_{u,c,t} = \frac{y_{u,c,t}}{y_{u,c,t}^{\mathrm{SM}}}, \qquad R_{d,s,b} = \frac{y_{d,s,b}}{y_{d,s,b}^{\mathrm{SM}}}, \qquad R_{e,\mu,\tau} = \frac{y_{e,\mu,\tau}}{y_{e,\mu,\tau}^{\mathrm{SM}}}. \quad (5.8)$$

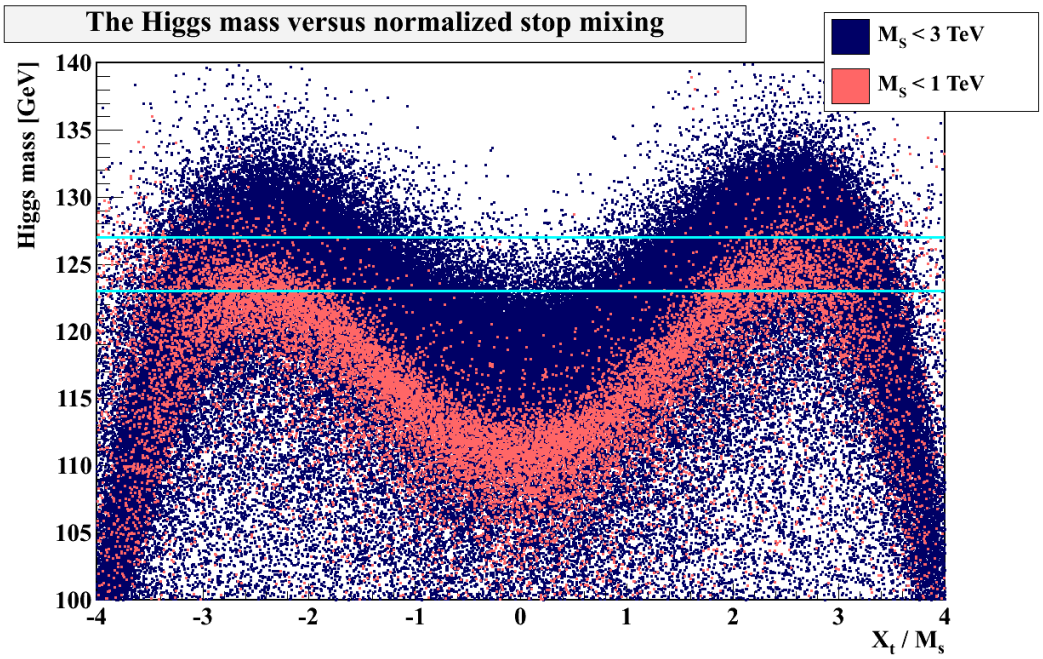

Figure 5.2: The mass of h^0 versus the stop mixing divided by the SUSY scale.

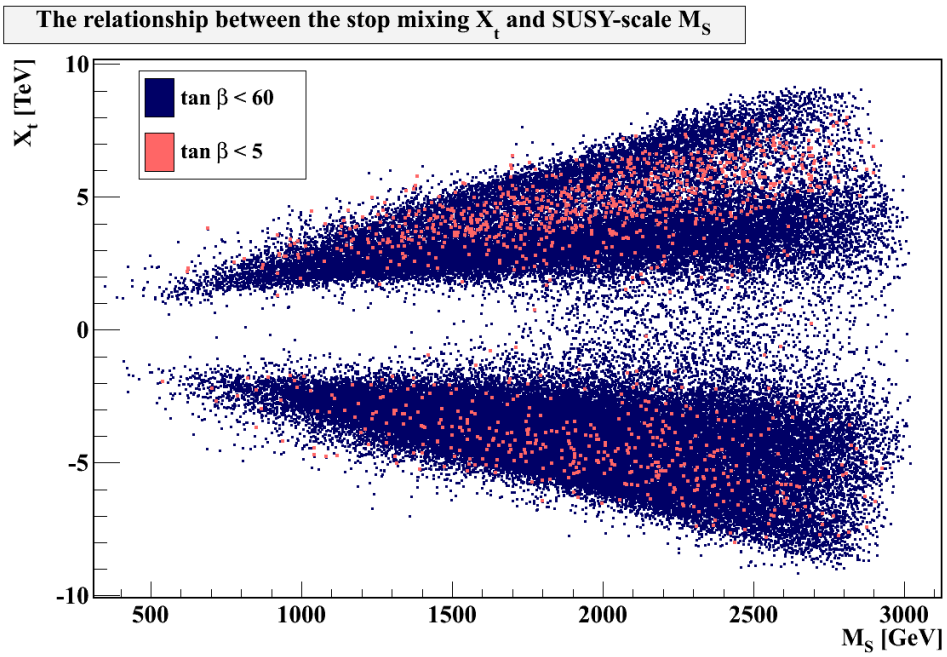

Figure 5.3: The stop mixing versus the SUSY scale. Constraints on the light Higgs mass ($m_h \in [123, 127]$ GeV) and $\tan\beta$ are placed.

The couplings acquire the factors R_i, which are given in [95]. For vectors and up- and down-type fermions, they are

$$R_V \equiv R_W = R_Z = \sin(\beta - \alpha), \qquad R_d = R_e = -\frac{\sin\alpha}{\cos\beta}, \qquad R_u = \frac{\cos\alpha}{\sin\beta}. \tag{5.9}$$

We can also define the normalized couplings between the heavy Higgs H^0 and the different particles:

$$R_V^H = \cos(\beta - \alpha), \qquad R_d^H = \frac{\cos\alpha}{\cos\beta}, \qquad R_u^H = \frac{\sin\alpha}{\sin\beta}. \tag{5.10}$$

Now, the decay widths for the different processes outlined in Section 3 are modified in different ways. For the tree-level (and some of the loop-mediated) processes, the new decay widths are $\Gamma_{\rm SM} R_i^2$, while the more complicated processes are altered in different ways. See Chapter 3 for details on $\Gamma_{\rm SM}$.

5.3.1 $h \to f\bar{f}$

The decay of h^0 to $f\bar{f}$ gets modified with the parameter R_f^2. At tree level, from Eq. (3.15) we get

$$\begin{aligned} \Gamma(h^0 \to f\bar{f}) &= \Gamma_{\rm SM}(H \to l^+l^-) N_c R_i^2, \\ \Gamma(H^0 \to f\bar{f}) &= \Gamma_{\rm SM}(H \to l^+l^-) N_c (R_i^H)^2, \end{aligned} \tag{5.11}$$

where $N_c = 3$ for quarks and 1 for leptons. For up-type particles like u and c (remember that $h^0 \to t\bar{t}$ is kinematically inaccessible), we find

$$\begin{aligned} \Gamma(h^0 \to q\bar{q}) &= \frac{3G_F m_q^2 m_{h^0}}{4\pi\sqrt{2}} \frac{\cos^2\alpha}{\sin^2\beta} \left(1 - 4\frac{m_q^2}{m_{h^0}^2}\right)^{3/2}, \\ \Gamma(H^0 \to q\bar{q}) &= \frac{3G_F m_q^2 m_{H^0}}{4\pi\sqrt{2}} \frac{\sin^2\alpha}{\sin^2\beta} \left(1 - 4\frac{m_q^2}{m_{H^0}^2}\right)^{3/2}, \end{aligned} \tag{5.12}$$

where m_q is the quark mass. For down-type particles like d, s, b and the leptons e, μ and τ, we find

$$\begin{aligned} \Gamma(h^0 \to f\bar{f}) &= \frac{G_F N_c m_f^2 m_{h^0}}{4\pi\sqrt{2}} \frac{\sin^2\alpha}{\cos^2\beta} \left(1 - 4\frac{m_f^2}{m_{h^0}^2}\right)^{3/2}, \\ \Gamma(H^0 \to f\bar{f}) &= \frac{G_F N_c m_f^2 m_{H^0}}{4\pi\sqrt{2}} \frac{\cos^2\alpha}{\cos^2\beta} \left(1 - 4\frac{m_f^2}{m_{H^0}^2}\right)^{3/2}. \end{aligned} \tag{5.13}$$

5.3.2 $h \to V^*V$

The decay $h^0 \to VV$ is kinematically inaccessible, and we need one of the vectors to be virtual. In both cases, that is for W^*W and Z^*Z, the width is rescaled by R_V^2. This is a factor

$$R_V = \sin(\beta - \alpha), \tag{5.14}$$

for the light Higgs, and

$$R_V^H = \cos(\beta - \alpha) \tag{5.15}$$

for the heavy one. The latter can decay into two real vector bosons. See Eq. (3.24) for the complete expression of $H \to V^*V$. This process may also be applied when both vectors are off-shell, i.e. $h^0 \to V^*V^*$.

5.3.3 The loop-mediated decays

The loop mediated decays are affected by the new couplings. In Eqs (3.1), (3.40) and (3.32), the factors R_i^2 are added. Secondly, new charged SUSY particles will contribute in the loops: These are the charged Higgs bosons $H^\pm$, sleptons and squarks $\tilde{f}$, in addition to the charginos $\tilde{\chi}_i^\pm$. The gluon loops are only affected by squarks. For the case of SUSY loop particles, many different couplings are used – this is calculated through `HDECAY`.

5.3.4 Invisible decays

Decays of the Higgs boson into the SUSY particles $\tilde{f}_i\bar{\tilde{f}}_j$ and $\tilde{\chi}_i\tilde{\chi}_j$ are often hard to see in the detector, giving them the name *invisible decays*. Kinematically, this is more important for H^0 than for h^0, but if the SUSY particles are light (below around 60 GeV) we may see decays such as $h^0 \to \tilde{\chi}_1^0\tilde{\chi}_1^0$. In Chapter 7, we will look at the total branching ratio into invisible decays for different scenarios.

5.4 Production of MSSM Higgs bosons

As with the SM, there are many different production channels. In hadron colliders like the LHC, the gluon fusion process $gg \to h$ is still the dominant one. Approximating the production to only this channel is valid at the 10% level: See Fig. 41 in Dittmaier *et al.* [30]. There are many sources for an altered cross section: New couplings R_t, R_b and loop contributions from squarks are two examples. We ignore the effect from the latter, and focus on the new couplings. According to Dittmaier *et al.* [30], this is a reasonable approximation, and we remember that there are already some sources for uncertainty on the cross sections.

In Section 3.6.1, a method for calculating the SM cross section was outlined. If we assume the gluon loop process to consist of top and bottom quarks, the cross section has three contributions: Two pure quark terms σ_{bb} and σ_{tt}, and an interference term σ_{bt}. From J. Gunion *et al.* [9], the amplitude squared (and cross section) is proportional to

$$\sigma \sim \left| \tau_b[1 + (1 - \tau_b)f(\tau_b)] + \tau_t[1 + (1 - \tau_t)f(\tau_t)] \right|^2, \tag{5.16}$$

where $\tau_i = 4m_i^2/m_{h^0}^2$, and $f(\tau)$ is defined in Eq. (3.4). The real part of the loop integral, or $f(\tau)$, is negative for $2m_b < m_{h^0} < 2m_t$: The σ_{bt} interference is destructive.

Now we can calculate the MSSM h^0 production cross section with the method from S. Dittmaier *et al.* [30]:

$$\sigma^{\text{MSSM}} = R_t^2\sigma_{tt} + R_b^2\sigma_{bb} + R_tR_b\sigma_{bt}. \tag{5.17}$$

Practically, we find the separate terms by calculating the SM cross section in `HIGLU`, setting $g_b = 0$ for σ_{tt}, and conversely, $g_t = 0$ for σ_{bb}. The interference term is found by looking at the difference between σ^{SM} and $\sigma_{tt} + \sigma_{bb}$.

In Fig. 5.4 we compare the cross section calculated here with σ^{SM}. Note that most of the non-SM-like cross sections in pMSSM disappear when we apply the constraints (red points), which are described in Chapter 6.

5.5 Corrections to the parameters

In essence, the electroweak and QCD-corrections we found in Chapter 3 can be used here as well. Care must be taken when doing loop corrections, to account for modified couplings and new SUSY particles in the loops. The details of this will not be treated here, but some qualitatively new corrections will be mentioned.

Two of the methods to implement higher-order corrections (apart from the corrections to m_h, which were discussed in Section 5.1) are to include loop effects in the heavy quark masses m_b and m_t, and in the angle α used in couplings to the Higgs bosons.

5.5.1 Corrections to the mixing angle: $\bar{\alpha}$

The same radiative corrections which affect the neutral Higgs bosons also affect the angle α. Therefore, we can use the same approximation scheme: A correction to $\epsilon/\cos 2\beta$ is added to the denominator in Eq. (4.22). From A. Djouadi [26], this is

$$\tan 2\bar{\alpha} = \tan 2\beta \frac{m_A^2 + m_Z^2}{m_A^2 - m_Z^2 + \epsilon/(\sin^2\beta\cos 2\beta)}, \qquad -\frac{\pi}{2} \leq \bar{\alpha} \leq 0. \tag{5.18}$$

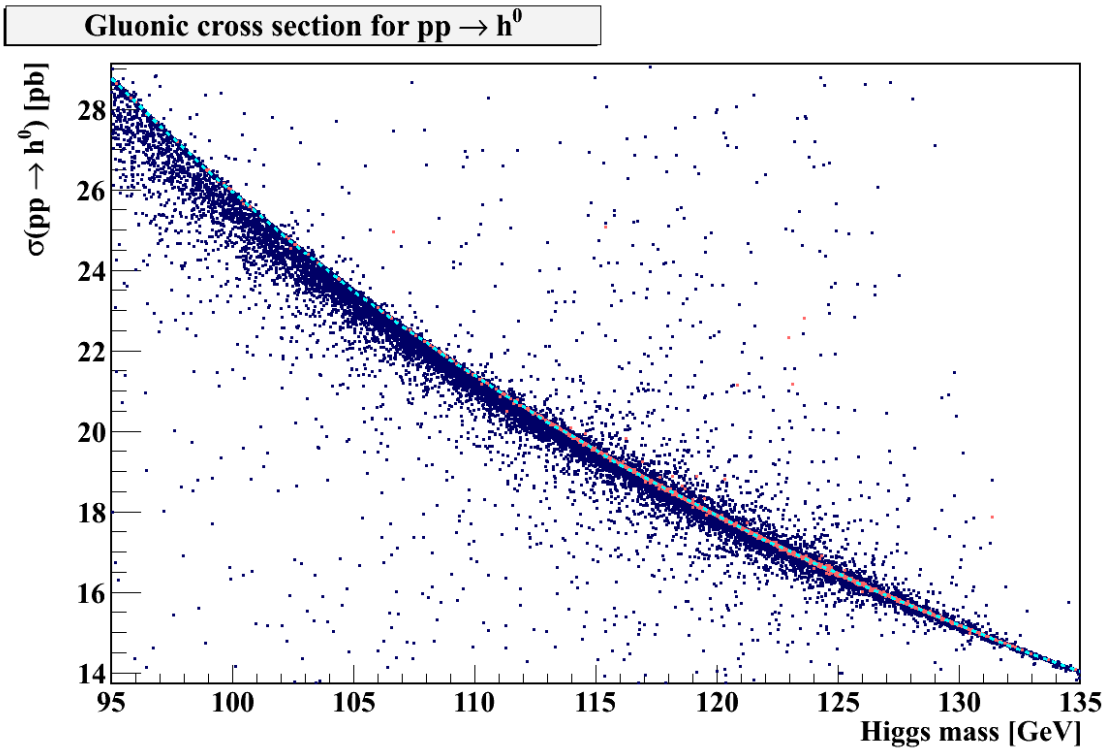

Figure 5.4: The gluonic contribution to the cross section $pp \to h^0$. The blue points are all models, whereas the red points follow the tight constraints described in the next chapter. The dashed cyan line signifies the SM value.

The correction ϵ was defined in Eq. (5.5). Now, this $\bar{\alpha}$ may be used in any place where α was earlier used. As an example, the g_{h^0VV} coupling becomes

$$R_V = \sin(\beta - \bar{\alpha}). \tag{5.19}$$

5.5.2 Corrections to the heavy quark masses: Δ_b, Δ_t

The heavy quarks (and τ) are affected by SUSY-QCD corrections from squark/gluino loops (see Section 1.1.6 of A. Djouadi [26]), parametrized by Δ_b and Δ_t. The functions Δ_q are defined as the ratio

$$\Delta_q \equiv \frac{\Delta m_q}{m_q}. \tag{5.20}$$

With the auxiliary function

$$I(x,y,z) = \frac{xy\ln(x/y) + yx\ln(y/z) + xz\ln(z/x)}{(x-y)(y-z)(z-x)}, \tag{5.21}$$

we can write the approximate corrections to the 3rd generation fermion masses from:

$$\begin{aligned}
\Delta_\tau &\simeq \frac{\alpha}{4\pi}\left[\frac{M_1\mu}{\cos^2\theta_W} I(M_1^2, m_{\tilde{\tau}_1}^2, m_{\tilde{\tau}_2}^2) - \frac{M_2\mu}{\sin^2\theta_W} I(M_2^2, m_{\tilde{\nu}_\tau}^2, \mu^2)\right]\tan\beta, \\
\Delta_b &\simeq \left[\frac{2\alpha_s}{3\pi}\mu m_{\tilde{g}} I(m_{\tilde{g}}^2, m_{\tilde{b}_1}^2, m_{\tilde{b}_2}^2) + \frac{m_t^2}{8v^2\pi^2\sin^2\beta} A_t\mu I(\mu^2, m_{\tilde{t}_1}^2, m_{\tilde{t}_2}^2)\right]\tan\beta, \\
\Delta_t &\simeq -2\frac{\alpha_s}{3\pi} m_{\tilde{g}} A_t I(m_{\tilde{g}}^2, m_{\tilde{t}_1}^2, m_{\tilde{t}_2}^2) - \frac{m_b^2}{8v^2\pi^2\cos^2\beta}\mu^2 I(\mu^2, m_{\tilde{b}_1}^2, m_{\tilde{b}_2}^2).
\end{aligned} \tag{5.22}$$

This is most important for Δ_b, and will in turn affect the coupling R_b. From [26, 30],

$$R_b \simeq -\frac{\sin\bar{\alpha}}{\cos\beta}\left[1 - \frac{\Delta_b}{1+\Delta_b}(1 + \cot\bar{\alpha}\cot\beta)\right]. \tag{5.23}$$

For completeness, the correction for R_b^H is given by

$$R_b^H \simeq \frac{\cos\bar{\alpha}}{\cos\beta}\left[1 - \frac{\Delta_b}{1+\Delta_b}(1 - \tan\bar{\alpha}\cot\beta)\right]. \tag{5.24}$$

Chapter 6

Scans of the pMSSM parameter space

The large number of parameters in the pMSSM makes detailed analyses hard to do analytically. While a calculation of the tree level value of a decay channel may be trivial, higher order corrections on a number of the involved components will greatly increase the complexity.

In analyses involving 2 or 3 variables, one might picture a grid: Dividing each variable into partitions, creating unique areas or volumes. Each of these will correspond to a "point" in the parameter space. The number of different points increases as n^D, where n is the number of partitions per variable and D is the number of variables. In pMSSM, there are 22 parameters. Even with a very coarse-grained partitioning (say, 5 per variable), $5^{22} \sim 2$ quadrillion. This is clearly unfeasible.

The strategy, then, is to employ a random scan à la Monte Carlo. It will not exhaust the parameter space, but will give us a good idea of its structure. It is also scalable, since more points only will add to the statistics. A sample run with 100 models will most probably point in the same direction as a full run with 10^7 points, whereas in systematic "grid" scans this is often not the case.

For each model, each of these 22 parameters is generated as a random number within a given range, and then fed to different spectrum and decay calculators.

In the following sections, these parameters and calculators will be discussed. We will start with an outline of the parameters and their ranges in Section 6.1. After that, the different programs and some modifications which have had to be done on them are given in Sections 6.2 through 6.4. Sections 6.5 and 6.6 will be devoted to the numerous constraints we impose on the models.

Parameter	Range
$\lvert M_1, M_2\rvert$	[50, 1500] GeV
A_u, A_d, A_e	[-9000, 9000] GeV
A_t, A_b, A_τ	[-9000, 9000] GeV
μ	[-9000, 9000] GeV
m_A	[50, 3000] GeV
$m_{\tilde{\ell}}, m_{\tilde{e}_\mathrm{R}}, m_{\tilde{q}}, m_{\tilde{u}_\mathrm{R}}, m_{\tilde{d}_\mathrm{R}}$	[50, 3000] GeV
$m_{\tilde{L}}, m_{\tilde{\tau}_\mathrm{R}}, m_{\tilde{Q}}, m_{\tilde{t}_\mathrm{R}}, m_{\tilde{b}_\mathrm{R}}$	[50, 3000] GeV
M_3	[50, 3000] GeV
$\tan\beta$	[1, 60]

Table 6.1: Parameter ranges for the scans.

6.1 Parameters

In Section 4.6, the model pMSSM was outlined together with the parameters involved. Here, we will describe the bounds on each parameter in the scans performed. Many different schools of thought exist when placing such bounds. C. Berger *et al.* [86] use high bounds on the soft SUSY-breaking parameters (3 TeV in logarithmic scans, 1 TeV in linear scans). Some argue that a low m_A (already at a few hundred GeV) triggers the decoupling limit, making it unnecessary to raise m_A further. Arbey *et al.* [96] use high limits for the trilinear couplings A_i.

Table 6.1 summarizes the limits used in the scans described above. See Table 4.4 for a description of each parameter. Each value is chosen uniformly (or linearly) between the bounds. The result is saved to an SLHA file, which is used as input for `SuSpect`. If no error flags are raised, the result is saved to a new SLHA file, on which further manipulations are done.

6.2 The SUSY Les Houches Accord (SLHA) format

The plethora of different SUSY model generators, spectrum calculators, decay packages and event generators creates the need for a standardized interface. Following the philosophy of `FORTRAN`, The SUSY Les Houches Accord [97] provides a framework for storing information about a supersymmetric model in different `BLOCK` sectors: `EXTPAR`, `SMINPUTS`, `MASS` and

DECAYS are such examples. As an example, the format of the MASS block is

```
BLOCK  MASS
PID1   VALUE1
PID2   VALUE2
```
(6.1)

PID is the particle ID in the *Monte Carlo numbering scheme*, described in chapter 35 of the PDG review [2]. An SLHA file is usually readable by programs calculating SUSY quantities, both by input and output. Often, a specific calculator will take an input SLHA file, outputting the same file but with its own values added.

6.3 The programs

6.3.1 SuSpect

SuSpect, or SUpersymmetric SPECTrum calculator, is created by A. Djouadi *et al.* [98]. It takes a parameter point, a number of options, and calculates:

1. All the masses of the supersymmetric particles in pMSSM. It evaluates two-loop expressions for the renormalization group equations, for the radiative corrections to the Higgs boson masses, and also radiative corrections to the masses of the squarks and gauginos.

2. Values for different experimental processes to be used as constraints. These are the supersymmetric contributions to the muon magnetic dipole moment, electroweak corrections and the rate for $b \to s\gamma$.

The output is stored as SLHA files. It should be said that SuSpect provides its own caller file suspect2_call.f, where all the parameters can be initialized. Here, each model point is defined, and the main program suspect2.f is looped over with a new model each time. The end result is a folder containing multiple SLHA files.

There are two main ways of generating a parameter point: Either through a loop in the caller file, or through an input SLHA file. In the latter case, an external program must create the necessary parameters. Both of these will be mentioned shortly in Section 6.4.

6.3.2 HDECAY

The program HDECAY, also developed by A. Djouadi *et al.* [99], adds decay tables for each model provided. It calculates the width and branching ratio for each of the five Higgs bosons

in the MSSM. Their mixing angles and couplings are also found. `HDECAY` uses complete radiative corrections due to top/bottom quark and squark loops, next-to-leading order QCD corrections and full mixing in the stop and bottom sectors.

It can also be used as a SM Higgs decay calculator, which was done to check the results in Section 3. Practically, a `Python` program controls the work flow: An input SLHA file from `SuSpect` is given to `HDECAY`, the output SLHA file copied to a new directory.

6.3.3 `HIGLU`

The program `HIGLU` [45], created by M. Spira, calculates the production cross section for the Higgs, through the gluon-fusion contribution to the process $pp \to H$. This is the leading production channel at the LHC. The cross section is calculated with next-to-leading order QCD corrections, both in the case of the SM and the MSSM. See Sections 3.6.1 and 5.4 for more information on the production mechanisms through gluon fusion.

The integration of the parton density functions (PDFs) is a time demanding process, and due to some other limitations like theoretical uncertainties in the Higgs boson mass, we limit the program to SM calculations. It is possible to set the couplings between Higgs and the quarks separately, which is needed when the MSSM cross sections are calculated. This process is described in Section 5.4, and the PDFs in Section 2.9.1.

In order to interface `HIGLU` with the PDFs, the framework `LHAPDF` [100] is used.

6.3.4 `DarkSusy`

In Section 4.1.2, the neutralino $\tilde{\chi}_0^1$ was proposed as a dark matter candidate. There are a number of ways to test a given pMSSM model against the constraints from astrophysical data and scattering experiments on earth. The program `DarkSusy` [101] will calculate all these values: The LSP relic density in terms of $\Omega_{\mathrm{DM}}h^2$, and the spin dependent, independent and thermally averaged cross sections.

The program uses SLHA files, and writes the output as a simple text file with the desired information. This is appended to the input SLHA file, in a new structure we have called `BLOCK RELICS`.

6.4 Modifications to the standard program files

In order for the programs to perform optimally, some modifications and even bug fixes had to be made.

In `SuSpect`, the follow changes have been done:

1. Generation of the random parameters, looping over each model, and copying of the result files. This was done in `suspect2_call.f`.

2. An extra test condition `.or.input.eq.11` in `suspect2.f`, line 524. Without this, some variables are not transferred correctly before calculations, and the output file is useless. This error is known, but not corrected in the public version 2.41, as stated by J-L. Kneur [102].

3. Corrections to the neutralinos will sometimes yield a `NaN` ("Not a Number") for their masses. This will create a segmentation fault, aborting the scan. A test for this has been implemented, gracefully aborting, allowing the routine to continue with the next model. The test is inserted in the main program `hdecay.f`, before the `SU_GAUGINO` call in line 1910. The authors have been notified [102].

4. There are different ways to create the points, and some care must be taken when looping inside the caller file `suspect_call.f`. Not every shared variable (those inside the common blocks) is reset after the point is generated. This will cause an asymmetry in the distribution of the models generated, see Fig. 6.1. The sign of the parameter μ plays a vital role in this case. If a line `sgnmu0 = 0` is added before a new parameter point is generated, this asymmetry disappears. It should also be noted that using SLHA input may distort the Higgs masses: This behavior was observed, and these kinds of scans were abandoned. See Fig. 6.2 for an example of this.

In `HDECAY`,

1. The SUSY-QCD correction factor to the $h^0 \to b\bar{b}$ rate can deviate wildly from its intended value of ~ 1. This in turn will create negative values for the width. According to the author, this behavior is known but not documented. Those models should be discarded, which M. Spira pointed out in [103].

2. The particle ID for the light CP-even Higgs h^0 is wrongly set to 26 in the SLHA output. In line 1844 of `hdecay.f`, the number 26 should be 25, which is the correct PID for h^0.

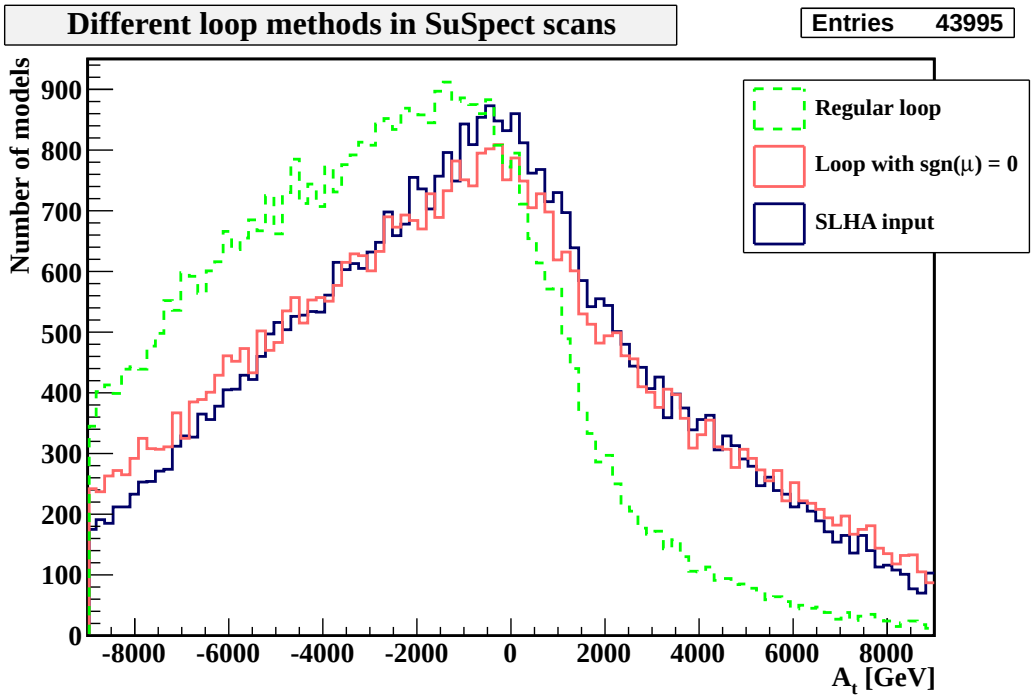

Figure 6.1: Three different ways of generating points in `SuSpect`*: With and without resetting the value of* `sgnmu0`*, and using SLHA input files. See the text for more information.*

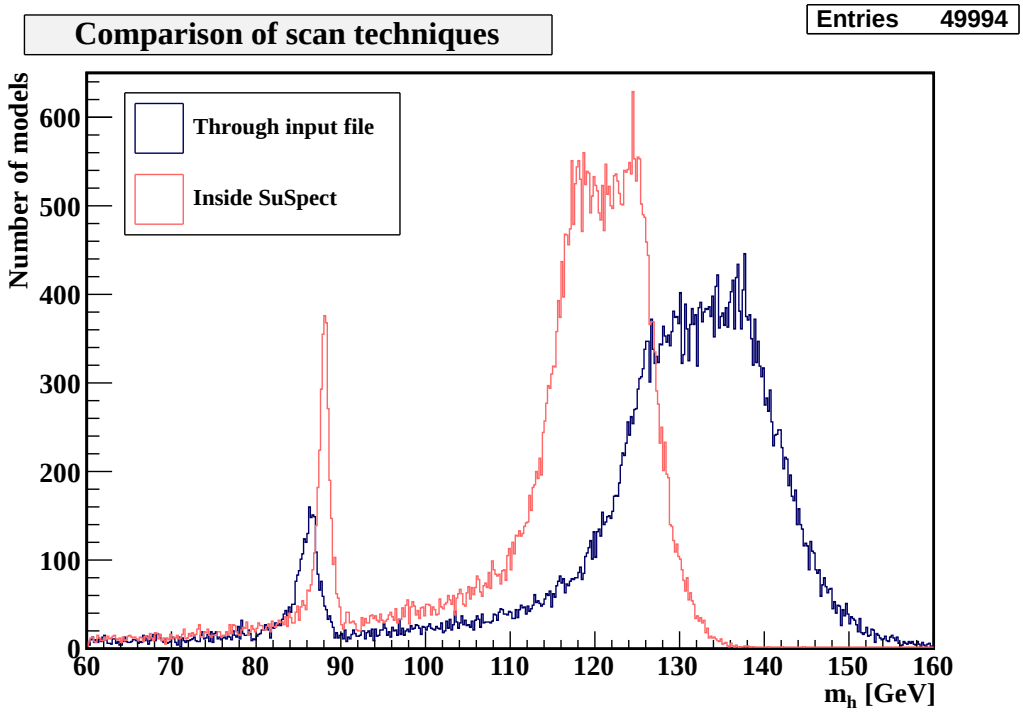

Figure 6.2: Difference in light Higgs masses between internal `SuSpect` *loop and SLHA input.*

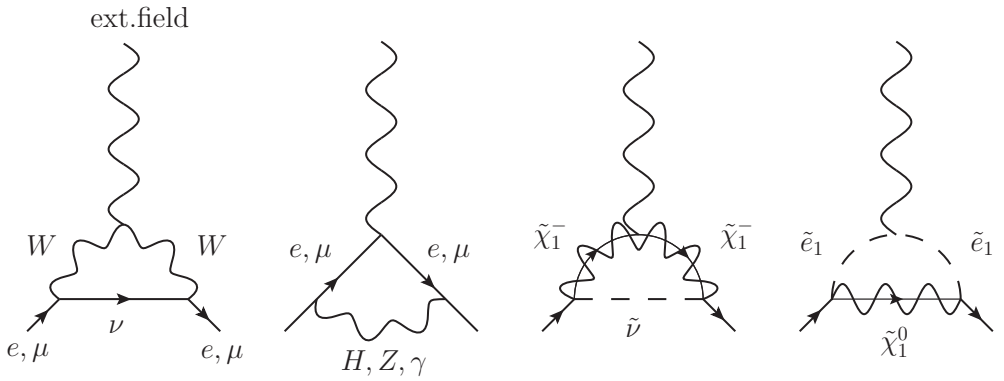

Figure 6.3: Some of the loops for the dipole moment of electrons and muons. The two first are from the SM, while the last two are from the MSSM.

6.5 Bounds from experimental results

6.5.1 The anomalous dipole moment of the muon: $g - 2$

The magnetic moment of a spin 1/2 particle can be derived from the Dirac equation, and is on the form

$$\mu = -\frac{e}{2m}. \tag{6.2}$$

Higher order corrections have been calculated both for the muon and the electron. In both cases a first order correction from the loops in Fig. 6.3 is applied, with the result

$$\mu = -\frac{e}{2m}\left(1 + \frac{\alpha}{2\pi}\right) \equiv -\frac{e}{2m}\left(1 + a_e\right). \tag{6.3}$$

This correction was derived by Schwinger in 1948 [104]. Later results (experimental and theoretical up to $\mathcal{O}(\alpha^4)$, from F. Mandl and G. Shaw [24]) give the value for the electron

$$\begin{aligned} a_e^{th.} &= (1159652183 \pm 8) \cdot 10^{-12} \\ a_e^{exp.} &= (1159652181 \pm 7) \cdot 10^{-12} \end{aligned} \tag{6.4}$$

These results are in excellent agreement with each other.

For the muon, the agreement is not so good. Theoretical values from different processes are given in [105–109], summarized by F. Jegerlehner and A. Nyffeler in [110]. Experimental values from the E821 experiment at Brookhaven [111] are also given below:

$$\begin{aligned} a_\mu^{th.} &= (11659180 \pm 5) \cdot 10^{-10} \\ a_\mu^{exp.} &= (11659209 \pm 6) \cdot 10^{-10} \end{aligned} \tag{6.5}$$

This discrepancy is often attributed to new physics, which will create new loop diagrams and push the theoretical value up or down. The discrepancy is

$$\Delta a_\mu = a_\mu^{exp.} - a_\mu^{\mathrm{SM}} = (290 \pm 90) \cdot 10^{-11}. \tag{6.6}$$

The leading contributions from MSSM is through chargino and neutralino loops. From F. Jegerlehner and A. Nyffeler [110],

$$\begin{aligned} a_\mu^{\mathrm{SUSY}} &\simeq a_\mu^{\tilde{\chi}^\pm} + a_\mu^{\tilde{\chi}^0} \\ &\simeq \frac{\mathrm{sgn}(\mu M_2)\alpha}{8\pi \sin^2\theta_W} \frac{(5+\tan^2\theta_W)}{6} \frac{m_\mu^2}{M_S^2} \tan\beta \left(1 - \frac{4\alpha}{\pi} \ln\frac{M_S}{m_\mu}\right). \end{aligned} \tag{6.7}$$

The program `SuSpect` returns the value a_μ^{SUSY}, and a constraint here may be placed early in the process. Fig. 6.4 shows the distribution of a_μ^{SUSY} versus both the SUSY scale M_S and $\tan\beta$, together with a $\pm 3\sigma$ band. Models that give a_μ a correct contribution can be characterized by a central M_S value

$$1000 \text{ GeV} < M_S < 2500 \text{ GeV}, \tag{6.8}$$

and values of $\tan\beta$ above 5-6, as a_μ^{SUSY} grows as $\tan^2\beta$.

This constraint is not always taken as absolute. For example, J. Ellis *et al.* [112] points out that the calculation of a_μ^{SM} is not completely certain. In addition, we do not know if the whole discrepancy Δa_μ needs to be closed by MSSM. In constrained MSSM models like mSUGRA, a very large fraction of the models will fail the $g-2$ test, so this constraint is often overlooked.

6.5.2 Electroweak corrections: $\Delta\rho$

In the standard model, the self energy corrections to the massive gauge bosons is defined as

$$\frac{1}{1-\Delta\rho} = \frac{\Pi_{ZZ}(0)}{M_Z^2} - \frac{\Pi_{WW}(0)}{M_W^2}, \tag{6.9}$$

where Π_{ZZ} and Π_{WW} are the radiative self energy corrections (or vacuum polarizations) to the Z and W bosons, evaluated at zero momentum transfer. In the standard model, $\Delta\rho$ is dominated by the top quark. From A. Djouadi [113],

$$\Delta\rho^{(t)} = \frac{3\alpha}{16\pi \sin^2\theta_W \cos^2\theta_W} \frac{m_t^2}{m_Z^2} \sim 9 \times 10^{-3}. \tag{6.10}$$

Some one-loop and two-loop contributions are shown in Fig. 6.5.

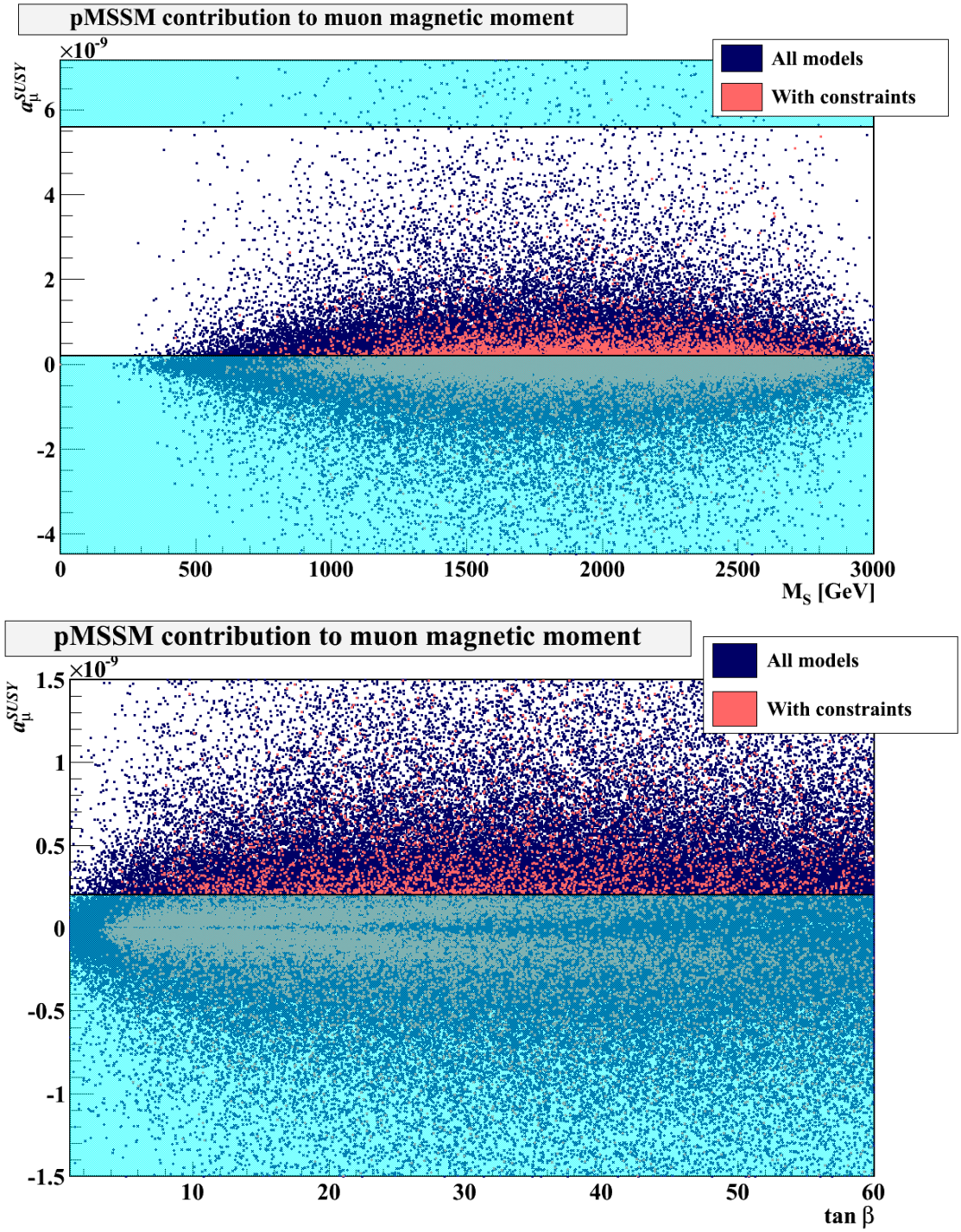

Figure 6.4: The M_S and $\tan\beta$ dependence on the pMSSM *contribution for a_μ in a scan. Note the lines at $\Delta a_\mu \pm 3\sigma$.* **Top***: M_S,* **Bottom***: $\tan\beta$.*

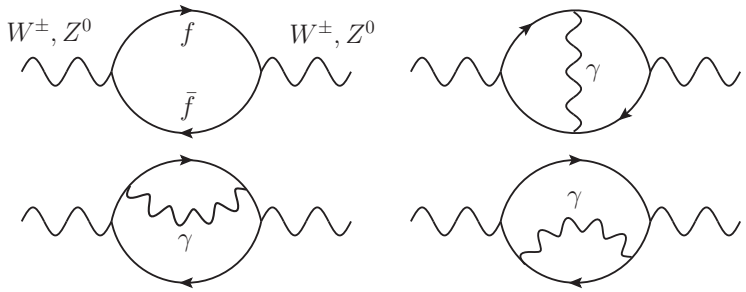

Figure 6.5: One- (upper left) and two-loop contributions to the gauge boson self energy, from A. Djouadi [114].

The supersymmetric contributions can grow large if there are large mass splittings in the same SU(2) doublet. There is also a contribution from the Higgs bosons. We first define some functions

$$\begin{aligned} f(x,y) &= x + y - \frac{2xy}{x-y}\ln x/y, \qquad \tau_i = \frac{m_i^2}{m_W^2}, \qquad \eta_i = \frac{m_i}{m_Z^2} \\ f_1(x) &= x\left[\frac{\ln\cos^2\theta_W - \ln x}{\cos^2\theta_W - x} + \frac{\ln x}{\cos^2\theta_W(1-x)}\right] \\ f_2(x,y) &= \frac{xy}{x-y}\ln\frac{x}{y} + \frac{1.165}{2}(x+y), \end{aligned} \tag{6.11}$$

and given in Chapter 1 of A. Djouadi [26], the SUSY contributions from squarks and Higgs bosons to $\Delta\rho$ are

$$\Delta\rho^{\text{SUSY}} = \Delta\rho^{\text{Higgs}} + \Delta\rho^{\tilde{t},\tilde{b}}, \tag{6.12}$$

where the Higgs contribution is

$$\begin{aligned} \Delta\rho^{\text{Higgs}} = -\frac{G_F m_W^2}{8\sqrt{2}\pi^2}\Big\{ & 3\sin^2(\beta-\alpha) f_1(\eta_{h^0}) + 3\cos^2(\beta-\alpha) f_1(\eta_{H^0}) \\ & + \sin^2(\beta-\alpha)\left[f_2(\tau_{H^\pm},\tau_{H^0}) - f_2(\tau_{A^0},\tau_{H^0})\right] + f_2(\tau_{H^\pm},\tau_{A^0}) \\ & + \cos^2(\beta-\alpha)\left[f_2(\tau_{H^\pm},\tau_{h^0}) - f_2(\tau_{A^0},\tau_{h^0})\right]\Big\}, \end{aligned} \tag{6.13}$$

and the stop/sbottom contribution is

$$\Delta\rho^{\tilde{t},\tilde{b}} = \frac{3G_F}{4\pi^2\sqrt{2}}\left[\cos^2\theta_t f(m_{\tilde{t}_1}^2, m_{\tilde{b}_1}^2) + \sin^2\theta_t f(m_{\tilde{t}_2}^2, m_{\tilde{b}_1}^2) - \cos^2\theta_t \sin^2\theta_t f(m_{\tilde{t}_1}^2, m_{\tilde{t}_2}^2)\right]. \tag{6.14}$$

The angle θ_t is the stop mixing angle, defined in Eq. (4.25).

`SuSpect` also calculates $\Delta\rho$, and with more contributions than we have showed here. It is possible to only keep models where this extra contribution is within 3σ of the SM value:

$$\left|\Delta\rho^{(\text{SUSY})}\right| < 3\cdot 10^{-3}. \tag{6.15}$$

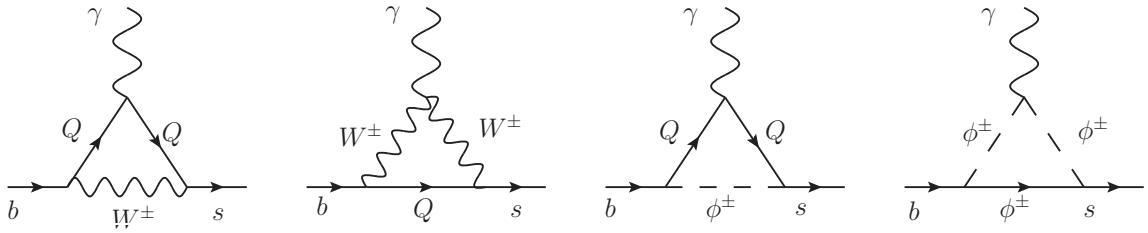

Figure 6.6: Different diagrams contributing to $b \to s\gamma$. The two to the left are from the SM [115]*, while the two to the right are from MSSM* [116, 117]*. q_i is any quark, u_i is any up-type quark. $\phi = H^\pm, G^\pm$.*

In Fig. 6.8 we show this contribution, where the cyan area is excluded by 3σ. Only models below should be considered.

6.5.3 Precision flavor physics: $b \to s\gamma$

Decays like $B \to X_s\gamma$ happen at loop level in the SM, involving charge up-type quarks and W bosons. In SUSY theories, this will happen at the same level of perturbation theory, involving charginos, stops, top quarks and charged Higgs bosons. This decay is calculated by M. Misiak *et al.* [118]:

$$[\mathrm{BR}(b \to s\gamma)]_{th.} = (3.15 \pm 0.23) \times 10^{-4}. \tag{6.16}$$

Fig. 6.6 shows the diagrams at leading order. The Babar [119] and Belle [120] collaborations have measured the rate $b \to s\gamma$, and we use some extrapolations from the PDG [2]:

$$[\mathrm{BR}(b \to s\gamma)]_{exp.} = (3.61 \pm 0.49) \cdot 10^{-4}. \tag{6.17}$$

`SuSpect` outputs the value of $\mathrm{BR}(b \to s\gamma)$, these are shown in Fig. 6.7.

6.5.4 Light charginos

A (still unpublished) combination of the four LEP experiments gives a limit on the lightest chargino $\tilde{\chi}_1^\pm$ in the general MSSM, which is the kinematical limit from e^+e^- collisions at $\sqrt{s} \simeq 209$ GeV. From the PDG [2], this lower limit is

$$\tilde{\chi}_1^\pm > 103.5 \text{ GeV}. \tag{6.18}$$

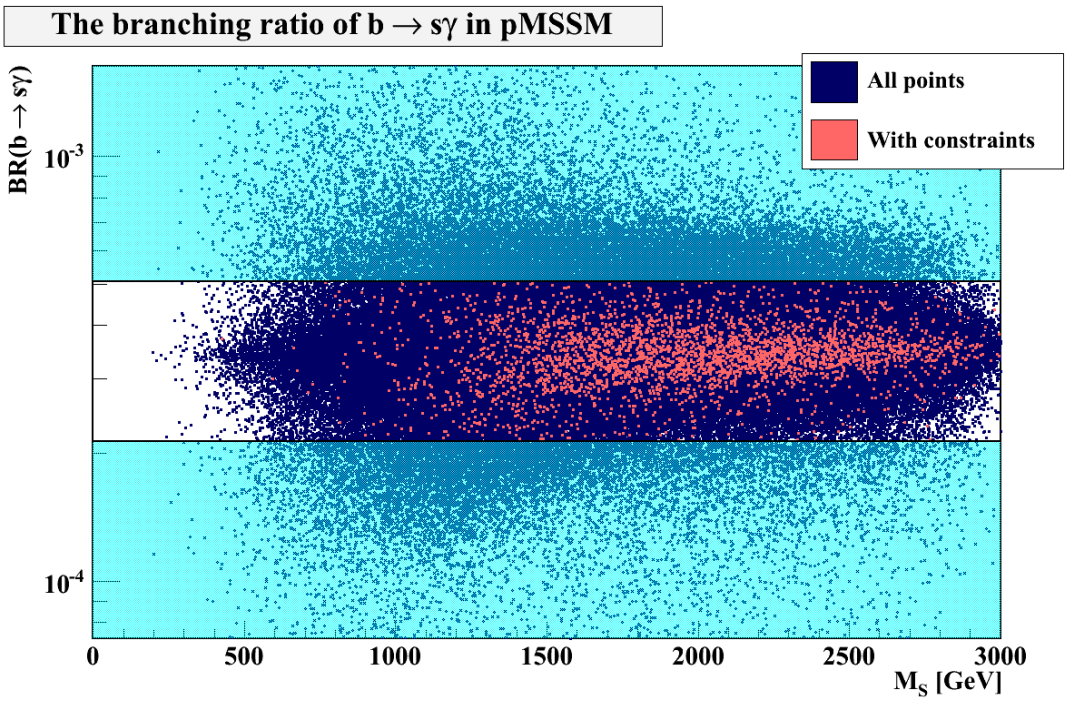

Figure 6.7: The $b \to s\gamma$ dependence on M_S, as defined in (6.17).

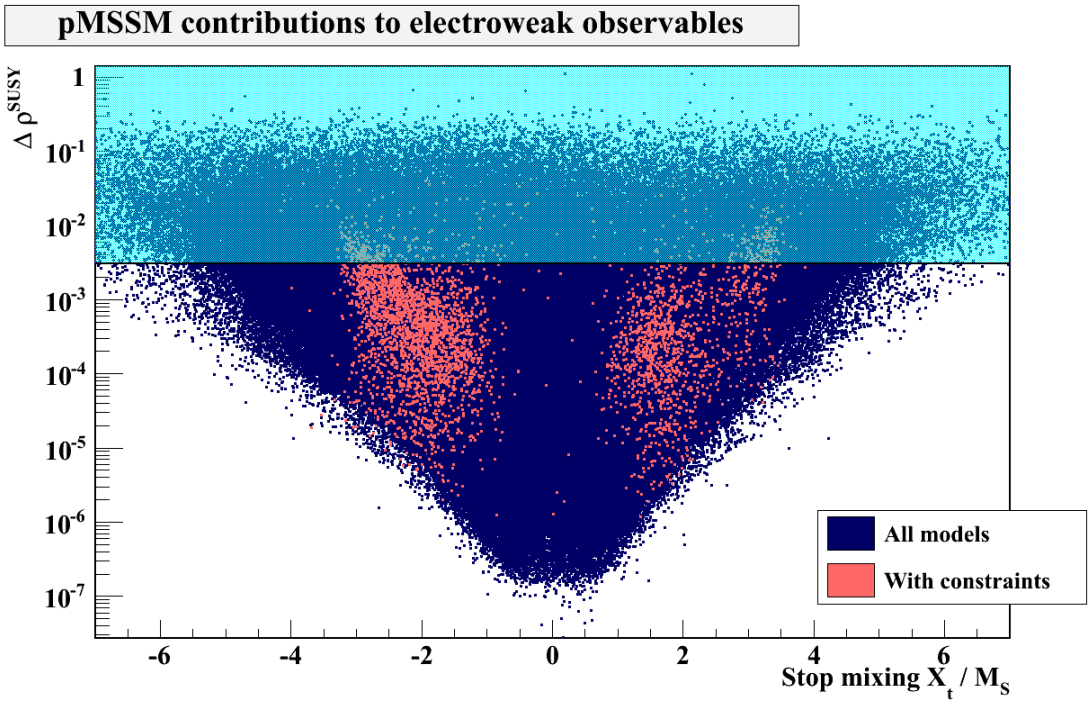

Figure 6.8: The pMSSM contributions to $\Delta\rho$, as a function of the stop mixing, normalized to the SUSY mass scale.

6.5.5 Relic neutralino density

The relic density of the neutralino is calculated from its cross section to different particles, together with thermal averaging with the Boltzmann equation. See J. Edsjo and P. Gondolo [121]. This is done using the program `DarkSusy` [101] as described earlier. The value found is compared to the one from the WMAP data [69]:

$$\Omega_{\mathrm{DM}} h^2 = 0.1123 \pm 0.0035. \tag{6.19}$$

From `DarkSusy`, these values are shown in Fig. 6.9.

If there is a small mass splitting between the next-to-lightest SUSY particle (NLSP) and the LSP $\tilde{\chi}_1^0$, *coannihilation* may occur, see J. Ellis [122]. These are processes like $\tilde{\tau}_1 \tilde{\chi}_1^0 \to Z\tau$. A small mass splitting means that they are thermally available in the same time frame since Big Bang. This way, a large fraction of the $\tilde{\chi}_1^0$ can coannihilate before they are "frozen out", and the relic density will be much lower. Fig. 6.10 shows the correlation between the mass splitting and $\Omega_{\mathrm{DM}} h^2$.

With this constraint, a large portion of the models are rejected: Almost every model with a mass splitting

$$m_{\mathrm{NLSP}} - m_{\tilde{\chi}_1^0} > 70 \text{ GeV} \tag{6.20}$$

will create huge relic densities, far above the measured values.

6.5.6 Dark matter detection experiments

There are two main methods for searching for a weakly interacting massive particle (WIMP):

1. **Direct detection**, where neutralinos scatter on atomic nuclei. The XENON experiment in Gran Sasso [61] gives spin-independent limits on the WIMP-nucleon cross section. Fig. 6.11 shows these limits against values from `DarkSusy`.

2. **Indirect detection**, where annihilation products are observed in telescopes: Gamma rays at the Fermi Large Area Telescope [58], Cherenkov radiation at HESS [59, 62] and neutrinos at XENON [61] in the Antarctic. Each of these is shown against their respective calculated values (spin dependent WIMP-nucleon cross section for IceCube and the thermally averaged one for Fermi-LAT and HESS in Figs. 6.12 and 6.13.

We require that the cross sections generated from `DarkSusy` are below the limits set by these experiments.

Many of these experiments are still in their relative infancy, and as they collect more data they will be able to set lower limits or find signals. As an example, the "100" in XENON100

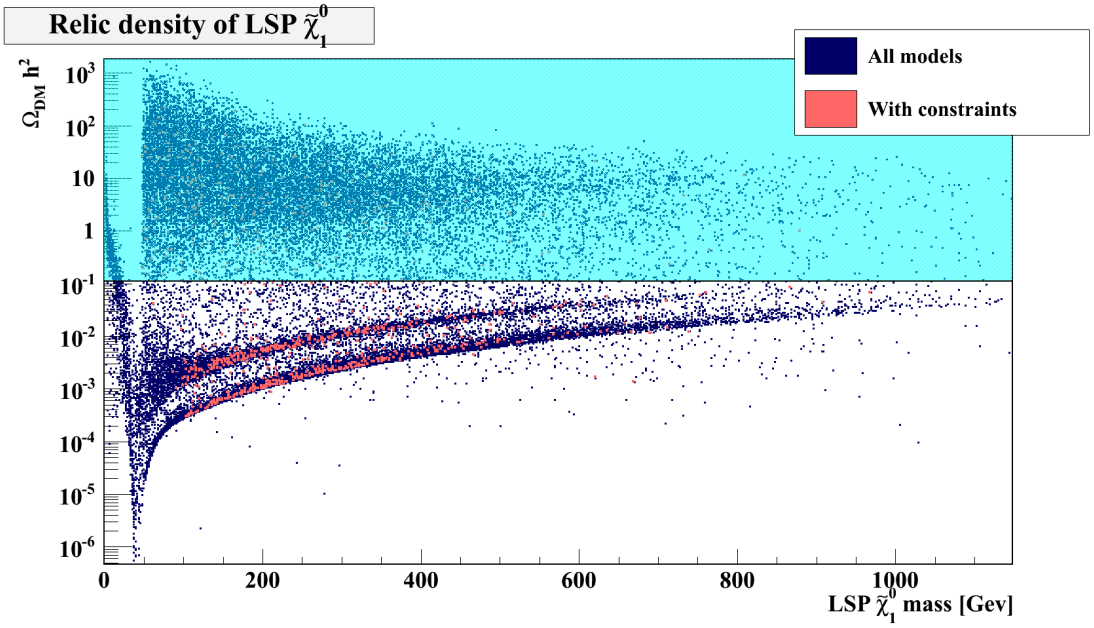

Figure 6.9: The calculated relic density versus $\tilde{\chi}_1^0$ mass. The constrains on the red dots are $m_{h^0} \sim 125$ GeV, $m_{\tilde{\chi}_1^\pm} > 103.5$ GeV and $\Delta\rho, \Delta a_\mu, b \to s\gamma$.

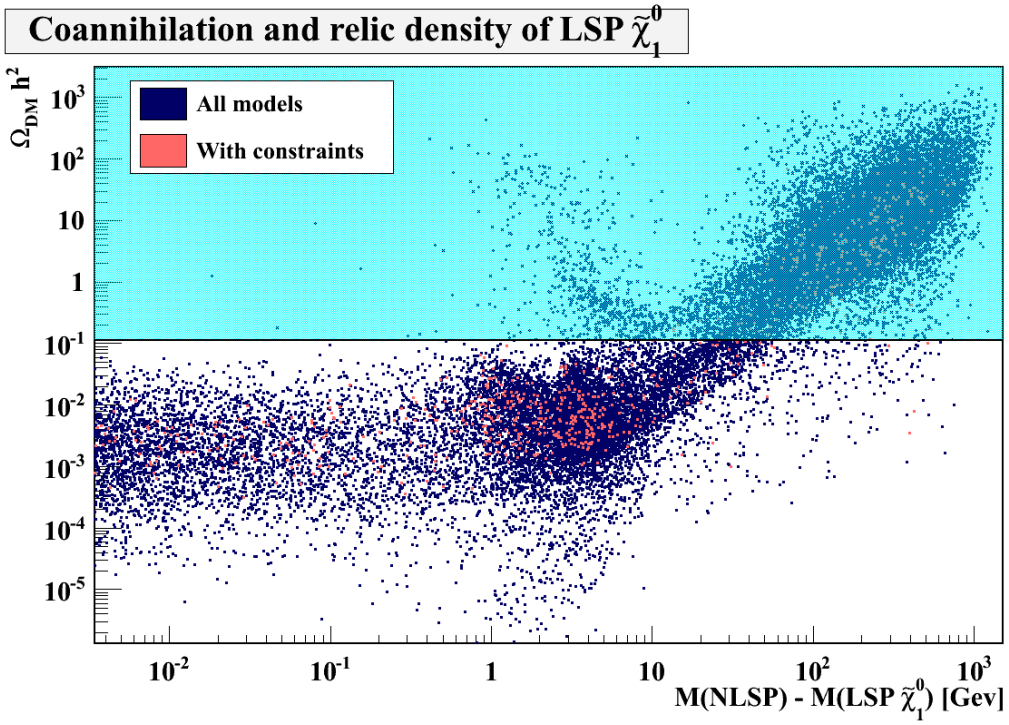

Figure 6.10: Same as above, but with the mass splitting between the NLSP and LSP on the x axis. A low mass splitting means large coannihilation, and a lower resulting relic density.

refers to just 100 days of data taking. As for a signal example, Fermi-LAT has found a preliminary photon signature at 130 GeV. C. Weniger [123] was the first to report this from the Fermi-LAT data. Further independent studies have confirmed the result [124–126], although the official collaboration has failed to find any such signature [127]. We will check if our models can accommodate such a result in Chapter 7.

6.6 Summary of constraints

At the end of this chapter, we summarize how the pMSSM models are affected by the constraints outlined above.

Table 6.2 shows the survival rate of 500 000 created models, using each of the constraints from the above sections. The "consistency check" is the survival after `HDECAY` and `DarkSusy`, where some of the models are flagged as bad. It should be noted that the total fraction of models which survive, about 0.7%, is exactly the number found by C. Berger *et al* [86]. They use a different set of constraints with sometimes different limits, so this is a coincidence.

We can compare these numbers with mSUGRA, one of the constrained MSSMs mentioned in Section 4.7. A quick scan over the mSUGRA parameters done by J. Lindroos [128], using analogous limits: m_0 with our M_1, M_2 and M_3 ranges, $m_{1/2}$ with our sfermion ranges and A_0 with our A_i ranges. Our ranges were listed in Table 6.1. The obtained survival rates are shown in Table 6.2. We use $|\Delta\rho|^{\text{SUSY}} < 1.3 \cdot 10^{-3}$ for $\Delta\rho$ this time, but the limits for the rest of the constraints stay the same. We generated a total of 90351 models for this scan, all of which had a $\tilde{\chi}_1^0$ LSP. Of special interest is the dark matter relic density $\Omega_{\text{DM}}h^2$, where only 4.2% models survive in mSUGRA, against 58.2% in pMSSM. This may be due to larger coannihilation regions in pMSSM, with higher occurrences of small mass differences between the NLSP and $\tilde{\chi}_1^0$.

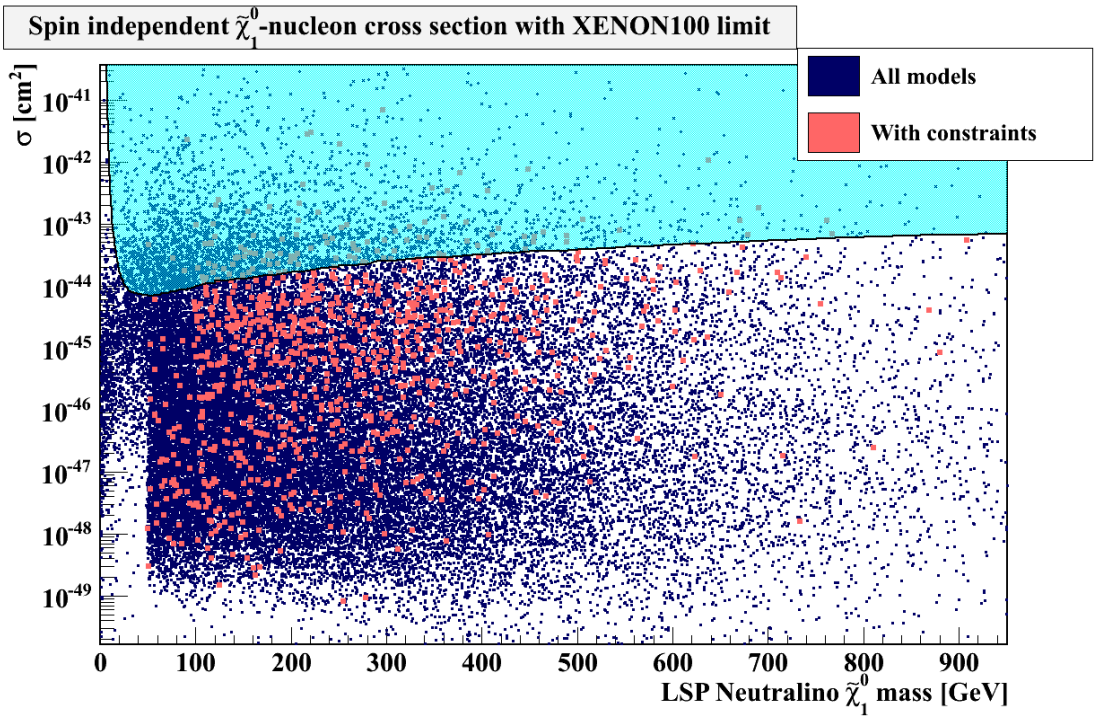

Figure 6.11: The calculated spin independent $\tilde{\chi}_1^0$-nucleon cross section versus the $\tilde{\chi}_1^0$ mass.

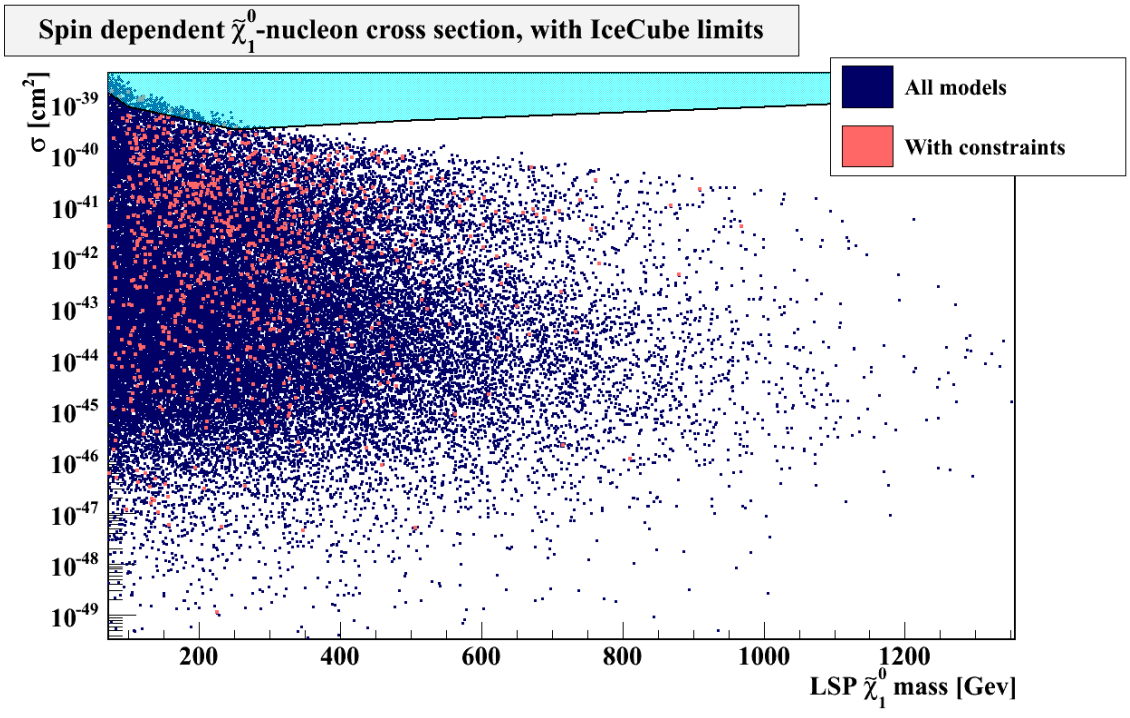

Figure 6.12: The calculated spin dependent $\tilde{\chi}_1^0$-nucleon cross section versus the $\tilde{\chi}_1^0$ mass.

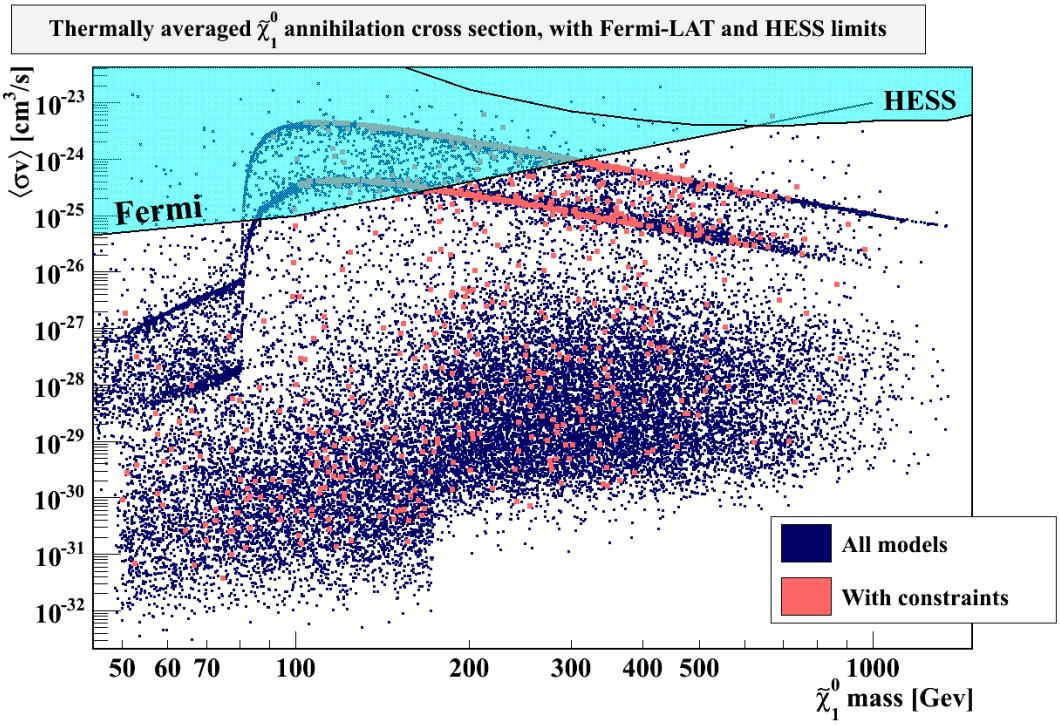

Figure 6.13: The thermally averaged cross section $\langle\sigma_{\tilde{\chi}_1^0\tilde{\chi}_1^0}v\rangle$, with Fermi-LAT [58] and HESS [62] limits. The constraints are: $m_h \sim 125$ GeV, $m_{\tilde{\chi}_1^\pm} > 103.5$ GeV, and from $\Delta\rho, \Delta a_\mu$ and $b \to s\gamma$.

Constraint	Remaining models	SR	mSUGRA SR
None	500000	100%	
Consistency	378221	75.6%	
$g-2$	52422	13.9%	15.7%
Higgs mass	12379	20.3%	12.8%
$\Omega_{\text{DM}}h^2$	9116	58.2%	3.24%
Fermi-LAT / HESS	6612	83.9%	
$\tilde{\chi}_1^\pm$ mass	5216	87.2%	98.1%
$\Delta\rho$	4582	74.6%	100%
$b \to s\gamma$	4085	90.1%	98.3%
XENON100	3363	91.6%	
IceCube	3362	97.8%	

Table 6.2: The effect of the different constraints. The number of remaining models is the number after each constraint has been successively applied, and the survival rate (SR) is the fraction of surviving models to all models when confronted with the constraint. The survival rates for some of the constraints in a scan over mSUGRA are also shown.

Chapter 7

Results

In Chapter 3, the different observables of the Standard Model Higgs boson were given with a certain precision. This was fairly easy as there is only one free parameter, and the different corrections are well known. Thus we reached a more or less complete picture of the different possible branching ratios, pictured in Fig. 3.3.

In the pMSSM, we encounter a more complex situation. The number of free parameters is $\mathcal{O}(20)$ (with $\mathcal{O}(100)$ in the unconstrained MSSM), and the different corrections play a bigger role than in the SM. In Chapter 5, the different observables of the pMSSM were outlined, as well as how they relate to their SM counterparts.

We will use the scan method described in Chapter 6 to visualize these observables, with the SM as a comparison. We will use them to find *accepted* models – models not yet excluded by the different constraints.

This chapter is organized as follows: In Section 7.1 we will discuss two specific accepted models, and describe their properties. After that, we will look at the different properties of the set of all models: Decay widths and branching ratios in Section 7.2, and cross sections in Section 7.3. For the remainder of the chapter, we will discuss how the models stand up against different experimental tests. The 125 GeV Higgs results from LHC will be tested in Section 7.4, and in Section 7.5 we check whether our models have large branching fractions into invisible decays. In the last two sections, we will see if the LHC data can accommodate a heavy MSSM Higgs, and then if we can recreate a 130 GeV neutralino to fit with the potential discovery at Fermi-LAT.

7.1 Two sample models

Later in this chapter, we will look at different characteristics of the many models generated. Before we do that, two specific models will be described. They are chosen randomly, based on experimental constraints: A light Higgs boson mass between 124 GeV and 126 GeV, and all the constraints from Section 6.5. We also look for some interesting mass hierarchies.

These two models ("A" and "B") are created with the input parameters listed in Table 7.1. After giving the parameters to the spectrum, decay and cross section calculators, some interesting properties of models A and B are listed in Table 7.2. We also give the SM values as a comparison.

While model B closely resembles the SM in terms of cross sections and branching ratios, we are looking at a different picture in Model A: A 35% increase in the $\gamma\gamma$ and VV rates, while the $b\bar{b}$ rate is down by 20%. Such low $b\bar{b}$ rates can often be attributed to a low (and negative) sbottom mixing X_b, defined in Eq. (5.7). See Fig. 7.1 for the $b\bar{b}$ decay rate versus sbottom mixing, divided by the sbottom mass scale $\sqrt{m_{\tilde{b}_1} m_{\tilde{b}_2}}$.

For the mass hierarchies, we have already demanded that the $\tilde{\chi}_1^0$ is the lightest SUSY particle (LSP) in both cases. In model A, we have the following hierarchy

$$h^0 < \tilde{\nu}_\tau < H^0 < \tilde{\tau}_1, \tag{7.1}$$

while for model B we have

$$h^0 < \tilde{\nu}_\tau < \tilde{\tau}_1 < H^0. \tag{7.2}$$

Both of these may lead to some interesting decay chains. A sneutrino $\tilde{\nu}_\tau$ is for example hard to find as an end-product in decay chains.

Only one of the models can produce a correct dark matter relic density. With model A, we have $\Omega_{\tilde{\chi}_1^0} h^2 = 0.1025$. Using $h^2 \simeq 0.52$, this is the same as a 20% DM component in the universe. With model B, on the other hand, there is a large discrepancy between the ideal value $\Omega_{\text{DM}} h^2 \simeq 0.13$ and $\Omega_{\tilde{\chi}_1^0} h^2 \simeq 6.2 \cdot 10^{-3}$, so in that case we need to explain dark matter with another mechanism.

7.2 Decays and branching ratios

We move from looking at specific models to extracting information from large data sets. We generated 500 000 models in Chapter 6, and after imposing the constraints listed there, as well as discarding models which did not pass consistency checks, we were left with 3362 accepted models. Both the full set and the subset of accepted models will be studied in this chapter.

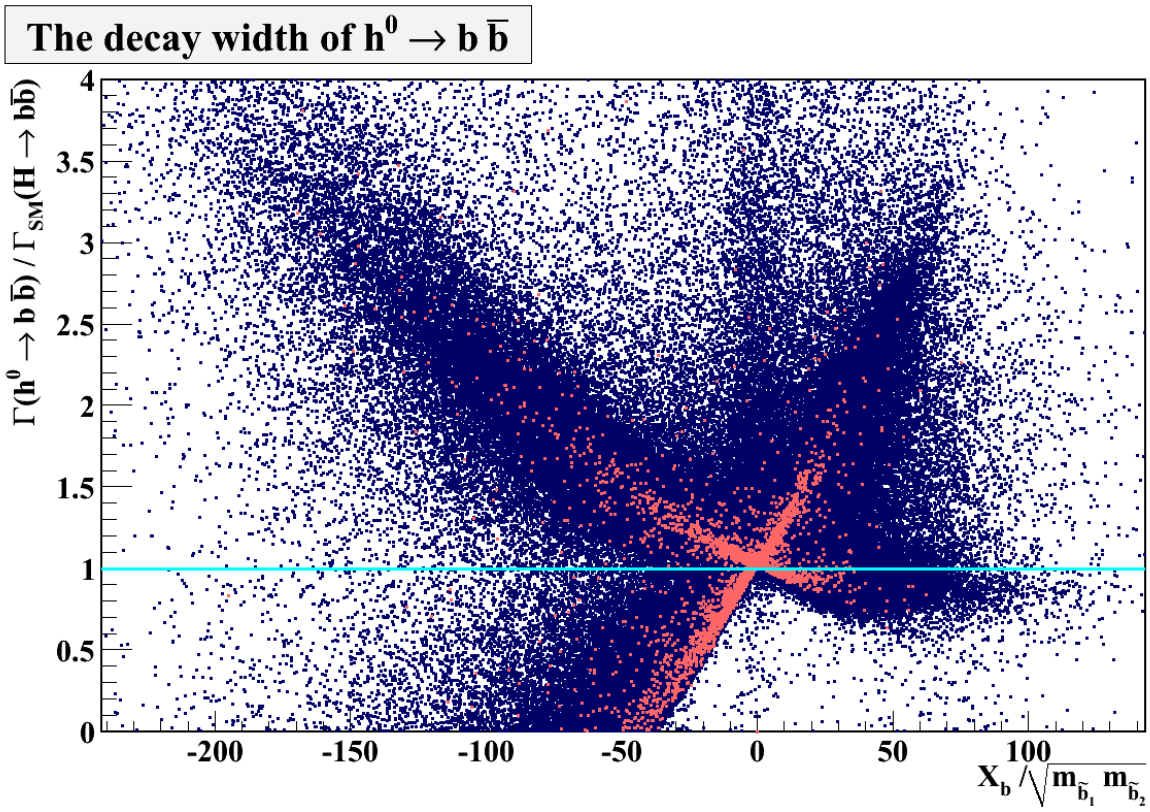

Figure 7.1: The decay width of $h \to b\bar{b}$ versus the sbottom mixing divided by the sbottom scale, normalized to the SM values (cyan line). The red and blue points are values from our scans, where the red ones satisfy the experimental constraints described in Section 6.5.

	Model A	Model B		Model A	Model B
M_1 [GeV]	360.0	-1147	m_A [GeV]	1474	2672
M_2 [GeV]	1375	-461.1	$m_{\tilde{e}_\mathrm{L}}$ [GeV]	719.1	279.9
M_3 [GeV]	1359	823.3	$m_{\tilde{\tau}_\mathrm{L}}$ [GeV]	2756	1069
A_t [GeV]	-3191	-3111	$m_{\tilde{e}_\mathrm{R}}$ [GeV]	2690	2060
A_b [GeV]	-1511	739.1	$m_{\tilde{\tau}_\mathrm{R}}$ [GeV]	1543	1511
A_τ [GeV]	-8765	3238	$m_{\tilde{q}}$ [GeV]	1200	2645
A_u [GeV]	-5594	18.74	$m_{\tilde{Q}}$ [GeV]	1769	1465
A_d [GeV]	-7026	8931	$m_{\tilde{u}_\mathrm{R}}$ [GeV]	1465	2707
A_e [GeV]	-876.9	2190	$m_{\tilde{t}_\mathrm{R}}$ [GeV]	1350	2138
μ [GeV]	376.7	-235.0	$m_{\tilde{d}_\mathrm{R}}$ [GeV]	2776	2404
$\tan\beta$	54.0	9.1	$m_{\tilde{b}_\mathrm{R}}$ [GeV]	1041	2558

Table 7.1: The input parameters for the models A and B.

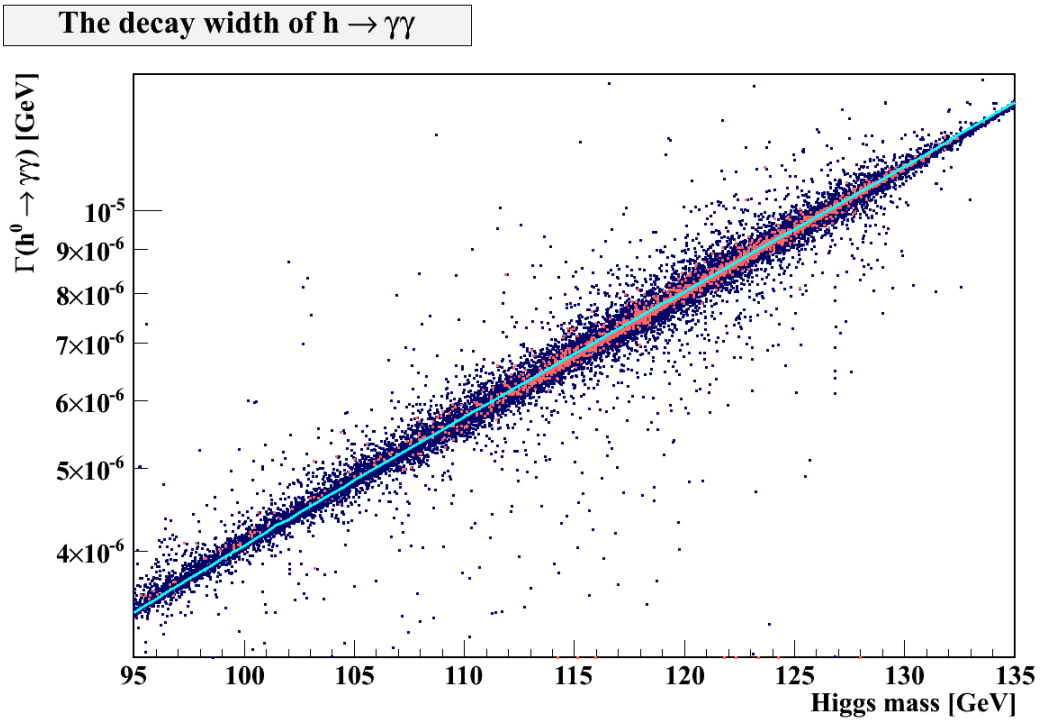

Figure 7.2: The decay width $\Gamma(h^0 \to \gamma\gamma)$. The cyan line signifies the SM value. The red and blue points are values from our scans, where the red ones are only the accepted models.

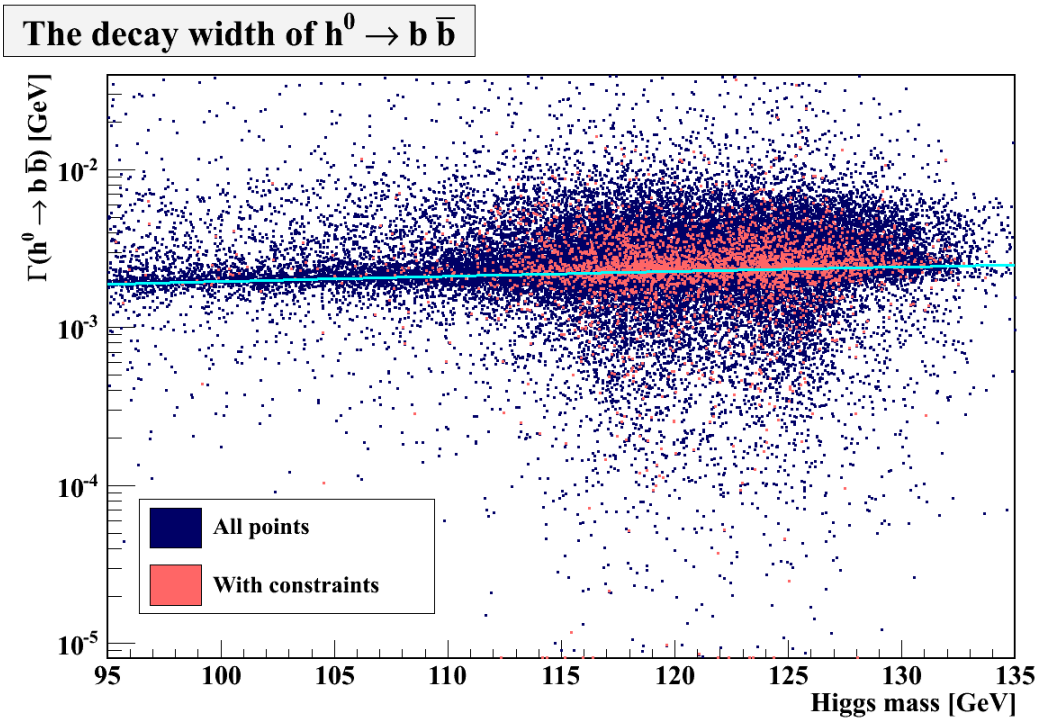

Figure 7.3: The decay width $\Gamma(h^0 \to b\bar{b})$. The cyan line signifies the SM values. The red and blue points are values from our scans, where the red ones are only the accepted models.

$h \to$	Model A	Model B	SM
$b\bar{b}$	48%	59%	58%
$\tau^+\tau^-$	8.9%	6.6%	6.3%
$\mu^+\mu^-$	0.031%	0.023%	0.022%
$s\bar{s}$	0.034%	0.025%	0.025%
$c\bar{c}$	3.8%	2.6%	2.9%
$g\bar{g}$	11%	8.3%	8.6%
$\gamma\gamma$	0.31%	0.24%	0.23%
$Z\gamma$	0.19%	0.15%	0.15%
W^+W^-	25%	20%	22%
Z^0Z^0	3.1%	2.6%	2.7%
$pp \to h$	16.7 pb	16.5 pb	17 pb

Table 7.2: Branching ratios and cross sections for the models A and B, including the SM. The cross section is purely gluonic.

We have spent some time on calculating the different decay widths, so this might be a good place to start. In general, the decay widths often match their SM values. Two examples of this are seen in Fig 7.2 and 7.3, where $\Gamma(h^0 \to \gamma\gamma)$ and $\Gamma(h^0 \to b\bar{b})$ are plotted. Note the wide spread in $\Gamma(h^0 \to b\bar{b})$ when compared to $\Gamma(h^0 \to \gamma\gamma)$.

However, such isolated decay widths can lack vital information. A SM-like channel in the MSSM may have a branching fraction far from the SM value if there are large deviations in other channels. The decay of h^0 into two b-quarks is an example of a channel which may affect the others. We saw this in the last section, where the low $b\bar{b}$ rate in model B increased the branching fraction of the other channels.

A large number of the models have a Higgs mass between 115 and 130 GeV. This is important to have in mind, and can be seen in Fig. 5.1, with the h^0 masses in a binned histogram. For example, the broader $\Gamma(h^0 \to b\bar{b})$ distribution around 125 GeV may be nothing more than a statistical effect, since there are more models with that Higgs mass.

The branching ratio of the light Higgs into $\gamma\gamma$, shown in Fig. 7.4, displays some of the features discussed above. There are two main differences between this branching ratio and the decay width in Fig. 7.2: The decay width rises sharply with the Higgs mass, and is concentrated about the SM value. For the branching ratio, the mass dependence is much weaker and the spread is larger.

As mentioned, there are many models with a low branching ratio compared to the SM, although not many of these are accepted after the constraints have been imposed. The invisible

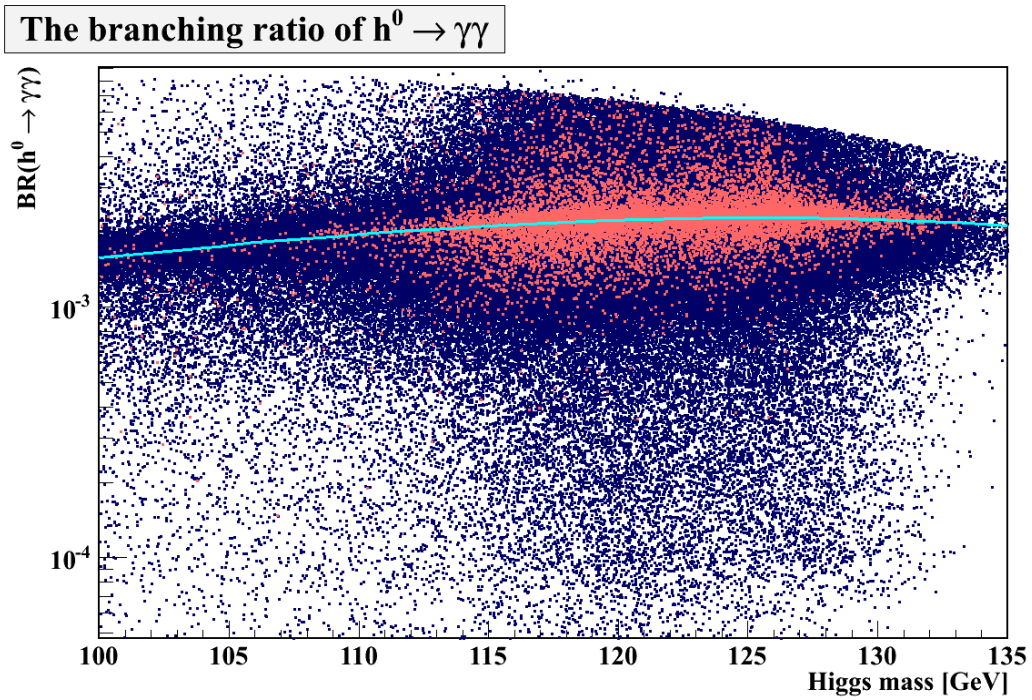

Figure 7.4: The branching ratio of the diphoton decay of the Higgs boson. The cyan line signifies the SM value. The red and blue points are values from our scans, where the red ones are only the accepted models.

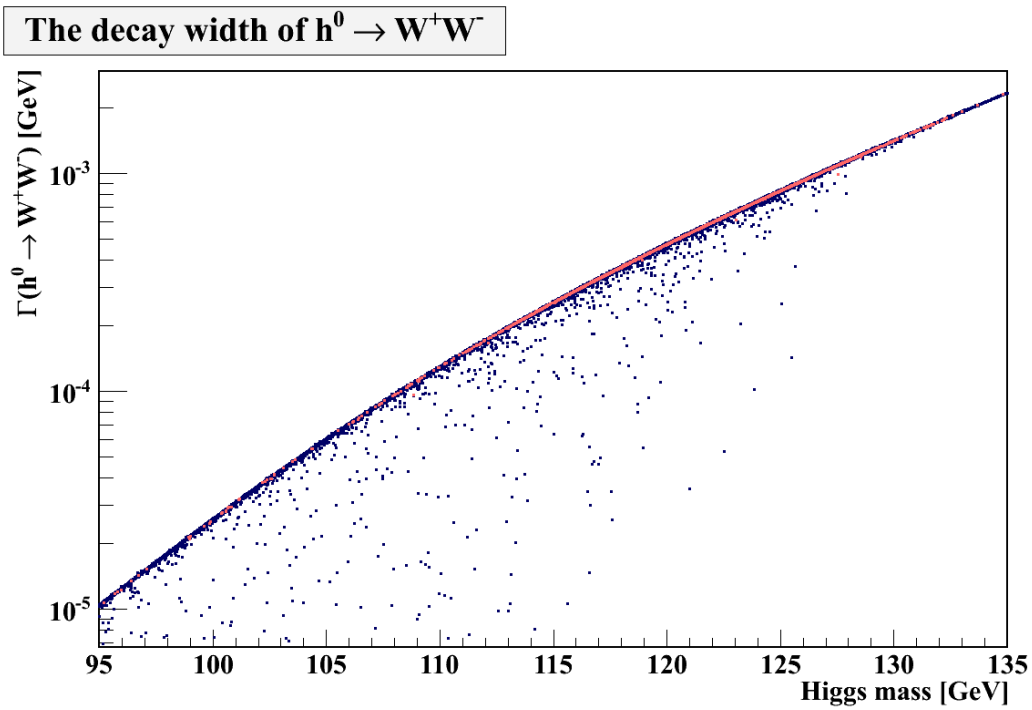

Figure 7.5: The decay width of the Higgs boson decaying into two W bosons. The cyan line signifies the SM value. The red and blue points are values from our scans, where the red ones are only the accepted models.

decays described in Section 5.3.4 will, when kinematically accessible, have considerable decay widths. This will decrease the other branching ratios. This effect will be further studied in Section 7.5.

There is also an effect from the $h^0 \to WW$ decay width. It goes as $\sim m_H^4$ (see Fig. 7.5), and above $m_h \simeq 100$ GeV it will act as a lower limit on the total width. This in turn will translate as an upper limit for the different branching fractions, as seen in Fig. 7.4.

7.3 Cross sections

To compare these results with real data, we need one more component: The cross section. Treated in Section 5.4, we have calculated the gluonic contribution to the cross section $\sigma(pp \to h^0)$ for every pMSSM model point.

The two processes we are going to use are of experimental interest. The channels $pp \to H \to \gamma\gamma$ and $pp \to H \to W^+W^-$ have been measured at the LHC [13, 14, 129, 130] and Tevatron [131].

Figs. 7.6 and 7.7 show these cross sections. Due to factors from the MSSM coupling strengths, which are often slightly below unity, the main body of MSSM cross sections are also slightly below the SM values. This is most prominent in the WW channel.

Individually, the $\gamma\gamma$ and WW channels can both produce SM-like cross sections. When put together, though, there are some interesting correlations. If we impose all the constraints, we *cannot* reproduce the SM. With a SM-like WW rate we get too high $\gamma\gamma$ rate, and with a SM-like $\gamma\gamma$ rate we are left wanting in the WW sector. Without the constraints, though, a few of the models reproduce the SM.

Fig. 7.8 shows the correlations between the normalized cross sections $\sigma_{\text{MSSM}}/\sigma_{\text{SM}}$ for the processes $pp \to h^0 \to W^+W^-$ and $pp \to h^0 \to \gamma\gamma$, one on each axis. The two cyan lines (one for each SM cross section) do not intersect in the red area, where every constraint is imposed. It should be stressed that there is a $\mathcal{O}(10\%)$ error on the SM cross section, from omitting squark loops and from the parton density functions. This might account for this discrepancy. In addition, these channels are not yet measured precisely, and we would rather be able to recreate Nature than one of our propositions on how she looks.

7.4 Comparison with LHC results

In the last section, we looked at the cross sections for $pp \to h^0 \to \gamma\gamma$ and $pp \to h^0 \to W^+W^-$. Preliminary measurements of these channels are available from the LHC and Tevatron

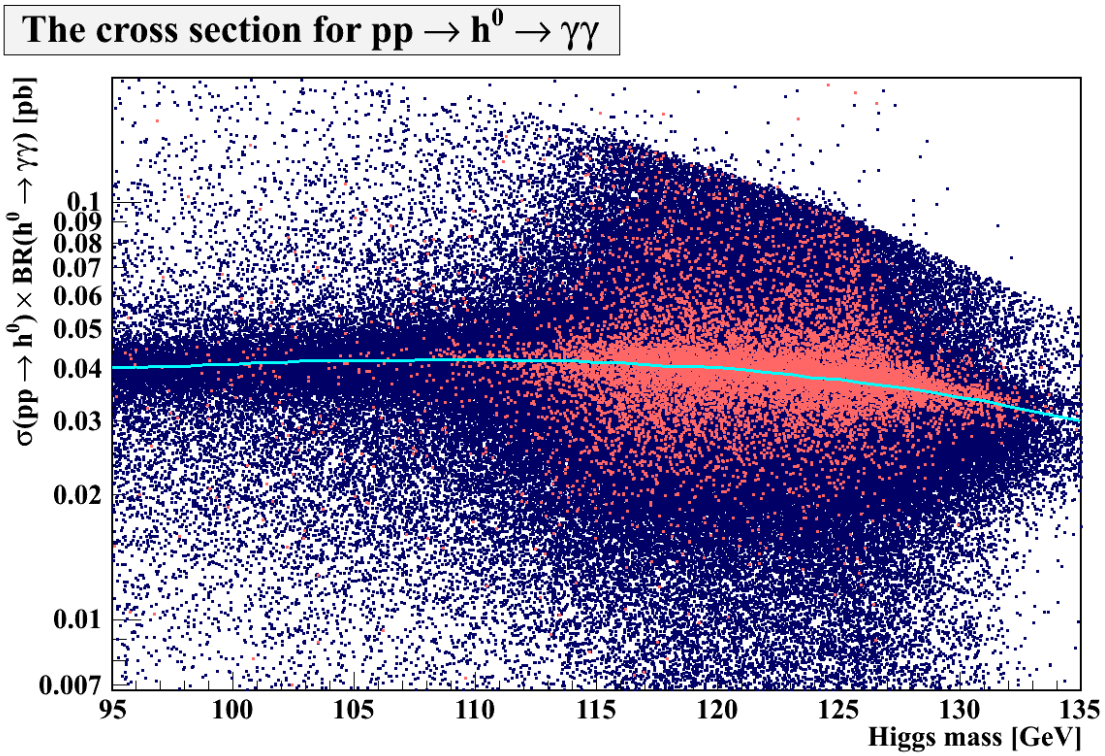

Figure 7.6: The cross section for $pp \to h^0 \to \gamma\gamma$. The cyan line signifies the SM value. The red and blue points are values from our scans, where the red ones are only the accepted models.

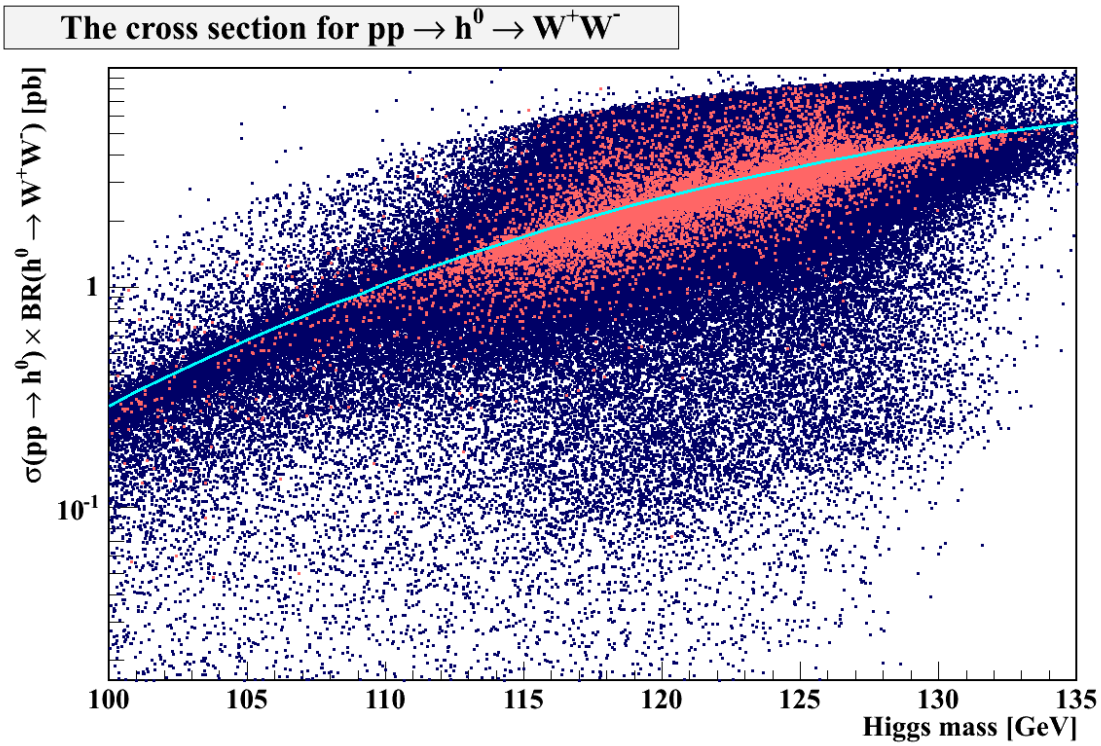

Figure 7.7: The cross section for $pp \to h^0 \to W^+W^-$. The cyan line signifies the SM value. The red and blue points are values from our scans, where the red ones are only the accepted models.

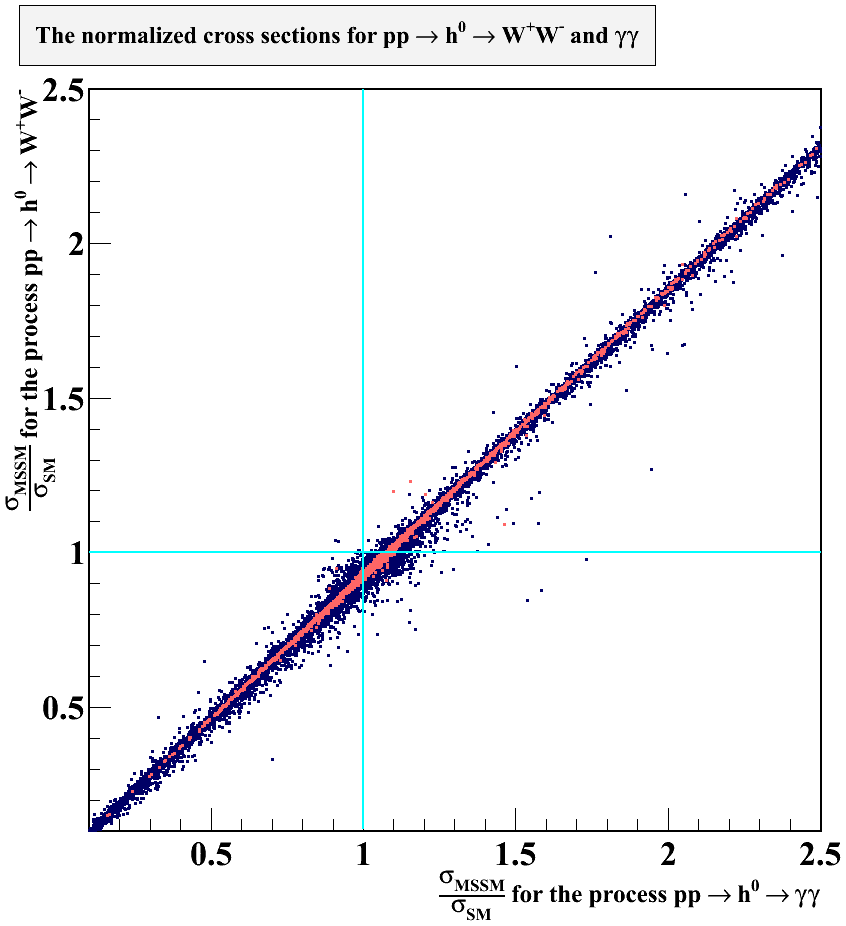

Figure 7.8: The normalized cross sections for $pp \to h^0 \to WW$ on the y axis, and $pp \to h^0 \to \gamma\gamma$ the x axis. The two cyan lines are the SM values for each of the processes.

collaborations. The official results are often experiment-specific (like analyses from the CMS [13, 129] and ATLAS [14, 130] experiments at CERN), and official combinations between experiments are scarce at this preliminary stage. Independent discoveries at both ATLAS and CMS is an argument for waiting with combined analyses, as this would be a stronger claim than a single discovery from a combined dataset. In addition, such analyses have a complex nature due to different systematical errors and from calibration. It is a good idea to have all of these under control before merging the data.

However, we will use unofficial analyses in order to obtain the largest amount of data. Philip Gibbs is known for combining results, often with good quality. See his "viXra log" [132] for a comparison between some of his unofficial combinations and the official ones.

The combination we will use is between the Tevatron and LHC data. For the former, an official combination for the CDF and D0 detectors is available [131], with a total integrated

luminosity of 10/fb each. From the LHC, we will use the ATLAS and CMS results from the 2011 dataset [13, 14, 129, 130], with a luminosity of almost 5/fb each. It should be pointed out that Tevatron has low sensitivity in the interesting mass range of $m_h \simeq 125$ GeV, while LEP had none. The interesting combination is therefore ATLAS + CMS. Nevertheless, both LEP and Tevatron are included in our combinations.

The best fit for signal strength $\sigma/\sigma_{\text{SM}}$ for the $\gamma\gamma$ and the W^+W^- channels is shown in Figs. 7.9 and 7.10. While the combination of every channel (not shown) fits well with a SM scenario ($\sigma/\sigma_{\text{SM}} = 1$), and while the statistical significance is still too low to make any strong conclusions, it looks like there is an excess of $\gamma\gamma$ events and a deficiency of W^+W^- events.

Since we have chosen a mass range of $m_h \in [124, 126]$ GeV in the $\gamma\gamma$ – W^+W^- plane, we find the signal strength at the three points $m_h \in \{124, 125, 126\}$ GeV in the combinations. This is done to see the "shape" of the uncertainty: The correlation between the systematic errors. The result of this is shown in Table 7.3. In the $\gamma\gamma$ case, the resolution is 0.5 GeV, so it is possible to directly read off the values. For W^+W^-, the mass resolution is only 5 GeV, and we must interpolate between the points to find the values. Since the signal strength $\sigma/\sigma_{\text{SM}}$ is just the quantity we have calculated in Fig. 7.8, we can include the fit there. This is done in Fig. 7.11.

Process	$\frac{\sigma}{\sigma_{\text{SM}}}$ at 124 GeV	$\frac{\sigma}{\sigma_{\text{SM}}}$ at 125 GeV	$\frac{\sigma}{\sigma_{\text{SM}}}$ at 126 GeV
$pp \to h^0 \to W^+W^-$	0.35 ± 0.35	0.31 ± 0.33	0.32 ± 0.33
$pp \to h^0 \to \gamma\gamma$	1.33 ± 0.40	1.78 ± 0.37	1.68 ± 0.40

Table 7.3: The signal strength for different h^0 masses, from a global data fit by P. Gibbs [133].

We might be fitting the fluctuations of the still-early data of LHC, however the fit for $m_h = 125$ GeV is about 3σ away from the SM value. This can be seen geometrically from the figure. With the same technique, we find that the 125 GeV fit is 2.7σ (2.6σ) away from the main body of pMSSM values with (without) the different constraints. In other words: To a 3σ level, the current data can be accommodated by neither the SM nor by the pMSSM – but there is a pull towards pMSSM.

We reiterate that this short analysis should not be taken as conclusive. Uncertainties in the calculations of the cross sections may affect our values, and with new collision data being recorded at unprecedented rates[†], the scale may tip either way: Towards the rate predicted by SM or towards something else.

[†]The current 2012 dataset weighs in at 3.58 fb^{-1}, see the ATLAS `LuminosityPublicResults` website [134] for updated values.

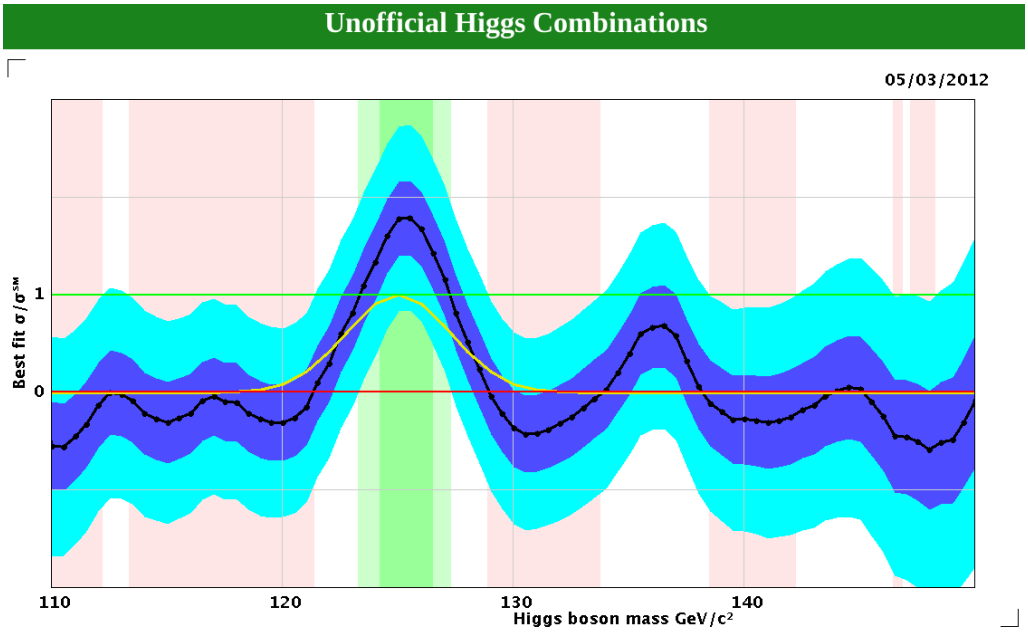

#	Collider	Experiment	Channel	Subchannel	Analysis	Conference	Date	Min Lumi	Max Lumi	Energy	Resolution	Quality
1	Tevatron	CDF	2gamma	2gamma	Any	Moriond12	29/01/2012	10/fb	10/fb	1.96 TeV	high	digitised
2	Tevatron	D0	2gamma	2gamma	Any	Thuile12	02/03/2012	9.7/fb	9.7/fb	1.96 TeV	high	digitised
3	LHC	ATLAS	2gamma	2gamma	Any	CCM11	13/12/2011	4.9/fb	4.9/fb	7 TeV	high	medium
4	LHC	CMS	2gamma	2gamma	Any	Moriond12	05/03/2012	4.76/fb	4.76/fb	7 TeV	high	digitised

Figure 7.9: Unofficial combinations for the σ/σ_{SM} fit in the $h \to \gamma\gamma$ channel at the LHC and Tevatron [133]*. The data used for the combination is listed, and the yellow curve is irrelevant.*

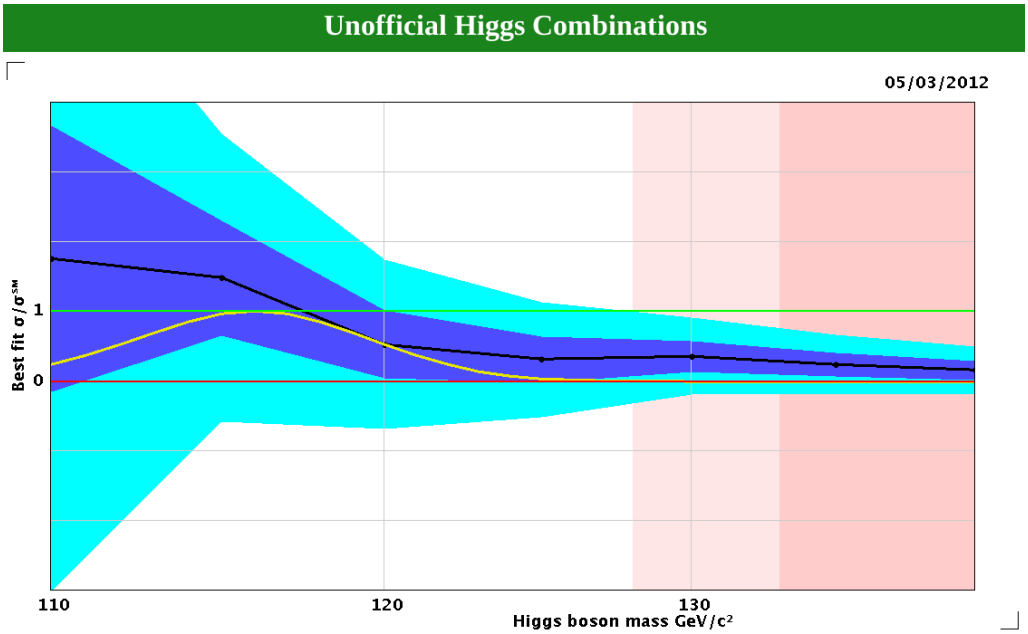

#	Collider	Experiment	Channel	Subchannel	Analysis	Conference	Date	Min Lumi	Max Lumi	Energy	Resolution	Quality
1	Tevatron	D0	WW	lvlv	CutMVA	Moriond12	05/03/2012	9.7/fb	9.7/fb	1.96 TeV	low	official
2	Tevatron	CDF	WW	lvlv	CutMVA	Thuile12	02/03/2012	9.7/fb	9.7/fb	1.96 TeV	low	digitised
3	Tevatron	CDF	WW	ltau	CutMVA	EPS11	22/07/2011	7.1/fb	7.1/fb	1.96 TeV	low	official
4	LHC	ATLAS	WW	lvqq	Any	Moriond12	05/03/2012	4.7/fb	4.7/fb	7 TeV	low	good
5	LHC	ATLAS	WW	lvlv	Any	Moriond12	05/03/2012	4.7/fb	4.7/fb	7 TeV	low	digitised
6	LHC	CMS	WW	lvlv	Cut	Moriond12	05/03/2012	4.6/fb	4.6/fb	7 TeV	low	digitised

Figure 7.10: Unofficial combinations for the σ/σ_{SM} fit in the $h \to W^+W^-$ channel at the LHC and Tevatron [133]*. The data used for the combination is listed, and the yellow curve is irrelevant.*

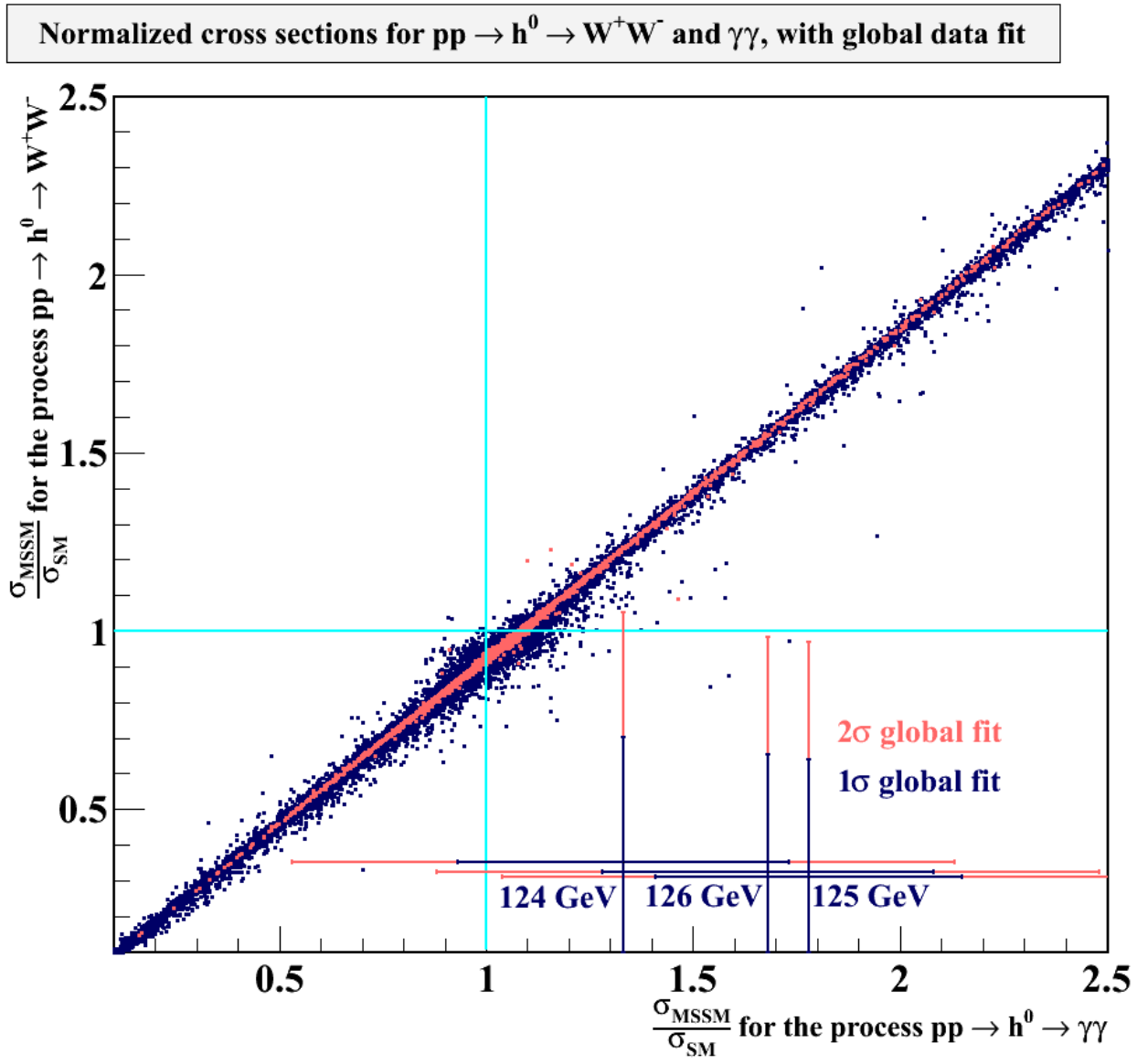

Figure 7.11: The global signal strength fits for $m_h = \{124, 125, 126\}$ GeV, overlaid with the signal strengths from our scans. The fit values are given at 1σ (blue cross) and 2σ (red cross). The red points signify the accepted models, and the blue ones are all models.

7.5 Invisible decays

For SUSY masses below about $2m_h$, the decay widths of both the light and heavy Higgs bosons into pairs of sfermions or gauginos can be huge when compared with the SM. Such decays are called *invisible*, and can be hard to find in the detector. This is especially true for decays into neutral SUSY particles like neutralinos and sneutrinos. About 6% of the 500 000 models generated have such channels.

In the diphoton branching fraction seen earlier in Fig. 7.4, much of the structure below the bulk of accepted models at $m_h \in [115, 130]$ GeV is due to such invisible decays. With them "turned off", much of this structure disappears.

In Fig. 7.12, we have plotted the sum of all invisible decays of the light Higgs boson. As most of the decays happen as pair annihilations to the lightest neutralino, the branching ratio is shown versus the $\tilde{\chi}_1^0$ mass. Note that very few of the models that do have invisible decays are accepted. In our scans, of the about $\mathcal{O}(25000)$ models with invisible decays, only $\mathcal{O}(10)$ survive. This is due to the constraint of the chargino mass – a light neutralino often leads to a light chargino[†], which have been excluded by the LEP2 data.

7.6 A Heavy Higgs

A heavy CP-even Higgs could in principle be detectable. If we use the separate data sets from CMS and ATLAS for the decay mode $H \to W^+W^-$, presented at the Moriond 2012 conference [129, 130], these can serve as upper bounds. In this mass region, the W^+W^- decay channel is the most prominent one. Having demanded a Higgs mass of about 125 GeV, this acts as a lower bound on the heavy Higgs boson mass of about 180 GeV. In addition to this, a SM-like light Higgs will trigger the decoupling limit, where the heavy Higgs has a very small coupling to the fermions and gauge bosons. The reasoning is this: If $\sin^2(\bar{\alpha} - \beta) \simeq 1$, then by construction $\cos^2(\bar{\alpha} - \beta) \simeq 0$.

Despite these shortcomings, there are still some models which could produce signals in the future. Fig 7.13 shows the accepted models which give cross sections inside a $\pm 20\%$ SM-band for $pp \to h^0 \to \gamma\gamma$ and $pp \to h^0 \to W^+W^-$, and have $m_{H^0} < 600$ GeV.

We see that there are a few models with cross sections above the signal fit, although the main body of decays are reduced to the percent level of σ_{SM}. As the LHC exclusion limit continue to shrink, maybe a novel structure will be found, unveiling a H^0 decay?

[†]This is because their mass matrices share some parameters: The SU(2) gaugino mass M_2 and the Higgsino mass parameter μ.

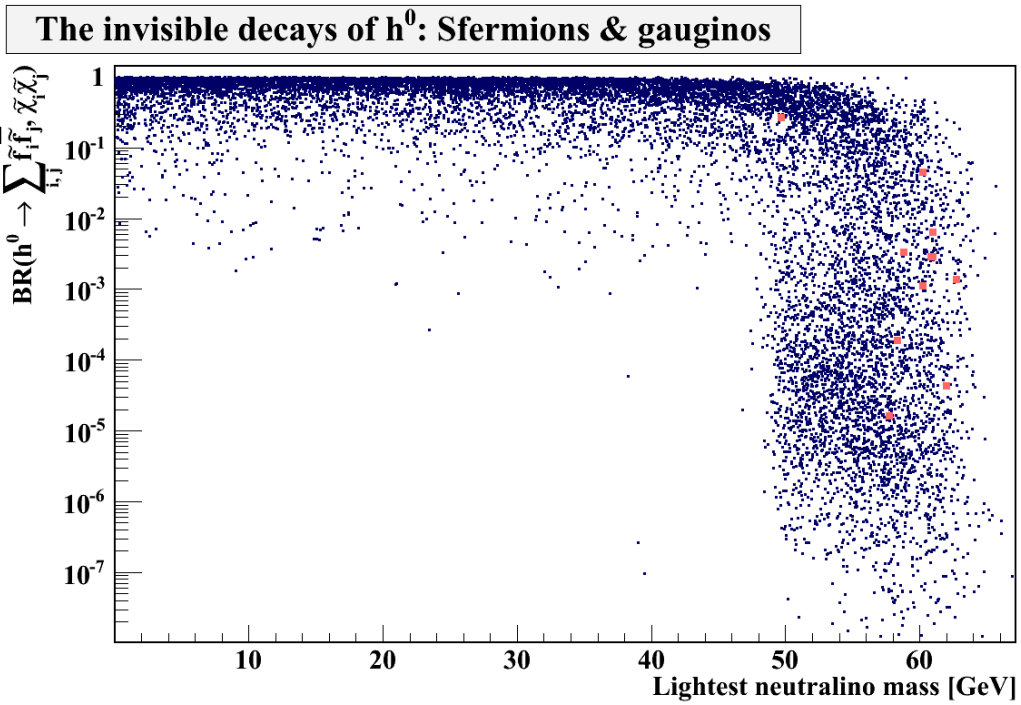

Figure 7.12: The sum of the invisible decays of the Higgs boson versus the $\tilde{\chi}_1^0$ mass. The (few) red points passes all the constraints.

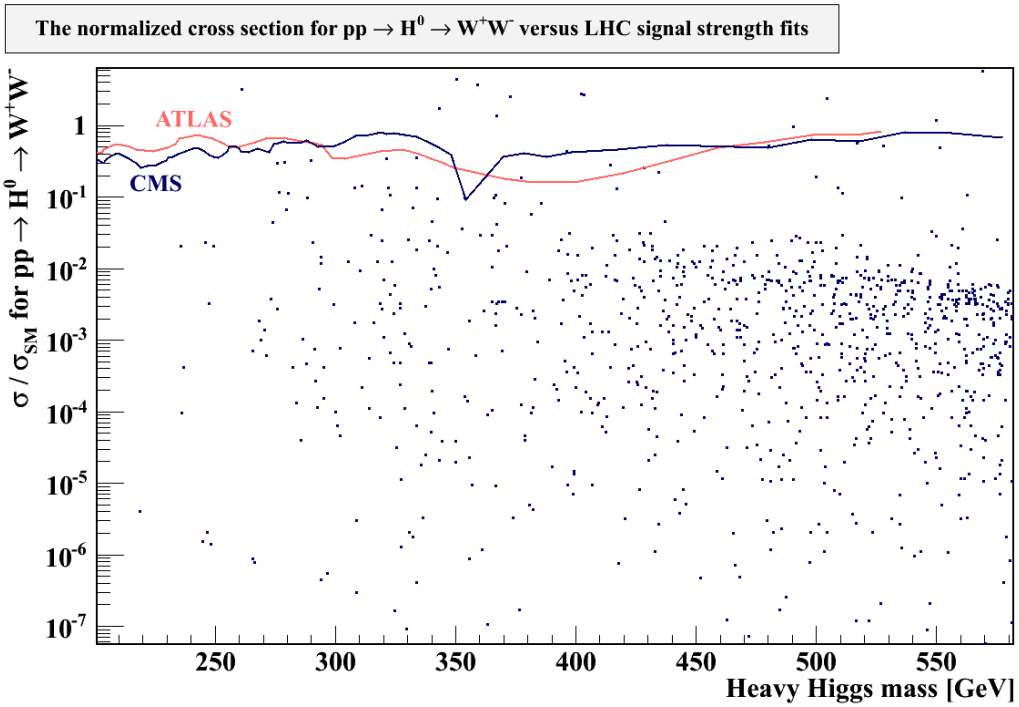

Figure 7.13: The normalized cross section for the process $pp \to H^0 \to W^+W^-$. The two lines are the signal fit from CMS and ATLAS. Every model displayed have survived the tight constraints, described in the text.

7.7 A 130 GeV neutralino

In Section 6.5.6 we said that the Fermi-LAT experiment has released data pointing to a potential WIMP annihilation signal at 130 GeV. See C. Weniger [123] for further details. We have no problems recreating a 130 GeV $\tilde{\chi}_1^0$ with the correct characteristics: A low μ, M_1 or M_2 can give us such a state, and this is not in direct conflict the the chargino mass limit of 103.5 GeV (although that constraint often requires μ or M_2 to be above 103.5 GeV). A total of 1.1% of our models had $m_{\tilde{\chi}_1^0} \in [128, 132]$ GeV, and of the accepted models 0.7% had this feature.

Chapter 8

Conclusion

In this thesis, we set out to see how supersymmetric theories hold up against experiments, with particular emphasis on the new results regarding the potential discovery of the Higgs boson at CERN.

We chose supersymmetry in the form of the Minimal Supersymmetric Standard Model (MSSM). Due to a complex picture, we imposed some phenomenological constraints: No CP-violation from the supersymmetric sector, no flavor-changing neutral currents and with no assumptions about unification of the forces at the Grand Unification scale. We simplified the problem by using the phenomenological MSSM (pMSSM), which is a version of MSSM following these assumptions.

We have detailed how to produce a large set of pMSSM models. This was done by a random scan in the formidable parameter space of pMSSM. Through the various existing programs, we have calculated the masses, branching fractions and cross sections for the pMSSM Higgs bosons. In addition, we have done the same calculations "by hand" for these quantities in the Standard Model.

We then put the models through an array of different constraints: From unobserved decay channels, through mass limits and constraints on the sizes of loop corrections to known observables, to limits on the observed influxes of dark matter from the galaxy. At the end, 0.7% of the models survived these tight constraints. This is orders of magnitudes above the survival rate in constrained theories like mSUGRA, which we also saw some examples of.

After imposing all the constraints, we were unable to find models which reproduced the SM in the case we studied. This was partly due to a reduced coupling strength between the light Higgs and the W boson in the pMSSM. We noted that uncertainties in the cross section calculations could help close this gap. However, the more constraints we impose, the less flexible is the pMSSM. If the Higgs boson turns out to be SM-like we may have to exclude

the pMSSM.

After this exercise, we applied our models to the recent data from (amongst other) the LHC. In order to obtain the best results, we used an unofficial combination of all the relevant data from different collaborations. The early data from the LHC shows an excess of diphoton decays $H \to \gamma\gamma$ and a deficit of vector decays $H \to WW$. This could be fluctuations which disappear with more statistics. However, we wanted to see how this would fit in with a pMSSM scenario. We found that there is a 3σ difference between the data and the SM, and a somewhat smaller difference between the data and the pMSSM. If this tendency does not disappear later on, we have an interesting situation. If we combine all the channels, however, the data fits well with a Standard Model scenario.

We have also seen how the heavy Higgs from the pMSSM can be observed at the LHC. With tight constraints from the light Higgs, the coupling strength of the heavy one is severely reduced. We find some models where H^0 would be observed at the LHC, although with very low production cross sections.

There have been some results on galactic photon signatures from the Fermi-LAT collaboration, which might be hints of a dark matter WIMP. We found that the pMSSM neutralino can accommodate this signal, without creating any trouble for the other constraints.

We are excited about how new data would affect this analysis, and others like it. Tighter constraints on the neutralino from dark matter searches, higher mass bounds on charged SUSY particles and of course measurements of the coupling strengths of the observed Higgs boson will all help to further uncover the theory behind. Even in the near future, for example at the summer conferences of 2012, the mystery of the Higgs could be unravelled.

Appendix A

Acronyms

2HDM	Two-Higgs-Doublet Model
ATLAS	A Toroidal LHC ApparatuS, LHC experiment
BR	Branching Ratio
BSM	Beyond the Standard Model
CMS	Compact Muon Solenoid, LHC experiment
cMSSM	constrained MSSM
CP	Charge-Parity
CTEQ6	A PDF
CoM	Center of Mass
DM	Dark Matter
`DarkSusy`	A program for generating relic densities
Fermi-LAT	Fermi-Large Angle Telescope
DoF	Degrees of Freedom
FCNC	Flavor-Changing Neutral Currents
GR	General Relativity
GUT	Grand Unification Theory
GeV	Giga electron Volt, equals $1.6 \cdot 10^{-10}$ J
`HDECAY`	A program for generating Higgs BRs
`HIGLU`	A program for generating Higgs cross sections
ILC	International Linear Collider
LEP	Large Electron-Positron collider
ΛCDM	Λ (dark energy) Cold Dark Matter
LHC	Large Hadron Collider
LSP	Lightest Supersymmetric Particle

MSSM	Minimal Supersymmetric Standard Model
MSTW2008	A PDF
mSUGRA	minimal SUperGRAvity
NLSP	Next-to-Lightest Supersymmetric Particle
PDF	Parton Density Function
PDG	Particle Data Group
pMSSM	phenomenological MSSM
QCD	Quantum ChromoDynamics
QED	Quantum ElectroDynamics
SLHA	SUSY Les Houches Accord
SM	Standard Model
SU(n)	Special Unitary group of degree n
SUSY	Supersymmetry
`SuSpect`	A program for generating SUSY mass spectra
U(n)	Unitary group of degree n
VBF	Vector Boson Fusion
vev	vacuum expectation value
WIMP	Weakly Interacting Massive Particle
WMAP	Wilkinson Microwave Anisotropy Probe

Bibliography

[1] Wikimedia Commons. Standard model of elementary particles — Wikipedia, the free encyclopedia. `http://en.wikipedia.org/wiki/File:Standard_Model_of_Elementary_Particles.svg`, 2004. [Online; accessed 23-May-2012].

[2] K. Nakamura *et al.* (Particle Data Group). Review of particle physics. *JP G*, **37**:075021, 2010.

[3] Wikimedia Commons. Elementary particle interactions — Wikipedia, the free encyclopedia. `http://en.wikipedia.org/wiki/File:Elementary_particle_interactions.svg`, 2008. [Online; accessed 23-May-2012].

[4] E. Schrödinger. Quantiserung als Eigenwertproblem. *Annalen der Physik*, **79**:361–376, 1926.

[5] J. Bjorken and S. Drell. *Relativistic Quantum Mechanics*. McGrawHill, paperback edition, 1998.

[6] P. A. M. Dirac. The Quantum theory of electron. *Proc.Roy.Soc.Lond.*, **A117**:610–624, 1928.

[7] E. Noether. Invariante Variationsprobleme. *Nachr. D. König. Gesellsch. D. Wiss. Zu Göttingen, Math-phys. Klasse*, pages 235–257, 1918.

[8] V. Barger and R. Philips. *Collider Physics*. Westview Press, updated edition, 1996.

[9] J. Gunion et. al. *The Higgs Hunter's Guide*. Westview Press, 2nd edition, 2000.

[10] P. Higgs. Broken symmetries and the masses for gauge bosons. *Phys. Rev. Lett.*, **13**:508–509, 1964.

[11] F. Englert and R. Brout. Broken symmetry and the mass of gauge vector mesons. *Phys. Rev. Lett.*, **13**:321–323, 1964.

[12] G. S. Guralnik *et al.* Global conservation laws and massless particles. *Phys. Rev. Lett.*, **13**:585–587, 1964.

[13] Serguei *et al.* Chatrchyan. Search for the standard model Higgs boson decaying into two photons in pp collisions at sqrt(s)=7 TeV. *Phys.Lett.*, **B710**:403–425, 2012, `arXiv:1202.1487 [hep-ex]`.

[14] ATLAS Collaboration. Search for the Standard Model Higgs boson in the diphoton decay channel with 4.9 fb^{-1} of pp collisions at $\sqrt{s} = 7$ tev with ATLAS. *Phys. Rev. Lett.*, **108**:111803, 2012, `arXiv:1202.1414 [hep-ex]`.

[15] O. W. Greenberg. Spin and unitary-spin independence in a paraquark model of baryons and mesons. *Phys. Rev. Lett.*, **13**:598–602, 1964.

[16] E. Henley and A. Garca. *Subatomic Physics*. World Scientific Publishing, 3rd edition, 2007.

[17] K. G. Wilson. Confinement of quarks. *Phys. Rev.*, **D10**:2445–2459, 1974.

[18] E. Klempt and A. Zaitsev. Glueballs, hybrids, multiquarks. Experimental facts versus QCD inspired concepts. *Physics Reports*, **454**:1–202, 2007, `arXiv:0708.4016 [hep-ph]`.

[19] J. Pumplin *et al.* New generation of Parton Distributions with uncertainities from global QCD analysis. *JHEP*, **0207**:012, 2002, `arXiv:hep-ph/0201195v3`.

[20] A. D. Martin *et al.* Parton distributions for the LHC. *Eur. Phys. J.*, **C63**:189–285, 2009, `arXiv:0901.0002v3 [hep-ph]`.

[21] J. D. Bjorken. Asymptotic sum rules at infinite momentum. *Phys. Rev.*, **179**:1547–1553, 1969.

[22] B. Adeva *et al.* Electroweak studies in e^+e^- collisions: $12 < \sqrt{s} < 46.78$ GeV. *Phys. Rev.*, **D38**:2665–2678, 1988.

[23] W. Heisenberg. Über den anschaulichen inhalt der quantentheoretischen Kinematik und Mechanik. *Z Phys.*, **43**:172–198, 1927.

[24] F. Mandl and G. Shaw. *Quantum Field Theory*. John Wiley & Sons, Ltd., 2nd edition, 2010.

[25] I. Aitchison. *Supersymmetry in Particle Physics*. Cambridge University Press, 2007.

[26] A. Djouadi. The anatomy of electro-weak symmetry breaking. II: The Higgs bosons in the Minimal Supersymmetric Model. *Phys. Rept.*, **459**:1–241, 2008, `arXiv:hep-ph/0503173v2`.

[27] Gerard 't Hooft. Dimensional regularization and the renormalization group. *Nucl.Phys.*, **B61**:455–468, 1973.

[28] Steven Weinberg. New approach to the renormalization group. *Phys.Rev.*, **D8**:3497–3509, 1973.

[29] B. Kniehl. Status of higher-order corrections in the standard electroweak theory. *Int. J. Mod. Phys A*, **10**:443–464, 1995, `arXiv:hep-ph/9410330`.

[30] S. Dittmaier *et al.* Handbook of LHC Higgs Cross Sections: 1. Inclusive Observables. 2011, `arXiv:1101.0593 [hep-ph]`.

[31] G. Degrassi and F. Maltoni. Two-loop electroweak corrections to the higgs-boson decay $H \to \gamma\gamma$. *Nucl. Phys*, **B724**:183–196, 2005, `arXiv:hep-ph/0504137`.

[32] M. Steinhauser. Higgs decay into gluons up to $\mathcal{O}(\alpha_s^3 g_f m_t^2)$. *Phys. Rev. D*, **59**:054005, 1999, `arXiv:hep-ph/9809507`.

[33] B. A. Kniehl. Higgs phenomenology at one loop in the standard model. *Phys. Rep.*, **240**:211–300, 1994.

[34] J. Fleischer and F. Jegerlehner. Radiative corrections to higgs-boson decays in the Weinberg-Salam model. *Phys. Rev.*, **D23**:2001–2026, 1981.

[35] B. A. Kniehl. Radiative corrections for $H \to ZZ$ in the standard model. *Nucl. Phys.*, **B352**:1–26, 1991.

[36] B. A. Kniehl. Radiative corrections for $H \to W^+W^-(\gamma)$ in the standard model. *Nucl. Phys.*, **B357**:439–466, 1991.

[37] W-Y. Keung and W. J. Marciano. Higgs-scalar decays: $H \to W^\pm + X$. *Phys. Rev.*, **D30**:248–250, 1984.

[38] E. Jones *et al.* `SciPy`: Open source scientific tools for Python. `http://www.scipy.org/`, 2001–.

[39] A. Grau *et al.* Contributions of off-shell top quarks to decay processes. *Phys. Lett.*, **B251**:293–293, 1990.

[40] A. Djouadi. The anatomy of electro-weak symmetry breaking. I: The Higgs boson in the Standard Model. *Phys. Rept.*, **457**:1–216, 2008, `arXiv:hep-ph/0503172v2`.

[41] M. Spira *et al.* QCD corrections to the HZγ coupling. *Phys. Lett.*, **B276**:350–353, 1992.

[42] A. Djouadi. Higgs Physics: Theory. 2012, `arXiv:1203.4199v1 [hep-ph]`.

[43] T. K. Nelson. Precision Measurements at the ILC. *AIP Conf. Proc.*, **870**:232–325, 2006.

[44] A. Djouadi *et al.* Production of Higgs bosons in proton colliders. QCD corrections. *Phys. Lett.*, **B264**:440–446, 1991.

[45] M. Spira. `HIGLU`: A Program for the Calculation of the total Higgs production cros section at hadron colliders via gluon fusion including QCD corrections. *DESY*, **T-95-05**, 1995, `arXiv:hep-ph/9510347`.

[46] A. Einstein. Die Grundlage der allgemeinen Relativitätstheorie. *Annalen Der Physik*, **49**:769–822, 1916.

[47] B. Bertotti *et al.* A test of general relativity using radio links with the Cassini spacecraft. *Nature*, **425**:374, 2003.

[48] G. t'Hooft. On the quantum structure of a black hole. *Nucl. Phys.*, **B256**:727–745, 1985.

[49] S. M. Maurer. Idea man. *Beamline (SLAC)*, **31**:1, 2001.

[50] RJE Clausius. On a mechanical theorem applicable to heat. *Philosophical Magazine, ser. 4*, **40**:122–127, 1870.

[51] F. Zwicky. On the masses of nebulae and of clusters of nebulae. *Astrophys. J.*, **86**:217–246, 1937.

[52] J. H. Oort. The force exerted by the stellar system in the direction perpendicular to the galactic plane and some related problems. *Bull. of the Astronomical Inst. of the Netherlands*, **6**:249–287, 1932.

[53] K. G. Begeman *et al.* Extended rotation curves of spiral galaxies – dark haloes and modified dynamics. *MMRAS*, **249**:523–537, 1991.

[54] J. Dunkley *et al.* Five-year Wilkinson Microwave Anisotropy Probe (WMAP) observations: Likelihoods and parameters from the WMAP data. *Astrophys. J. Suppl.*, **180**:306–329, 2009, `arXiv:0803.0586v2 [astro-ph]`.

[55] R. Massey *et al.* The dark matter of gravitational lensing. *Rep. Prog. Phys.*, **73**:086901, 2010, arXiv:1001.1739v2 [astro-ph.CO].

[56] L. Baudis for the XENON Collaboration. Results from the XENON100 Dark Matter search experiment. 2012, arXiv:1203.1589 [astro-ph.IM].

[57] C. H. Ha for the IceCube Collaboration. The first year IceCube-DeepCore results. *JCPS*, **TAUP**, 2011, arXiv:1201.0801v1 [hep-ex].

[58] M. Ackermann *et al.* Constraining Dark Matter Models from a Combined Analysis of Milky Way Satellites with the Fermi Large Area Telescope. *Phys. Rev. Lett.*, **107**:241302, 2011, arXiv:1108.3546 [astro-ph.HE].

[59] F. Aharonian *et al.* H.E.S.S. observations of the Galactic Center region and their possible dark matter interpretation. *Phys.Rev.Lett.*, **97**:221102, 2006, arXiv:astro-ph/0610509.

[60] R. Abbasi *et al.* Multi-year search for dark matter annihilations in the Sun with the AMANDA-II and IceCube detectors. *Phys. Rev.*, **D85**:042002, 2012, arXiv:1112.1840 [astro-ph.HE].

[61] E. Aprile *et al.* Dark Matter Results from 100 Live Days of XENON100 Data. *Phys. Rev. Lett.*, **107**:131302, 2011, arXiv:1104.2549 [astro-ph.CO].

[62] P. Brun *et al.* Searches for dark matter subhaloes with wide-field Cherenkov telescope surveys. *Phys.Rev.*, **D83**:015003, 2011, arXiv:1012.4766 [astro-ph.HE].

[63] B. W. Carroll and D. A. Ostlie. *An Introduction to Modern Astrophysics.* Pearson Education, Inc., 2nd edition, 2007.

[64] J. L. Feng *et al.* Supergravity with a Gravitino LSP. *Phys. Rev.*, **D70**:075019, 2004, arXiv:hep-ph/0404231v2.

[65] R. D. Peccei and Helen R. Quinn. CP conservation in the presence of pseudoparticles. *Phys. Rev. Lett.*, **38**:1440–1443, 1977.

[66] T. Padmanabhan. *Theoretical Astrophysics. Volume III: Galaxies and Cosmology.* Cambridge University Press, 1st edition, 2002.

[67] P. Sreekumar. EGRET Observations of the extragalactic gamma ray emmision. *Astrophys. J.*, **494**:523–534, 1988, arXiv:astro-ph/9709257v1.

[68] G. Lemaître. Un Univers homogène de masse constante et de rayon croissant rendant compte de la vitesse radiale des nébuleuses extra-galactiques.

[69] N. Jarosik *et al.* Seven-Year Wilkinson Microwave Anisotropy Probe (WMAP) Observations: Sky Maps, Systematic Errors, and Basic Results. *Astrophys.J.Suppl.*, **192**:14, 2011, `arXiv:1001.4744 [astro-ph.CO]`.

[70] P. J. E. Peebles and B. Ratra. The cosmoslogical constant and Dark Energy. *Rev. Mod. Phys.*, **75**:559–606, 2003, `arXiv:astro-ph/0207347v2`.

[71] S. Perlmutter *et al.* Measurements of ω and λ from 42 high-redshift supernovae. *Astrophys. J.*, **517**:565–586, 1999, `arXiv:astro-ph/9812133v1`.

[72] S. P. Ahlen. New limit on the low-energy antiproton/proton ratio in the galactic cosmic radiation. *Phys. Rev. Lett.*, **61**:145–148, 1988.

[73] K. R. Dienes. String theory and the path to unification: A review of recent developments. *Phys. Rept.*, **287**:447–525, 1997, `arXiv:hep-th/9602045v3`.

[74] J. C. Maxwell. A dynamical theory of the electromagnetic field. *Phil. Trans. of the Royal Society of London*, **155**:459–512, 1865.

[75] S. Weinberg. A model of leptons. *Phys. Rev. Lett.*, **19**:1264–1266, 1967.

[76] H. Georgi and S.L. Glashow. Unity of All Elementary Particle Forces. *Phys.Rev.Lett.*, **32**:438–441, 1974.

[77] J. Ellis. The superstring: theory of everything, or of nothing? *Nature*, **323**:595–598, 1986.

[78] Theodor Kaluza. On the Problem of Unity in Physics. *Sitzungsber.Preuss.Akad.Wiss.Berlin (Math.Phys.)*, **1921**:966–972, 1921.

[79] O. Klein. Quantum Theory and Five-Dimensional Theory of Relativity. (In German and English). *Z.Phys.*, **37**:895–906, 1926.

[80] A. Ashtekar. Introduction to loop quantum gravity. 2012, `arXiv:1201.4598v1 [gr-qc]`.

[81] S. Glashow and S. Weinberg. Natural conservation laws for neutral currents. *Phys. Rev.*, **D15**:1958–1965, 1977.

[82] G. C. Branco *et al.* Theory and phenomenology of two-Higgs-doublet models. 2011, arXiv:1106.0034v3 [hep-ph].

[83] P. Labelle. *Supersymmetry Demystified*. McGrawHill, 2010.

[84] D.Sutter S. Dimopoulos. The supersymmetric flavor problem. *Nucl. Phys.*, **B452**:496–512, 1995, arXiv:hep-ph/9504415.

[85] F. Gabbiani *et al.* A complete analysis of FCNC and CP constraints in general SUSY extensions of the standard model. *Nucl. Phys.*, **B477**:321–352, 1996, arXiv:hep-ph/9604387.

[86] C. Berger *et al.* Supersymmetry without prejudice. *JHEP*, **0902**:023, 2009, arXiv:0812.0980 [hep-ph].

[87] C. Csaki *et al.* Light stops from Seiberg Duality. 2012, arXiv:1201.1293v1 [hep-ph].

[88] D. Carmi *et al.* Interpreting LHC Higgs Results from Natural New Physics Perspective. 2012, arXiv:1202.3144v2 [hep-ph].

[89] P. Van Nieuwenhuizen. Supergravity. *Phys.Rept.*, **68**:189–398, 1981.

[90] L. Randall and R. Sundrum. Out of this world supersymmetry breaking. *Nucl.Phys.*, **B557**:79–118, 1999, arXiv:hep-th/9810155.

[91] Nelson A. E. Dine, M. and Y. Shirman. Low-energy dynamical supersymmetry breaking simplified. *Phys.Rev.*, **D51**:1362–1370, 1995, arXiv:hep-ph/9408384.

[92] M. Schmaltz and W. Skiba. The Superpartner spectrum of gaugino mediation. *Phys.Rev.*, **D62**:095004, 2000, arXiv:hep-ph/0004210.

[93] B. C. Allanach *et al.* Precise determination of the neutral higgs boson masses in the MSSM. *JHEP*, **0409**:044, 2004, arXiv:hep-ph/0406166v3.

[94] A. Arbey *et al.* Implications of a 125 GeV higgs for supersymmetric models. *Phys. Lett.*, **B708**:162–169, 2012, arXiv:1112.3028 [hep-ph].

[95] P. P. Giardino *et al.* Reconstructing Higgs boson properties from the LHC and Tevatron data. 2012, arXiv:1203.4254 [hep-ph].

[96] A. Arbey *et al.* Constrains on the MSSM from the Higgs Sector – A pMSSM study of Higgs searches, $B_s \to \mu^+\mu^-$ and Dark matter direct detection. *Eur. Phys. J.*, **C72**:1906, 2012, arXiv:1112.3032v3 [hep-ph].

[97] B. C. Allanach *et al.* Susy les houches accord 2. *Comp. Phys. Commun.*, **180**:8–25, 2009, `arXiv:0801.0045 [hep-ph]`.

[98] A. Djouadi *et al.* `SuSpect`: A `FORTRAN` code for the supersymmetric and higgs particle spectrum in the MSSM. *Comput. Phys. Commun.*, **176**:426–455, 2007, `arXiv:hep-ph/0211331v2`.

[99] A. Djouadi *et al.* `HDECAY`: A program for Higgs boson decays in the standard model and its supersymmetric extension. *Comp. Phys. Commun*, **108**:56–74, 1998, `arXiv:hep-ph/9704448`.

[100] D. Bourilkov M. R. Whalley and R. C. Group. The Les Houches Accord PDFs (LHAPDF) and Lhaglue. 2005, `arXiv:hep-ph/0508110`.

[101] P. Gondolo *et al.* `DarkSUSY`: Computing supersymmetric dark matter properties numerically. *JCAP*, **0407**:008, 2004, `arXiv:astro-ph/0406204`.

[102] J-L. Kneur. Personal communication, 2011.

[103] M. Spira. Personal communication, 2012.

[104] J. Schwinger. On quantum-electrodynamics and the magnetic moment of the electron. *Phys. Rev.*, **73**:416–417, 1948.

[105] T. Kinoshita and M. Nio. The tenth-order QED contribution to the lepton g-2: Evaluation of dominant α^5 terms of muon g-2. *Phys. Rev.*, **D73**:053007, 2006, `arXiv:hep-ph/0512330`.

[106] F. Jegerlehner. Muon g-2 update. *Nucl. Phys. Proc. Suppl.*, **181-182**:26–31, 2008.

[107] F. Jegerlehner. Precision measurements of σ_{hadronic} for $\alpha_{\text{eff}}(e)$ at ILC energies and $(g-2)_\mu$. *Nucl. Phys. Proc. Suppl.*, **162**:22–32, 2006, `arXiv:hep-ph/0608329`.

[108] M. Hayakawa *et al.* Hadronic light by light scattering effect on muon g-2. *Phys. Rev. Lett.*, **75**:790–793, 1995, `arXiv:hep-ph/9503463v1`.

[109] S. Peris *et al.* Two loop electroweak corrections to the muon g-2: A new class of hadronic contributions. *Phys. Lett*, **B355**:523–530, 1995, `arXiv:hep-ph/9505405`.

[110] F. Jegerlehner and A. Nyffeler. The muon $g-2$. *Physics Report*, **477**:1–110, 2009, `arXiv:0902.3360 [hep-ph]`.

[111] G. W. Bennett *et al.* Final report on the E821 muon anomalous magnetic moment measurement at bnl. *Phys. Rev.*, **D73**:072003, 2006, `arXiv:hep-ex/0602035`.

[112] John R. Ellis, Andy Ferstl, Keith A. Olive, and Yudi Santoso. Direct detection of dark matter in the MSSM with nonuniversal Higgs masses. *Phys.Rev.*, **D67**:123502, 2003, `arXiv:hep-ph/0302032`.

[113] A. Djouadi and C. Verzegnassi. Virtual very heavy top effects in LEP/SLC precision measurements. *Phys. Lett.*, **B195**:265–271, 1987.

[114] A. Djouadi and P. Gambino. Electroweak gauge boson self-energies: Complete QCD corrections. *Phys. Rev.*, **D49**:3499–3511, 1994, `arXiv:hep-ph/9309298`.

[115] M. Misiak and M. Steinhauser. Three-loop matching of the dipole operators for $b \to s\gamma$ and $b \to sg$. *Nucl. Phys.*, **B683**:277–305, 2004, `arXiv:hep-ph/0401041v1`.

[116] F. Borzumati *et al.* Beyond leading-order corrections to $\bar{B} \to X_s\gamma$ at large tan beta: The charged Higgs boson contribution. *Phys. Rev.*, **D69**:055005, 2004, `arXiv:hep-ph/0311151v2`.

[117] G. Degrassi *et al.* QCD corrections to radiative B decays in the MSSM with minimal flavor violation. *Phys. Lett.*, **B635**:335–342, 2006, `arXiv:hep-ph/0601135v2`.

[118] M. Misiak *et al.* Estimate of BR($B \to X_s\gamma$) at $\mathcal{O}(\alpha_s^2)$. *Phys. Rev. Lett.*, **98**:022002, 2007, `arXiv:hep-ph/0609232`.

[119] B. Aubert *et al.* For the BABAR Collaboration. Measurement of the $B \to X_s\gamma$ branching fraction and photon energy spectrum using the recoil method. *Phys. Rev.*, **D77**:051103, 2008, `arXiv:0711.4889 [hep-ex]`.

[120] A. Limosani *et al.* for the Belle Collaboration. Measurement of inclusive radiative B-meson decays with a photon energy threshold of 1.7 GeV. *Phys. Rev. Lett.*, **103**:241801, 2009, `arXiv:0907.1384 [hep-ph]`.

[121] J. Edsjo and P. Gondolo. Neutralino relic density including coannihilations. *Phys.Rev.*, **D56**:1879–1894, 1997, `arXiv:hep-ph/9704361`.

[122] K. A. Olive J. Ellis and Y. Santoso. Calculations of neutralino stop coannihilation in the CMSSM. *Astropart.Phys.*, **18**:395–432, 2003, `arXiv:hep-ph/0112113`.

[123] Christoph Weniger. A Tentative Gamma-Ray Line from Dark Matter Annihilation at the Fermi Large Area Telescope. 2012, `arXiv:1204.2797 [hep-ph]`.

[124] Bumseok Kyae and Jong-Chul Park. 130 GeV Gamma-Ray Line from Dark Matter Decay. 2012, arXiv:1205.4151 [hep-ph].

[125] James M. Cline. 130 GeV dark matter and the Fermi gamma-ray line. 2012, arXiv:1205.2688 [hep-ph].

[126] Elmo Tempel, Andi Hektor, and Martti Raidal. Fermi 130 GeV gamma-ray excess and dark matter annihilation in sub-haloes and in the Galactic centre. 2012, arXiv:1205.1045 [hep-ph].

[127] M. Ackermann et al. Fermi LAT Search for Dark Matter in Gamma-ray Lines and the Inclusive Photon Spectrum. 2012, arXiv:1205.2739 [astro-ph.HE].

[128] J. Lindroos. Personal communication, 2012.

[129] CMS Collaboration. Search for the standard model Higgs boson decaying to W^+W^- in the fully leptonic final state in pp collisions at $\sqrt{s} = 7$ TeV. *Phys. Lett.*, **B710**:91–113, 2012, arXiv:1202.1489v1 [hep-ex].

[130] ATLAS Collaboration. Seach for the Higgs boson in the $H \to WW^{(*)} \to l^+\nu l^-\bar{\nu}$ decay channel in pp collisions at $\sqrt{s} = 7$ TeV with the ATLAS detector. *Phys. Rev. Lett.*, **108**:111802, 2012, arXiv:1112.2577v3 [hep-ex].

[131] Combined CDF and D0 Search for Standard Model Higgs Boson Production with up to 10.0 fb^{-1} of Data. 2012, arXiv:1203.3774 [hep-ex].

[132] P. Gibbs. New Higgs Combinations Released. http://blog.vixra.org/2011/11/18/new-higgs-combinations-realeased/, 2011. [Online; accessed 23-May-2012].

[133] P. Gibbs. Higgs combination applet. http://vixra.org/Combo/, 2012. [Online; accessed 23-May-2012].

[134] Georges *et al.* Aad. ATLAS EXPERIMENT – Luminosity Public Results. https://twiki.cern.ch/twiki/bin/view/AtlasPublic/LuminosityPublicResults, 2012. [Online; accessed 25-May-2012].